On the theory of dark matter superfluidity

Pål Valberg

Thesis submitted for the degree of
Master of Science in Astronomy

Institute of Theoretical Astrophysics
University of Oslo

1st June 2018

Abstract

The "theory of dark matter superfluidity" [1] is reproduced in SI units with the inclusion of intermediate, and precise, steps in the calculations. By use of another measure of the mean interparticle separation, the bound on dark matter particle mass is less stringent than in [1], though the sub-eV mass range is still found. Using the conjectured superfluid phonon effective field theory, the equation of state is found to be polytropic $P \propto \rho^3$. Due to the increased precision in calculations, the resulting condensate halo radius is found to be less than in [1]. The proper acceleration needed is derived in higher precision than in [1], though, when compared to standard gravitational acceleration, is not dominant on large scales ($\sim 100\,\mathrm{kpc}$). Superfluid phonons are generated in galaxies, and breakdown of coherence within the fluid occurs closer to the source than in [1], though dark matter is still found to exist in its normal phase within the Solar System. A relativistic theory that produces proper dynamics in the non-relativistic, weak-field limit is considered, and a starting point for the inclusion of coupling to baryonic matter is suggested. Cosmological dark matter is found in the superfluid state, and the theory is altered to account for this in order to obtain "cold dark matter" on these scales. In addition to this, the evolution of the condensate mass density is found to reveal a finite (non-zero) scale factor for which it diverges. Finally, consequences to this theory, mostly considering Bose-Einstein condensate theory, is discussed in short, as well as the same points regarding astrophysics discussed in [1].

Acknowledgments

I would like to thank Øystein Elgarøy for being the voice of reason when I really needed it, as well as the rest of the Master students for providing an endless source of great fun.

Contents

Abstract **iii**

Acknowledgments **v**

List of Figures **viii**

1 Introduction **1**
1.1 Dark Matter 1
1.2 Modified Newtonian Dynamics 4
1.3 Reconciling CDM and MOND - Bose-Einstein Condensation and Superfluidity 5

2 Conditions for Dark Matter Condensation **9**
2.1 The first condition 9
2.2 The second condition 13
2.3 Critical temperature 15

3 Dark matter superfluid phase **17**
3.1 Finite temperature effective field theory for relativistic superfluids 17
3.1.1 Relativistic superfluids 18
3.1.2 Newtonian limit 20
3.1.3 Superfluid EFT in Newtonian limit 22
3.2 Condensate and phonon properties 22
3.2.1 Condensate equation of state 23
3.2.2 Phonons 23
3.3 Halo density profile 26

4 Including Baryons: Phonon Mediated Force **35**
4.1 Zero-temperature analysis 35
4.1.1 Determining the acceleration of baryons 36
4.1.2 Stability of phonon perturbations 39
4.2 Finite-temperature effects 42
4.2.1 Toy theory 43

5 Validity of EFT and the Solar System **57**
5.1 Superfluid stability 57
5.2 Higher-order derivatives 58
5.3 Local breakdown of coherence 59

6 A relativistic completion **63**
6.1 The theory 63
6.2 Future considerations 68

7 Cosmology **69**
7.1 Cosmological dark matter condensate 69
7.2 Equation of state 70
7.3 Coupling to baryons 72

8 Other consequences **75**
8.1 Bose-Einstein condensate theory 75
8.2 Astrophysics 78

9 Summary **81**

Bibliography **83**

List of Figures

2.1 The colored area shows the particle mass m and halo mass M for which dark matter can form a BEC, assuming the condition (2.3) and $z_{\rm vir} = 2$. 13
2.2 Fraction of condensed particles in halos with mass M for various particle masses m, assuming free particles and $z_{vir} = 0$. 16

3.1 Numerical solution (blue solid line) to the $n = 1/2$ Lane-Emden equation. The red dotted line is the analytical approximation to the numerical solution, and is a cosine-function. 29
3.2 Difference between the analytical approximation and the numerical solution to the $n = 1/2$ Lane-Emden equation. 30
3.3 Numerically calculated density profile corresponding to the $n = 1/2$ Lane-Emden equation (blue solid line). The analytical approximations (red and black dotted lines) are the square root of a cosine and the $(x, y) = (+, +)$ quadrant ellipse respectively. 31
3.4 Logarithmic absolute difference between the analytical approximations and the density profile corresponding to numerical solution to the $n = 1/2$ Lane-Emden equation. The solid and dotted lines are the cosine and ellipse approximations respectively. 32

4.1 The ϕ-mediated acceleration plotted with fiducial values alongside the MONDian expression on a test baryonic particle. The yellow star represents the transition radius $r_\star$. 48
4.2 The ratio between ϕ-mediated acceleration with fiducial values and MONDian acceleration on a test baryonic particle. The yellow star represents the transition radius $r_\star$. 48

Chapter 1

Introduction

This thesis serves as a review of the theory of dark matter superfluidity, as presented in Berezhiani and Khoury's paper "Theory of Dark Matter Superfluidity" [1], and hence follows the general layout of [1]. The key difference is the inclusion of more intermediate steps of the calculations, and that they are done in SI-units (as opposed to natural units given in [1]). Other things that [1] did not mention are brought up, mostly with regards to the consequences of the theory.

This introductory chapter differs from [1] by giving a more detailed history and motivation of astronomical dark matter, based on [2]. The section about Modified Newtonian Dynamics (hereby denoted MOND) is mostly the same. The third is about reconciling the two phenomena, and goes through the concept of how this is accomplished in [1]. Included in this thesis is some background information about Bose-Einstein condensates and superfluidity to make it a little more understandable.

1.1 Dark Matter

The observed velocity dispersion of galaxies in the Coma Cluster far exceeded what was inferred from the virial theorem [3]. The conclusion was that there was a significant amount of non-luminous matter present in the system, a result further backed by much higher *mass-to-light ratios* than inferred from observed baryonic matter in the form of luminous stars [4]. This "dark matter" was, at the time, believed to be baryonic - it was thought to be in the form of cold stars, solid bodies, and gas - an interpretation much akin to that of the Massive Compact Halo Objects model (MACHO). Multiple waveband surveys, [5, 6, 7, 8], eventually ruled out gas in the intergalactic space within the cluster - *intracluster gas* - as dark matter, seeing it was not nearly enough. Based on optical spectrography [9] and radio measurement of the 21 cm-line [10], along with later observations [11], it was determined that more matter in the outer regions of spiral galaxies was needed to explain the asymptotically flat rotation curves that had been observed - the rotational velocity of stars moving in circular orbits are expected to decline as $v_{\text{circ}} \propto r^{-1/2}$ according to Newtonian mechanics, but were observed to reach a constant value.

As for what constitutes dark matter, baryonic sources in the form of MACHOs - planets, dwarf stars, neutron stars and black holes - and primordial black holes were considered. Interest in the latter has been dwindling since it was discovered that the formation rate of such black holes is cosmologically negligible [2], and that in order to generate a necessary abundance of dark matter a large degree of non-gaussianity in the primordial power spectrum would have to be postulated [2]. The others could be identified through microlensing events, but were found to not contribute enough [12, 13]. In addition, the cosmic baryon content as measured by the Planck Collaboration from analysing the Cosmic Microwave Background was found to be $\Omega_{\mathrm{b}}h^2 = 0.02225 \pm 0.00016$ [14], a value which may also be inferred from Big Bang Nucleosynthesis coupled with observations of light element abundances - see e.g. [15]. Since baryonic matter thus make up only $\sim 20\%$ of the total matter density, there is left little room for MACHOs as dark matter.

Further indications for dark matter came from numerical simulations, one of which showed that rotationally supported galaxies with stellar disks are unstable [16, 17]. This contradicted observations, and a solution was presented where the disk was enveloped within a massive spherical halo [18]. Later cosmological simulations, which included a significant amount of dark matter, showed that the initial velocity distribution of dark matter did impact structure formation [19, 20]. Though the large-scale structures were insensitive to the velocity distribution, small-scale structures were not: if the thermal motions of dark matter particles were high ("hot" dark matter), small structures would be washed out, whereas low thermal motions ("cold" dark matter) would allow small structures to grow. The CfA survey revealed significant sub-cluster structures [21], much in opposition of "hot" dark matter simulations [22].

Thus cold dark matter (CDM) as a constituent of the cosmological Standrad Model ΛCDM seem to work very well on cosmological and extragalactic scales.

Dark matter candidates

As simulations and observations have ruled out "hot" candidates and baryons as constituents of dark matter, other candidates were considered. One which was quickly discarded was Standard Model neutrinos. Though not being baryons, they are very light thermal relics and are predicted to emerge form the early universe (decouple from the primordial bath) as highly relativistic particles, and would therefore be considered "hot" [23, 24].

Other candidates may be found within the frameworks of

- the minimal supersymmetric standard model (MSSM) in the form of neutralinos - the lightest, stable of which could be produced abundantly in the early universe, and with a mass in the GeV range would be very "cold" [25, 26]

- Peccei-Quinn theory in quantum chromodynamics - originally introduced to solve the strong *CP* problem (the problem of why QCD does not seem to break under the discrete charge-parity transformations when it is expected to from theory [27]), it brought with it the axion, a Goldstone boson of a spontaneously broken

$U(1)$ symmetry[1]. Its mass has been limited by astrophysical and cosmological observations to be in the sub-eV range [30], and can be considered "cold" only if they are produced from a misalignment mechanism in the early universe [31, 32, 33]

- Weakly Interacting Massive Particles (WIMPs) - for thermal relics to become cold, cosmological constraints on the mass (no less than 1 - 100 keV) combined with how such a species can match the observed dark matter density, the self-annihilation cross-section must be $\sigma v \sim 10^{-26}\text{cm}^3/\text{s}$, v being the relative particle speed. This is similar to that which arise in from the weak force, and when combined with theoretical arguments for new physics at the electroweak scale further bolster the WIMP as a dark matter candidate [34].

Failures of the cold dark matter paradigm

Though successful on very large scales, ΛCDM is not flawless. Cosmological simulations favors "collisionless" cold dark matter (for the purpose of structure formation, the relevant scales leave any fundamental force other than gravity ineffective), though the predicted abundance of dark subhalos orbiting Milky Way-sized galaxies is much more than observed [35]. Even though baryonic physics and other phenomena can be applied to bring down the predicted number, and the discovery of ultra-faint dwarf galaxies [36, 37, 38, 39] do increase the observed number, the discrepancy is still large. Along with this "missing satellite" problem, there is also the "too big to fail" problem [40, 41, 42]: the most massive simulated dark halos are too dense to host the brightest Milky Way satellites.

ΛCDM also predicts the distribution of dark satellites of Milky Way-sized galaxies to be isotropic, however the observed Milky Way satellites [43, 44, 45, 46] and Andromeda satellites [47, 48, 49] lie within vast planar structures and are co-rotating within these planes. This can be explained away if the Milky Way satellites are old tidal dwarfs created in an merger event early in the Milky Way's lifespan, as opposed to them being primordial subhalos [50]. This arise form the fact that the baryons within the galaxies are on nearly circular, coplanar orbits, whereas dark matter particles are on predominantly radial orbits in a quasi-spherical distribution. This corresponds to a difference in phase-space which leads to tidal tails which contain next-to-no dark matter [51] and thus exhibits no mass discrepancy, but do appear to contain dark matter [51] as well as fall within the *Baryonic Tully-Fisher Relation* (BTFR) [52].

This is an empirical relation in which the observed baryonic mass of a system is related to its circular velocity by a *power law*, or as a linear relation in log-log space,

$$\ln M_\text{b} \propto \alpha \ln v_\text{circ} \,. \tag{1.1}$$

[1]Goldstone's theorem states that for every spontaneously broken continuous symmetry, a given theory must contain a massless particle [28]. These are called *Goldstone bosons*. Massive Goldstone bosons can be generated if the continuous symmetry is also *explicitly* broken - *e.g.* within the Lagrangian formalism there are terms of the Lagrangian that breaks the symmetry, as opposed to spontaneous symmetry breaking where a solution to the equation of motion is not invariant under the breaking of a symmetry [29]

In the standard collapse model, the "spherical top-hat", matter is distributed in a sphere with uniform density, thus $M \propto R^3 \Rightarrow R \propto M^{1/3}$. For a rotationally supported self-gravitating distribution of matter the radial net force is zero, and centripetal acceleration is balanced out by Newtonian gravity,

$$\begin{aligned} \frac{M}{R^2} &\propto \frac{v_{\text{circ}}^2}{R} \\ M^{2/3} &\propto v_{\text{circ}}^2 \\ M &\propto v_{\text{circ}}^3 \end{aligned} \tag{1.2}$$

and the slope of the BTFR (in log-log space) is thus expected to be equal to 3. However, the observed slope (in log-log space) appears with very little scatter around 4, as can be seen in the Figure 3 in [53].

1.2 Modified Newtonian Dynamics

It therefore seems that ΛCDM works very well on the largest scales, but has problems on galactic scales. One proposition that works well *on* galactic scales is that of Modified Newtonian Dynamics (MOND). It completely does away with dark matter, so there are only baryons contributing to gravity.

First presented in [54, 55, 56] as an *ad hoc* modification of the traditional Newtonian inertial law in the limit of small acceleration, the acceleration experienced by a test mass changes with relation to some critical acceleration scale $a_0 \approx 1.2 \times 10^{-10}\,\text{m/s}$,

$$a_{\text{MOND}} \simeq \begin{cases} a_{\text{N}} & , \quad a_{\text{N}} \gg a_0 \\ \sqrt{a_0 a_{\text{N}}} & , \quad a_{\text{N}} \ll a_0 \end{cases} \tag{1.3}$$

where a_{N} is the standard Newtonian expression. With this, a rotationally supported self-gravitating distribution of matter is analyzed here in the context of MOND emerging as a consequence of an overlying theory of modified gravity[2]. Assuming dynamical equilibrium, the resulting expected BFTR slope (in log-log space) is precisely 4:

$$\begin{aligned} \sqrt{a_0 \frac{GM}{R^2}} &= \frac{v_{\text{circ}}^2}{R} \\ \sqrt{a_0 GM} &= v_{\text{circ}}^2 \\ M &= \frac{v_{\text{circ}}^4}{a_0 G}\,. \end{aligned} \tag{1.4}$$

Thus the BTFR favors MOND since its framework only consists of baryonic matter and is able to reproduce BTFR. As can be seen from eq. (1.4), the circular velocity is also independent of radius, which then reproduces the observed flat rotation curves in the outer regions of galaxies. However, two of the Milky Way dwarf spheroidals

[2]MOND therefore only affects Newtonian gravity.

[57, 58], and nearly all of the ultra faint dwarfs [59], are inconsistent with the BTFR, and the globular cluster NGC2419 also poses a challenge for MOND [60]. In opposition to the Milky Way satellites, MOND does well with the Andromeda satellites [61, 62], and it has been proposed that the discrepant dwarfs are undergoing tidal disruption [59] (this would bring the system out of equilibrium), or that the velocity estimates are complicated by interlopers [63]. It seems clear that more observations are in order as to not fall prey to a "sample size fallacy".

One situation where MOND succeeds is in explaining the planar structures in which the Milky Way and Andromeda satellites reside in, where they resulted due to a tidal stripping in an earlier fly-by event. With the MOND law a close encounter between the two galaxies has been estimated to have occured some 10 billion years ago with 55 kpc being the smallest distance between the two [64]. In ΛCDM, both galaxies would be enveloped in dark matter halos which would extend so far that in such a close encounter, dynamical friction would lead to a rapid merger of the two. In MOND there is only stellar dynamical friction, and a merger can be avoided [65, 66, 67]. MOND also predicts tidal dwarfs to fall within the BFTR, in agreement with the observed NGC5291 dwarfs mentioned above [51, 52].

In its earlier days, MOND faced challenges in not leading to conserved momentum, angular momentum and energy, and could not be generalized to general relativity [2]. The matter distribution of the merging "bullet cluster" [68], inferred from weak lensing observations, did not coincide with the observed baryon distribution, and thus meant even more trouble for MOND. The first realistic relativistic version of MOND, "Tensor-Vector-Scalar" theory (TeVeS) [69] predicts gravitational lensing due to baryonic matter alone to agree with observations as well as regular general relativity with a cold dark matter component does. Despite its successes, TeVeS cannot explain the observed lensing [70] of the "bullet cluster". Massive neutrinos and the theory's own vector field has been argued to alleviate this mismatch of prediction and observation [2]. TeVeS also predicts the wrong ratio between the second and third peaks in the CMB angular power spectrum, though this failure may be averted if some of the degrees of freedom of the theory behaved similarily to cold dark matter in the early universe [71, 72]. As a final note, numerical simulations of MONDian gravity with massive neutrinos fail to reproduce the observed cluster mass function [73, 74].

1.3 Reconciling CDM and MOND - Bose-Einstein Condensation and Superfluidity

As has been presented, the cold dark matter paradigm fits well on the largest of scales, whereas MOND fits well on galactic scales. It would appear that cold dark matter and MOND are mutually exclusive on their respective astronomical scales. This has prompted some hybrid models which includes both cold dark matter and MOND phenomena [75, 76, 77, 78, 79, 80, 81, 82].

The purpose of this thesis is to give more precise calculations and try to fill in some missing parts in one such hybrid model, first presented in [1]. In their proposal, dark

matter halos goes through Bose-Einstein condensation and forms a superfluid core with a coherence length[3] the size of galaxies, and the MONDian behaviour of baryons within this halo arise from a "fifth force" which occurs due to the baryons interacting with the dark matter superfluid phonons.

There will first be a short introduction to Bose-Einstein condensation and superfluids. Conditions for the onset of condensation are determined, a short but detailed derivation of the effective field theory that governs the superfluid phonons in included, then the superfluid phase itself is explored. The interaction theory is investigated and the "fifth force" acceleration is calculated in the context of zero- and finite temperature. Lastly, consequences of the theory are investigated.

Following is a short summary of Bose-Einstein condensation and superfluidity, as given in Pethick and Smith's book on Bose-Einstein condensation [83]. The purpose here is to provide the theoretical background necessary to work with dark matter in a superfluid context.

Bose-Einstein condensation

A key property of identical bosons is that they do not follow Pauli's exclusion principle. It follows that two or more particles can then occupy the same quantum state. For a system of many particles in thermal equilibrium, the mean occupation number of a state i with energy ϵ_i is given by the *Bose-Einstein ditribution*

$$f(\epsilon_i) = \frac{1}{e^{(\epsilon_i - \mu)/k_{\mathrm{B}}T} - 1},$$

where μ is the chemical potential and T is the temperature.

Above a critical temperature T_c all particles are in excited states, and as the temperature is lowered the ground state can become macroscopically occupied. The system is then said to have a *Bose-Einstein condensate* (BEC).

Superfluidity

One property a BEC can exhibit is that of *superfluidity*. It is the ability to flow around obstacles without dissipation (up to a limit):

- In the rest frame of the fluid: a moving obstacle in the fluid has a speed smaller than some critical value, there is not enough energy to create excitations in the fluid.
- In the rest frame of the moving obstacle: the fluid flows past without creation of excitations.

The obstacle can therefore be thought of as a time-dependent potential. Thus, for relative speeds between the fluid and the obstacle less than some critical value, no kinetic energy is lost since excitations are not created. Creation of an excitation is only

[3] The radius at which the condensate reaches its average value.

possible if its phase velocity equals that of the fluid velocity relative to the object. The lowest velocity for which this can occur, the *Landau critical velocity*, is given by the lowest phase velocity in an excitation spectrum ϵ_p for momentum p:

$$v_{\text{crit}} = \min\left(\frac{\epsilon_p}{p}\right), \tag{1.5}$$

for excitation momentum parallel to the relative velocity between the fluid and the object. Since this relative velocity is the superfluid velocity, there will not be created excitations if the fluid velocity is less than the Landau critical velocity,

$$v_s < v_{\text{crit}}\,, \tag{1.6}$$

and the system will exhibit superfluidity. Eq. (1.6) is therefore a criterion that must be satisfied for the superfluid to be stable, and is called *Landau's stability criterion* for superfluid flow.

It is clear that the lowest energy excitations that can be created are those with the lowest phase velocity. These are sound waves/phonons[4], so

$$v_s < c_s\,, \tag{1.7}$$

where v_s is the superfluid velocity and c_s the sound speed (propagation rate of the lowest energy excitation in the fluid).

A superfluid at finite temperature is usually described in *Landau's two-fluid picture*. The fluid is thought of as having two interpenetrating components - the **superfluid**, which is described as a $T = 0$ condensate, and the **normal fluid** which is described by the excited particles [83]. This is used in Chapter 3.

A peculiar property, that went unmentioned by [1], with such a picture is that the additional degrees of freedom associated with the superfluid yields a secondary sound mode. It rises from oscillatory solutions to the wave equations - which are derived hydrodynamically in [83] - yielding two coupled equations, for which a solution exists if the determinant vanishes. It becomes a second-order equation for the square of the phase velocity of the oscillation, and as such has two solutions - the "+" solution referred to as *first sound* and the "-" solution referred to as *second sound*.

A specific example provided in [83] is that of a uniform, interacting Bose gas. The first sound is a regular oscillation in density and thus propagates at sound speed c_s, while second sound corresponds to a temperature wave which propagates at $c_s/\sqrt{3}$. This is mentioned simply by the virtue that this happens only for superfluids, and that it may have some impact on the theory of dark matter that is the subject of this thesis. As such, it is not taken into proper consideration, though it is mentioned when appropriate.

[4] If the excitation spectrum is that of a *Bogoliubov* one - see [83]

Superfluidity and Dark Matter

In the context of superfluid dark matter [1], the obstacle that generate superfluid phonons is the gravitational potential set up by stars. The condensate remains coherent only when the gravitational potential is sufficiently weak. Close enough to the baryonic source (a star), the gravitational potential is so strong it brings the superfluid out of coherence and dark matter exists in its normal phase - *i.e.* the energy is sufficient to excite particles out of the ground state. This is studied in Chapter 5 with the Sun as an example.

Chapter 2

Conditions for Dark Matter Condensation

Since the model relies on dark matter particles existing in a condensed state, the conditions for condensation is, as in [1], here investigated.

For simplicity, [1] considers non-interacting particles, as is done here. This means that the dark matter particles are non-interacting in the *normal* phase. As will be shown in Chapter 6, the condensate requires significant three-body interactions in order to give MOND.

The estimation of the mean interparticle separation differs, in this thesis, from that used in [1]. This leads to a different bound on the particle mass, as well as the calculated condensed fraction of particles in a halo.

Virialized parameters are calculated using the standard collapse model, as opposed to simply mention this in passing as done in [1].

2.1 The first condition

The **first condition** is that the de Broglie wavelength of the dark matter particles be larger than the mean interparticle separation, the reason being that the individual particles enters a single, coherent quantum state when this is satisfied. The de Broglie wavelength is given as

$$\lambda_{\mathrm{dB}} = \frac{h}{mv} = \frac{2\pi\hbar}{mv}\,, \tag{2.1}$$

and the mean interparticle separation, here estimated by the *Wigner-Seitz radius*,

$$\frac{4}{3}\pi\rho\langle\ell\rangle^3 = m \Rightarrow \langle\ell\rangle = \left(\frac{3m}{4\pi\rho}\right)^{\frac{1}{3}}\,. \tag{2.2}$$

The radius itself is defined by the volume of a sphere that corresponds to the volume per particle of the system. These are different than in [1] by the inclusion of $2\pi\hbar$ in (2.1), and that [1] used $\rho\langle\ell\rangle^3 = m$ as the interparticle separation which is the volume of a cube that corresponds to the volume per particle of the system.

Taking the first condition into consideration, equations (2.1) and (2.2) gives an upper bound on the mass of the dark matter particles:

$$\frac{2\pi\hbar}{mv} \geq \left(\frac{3m}{4\pi\rho}\right)^{\frac{1}{3}} \Rightarrow m \leq \left(\frac{2^5\pi^4\hbar^3}{3}\frac{\rho}{v^3}\right)^{\frac{1}{4}} . \tag{2.3}$$

Here the difference in (2.1) and (2.2) from [1] by the factor $(2^5\pi^4/3)^{1/4} \approx 5.68$.

Virialization

The bound (2.3) is applied at virialization in [1], which only lists the virialized parameters. In this thesis they are derived from the standard *non-linear* spherical top-hat collapse model as presented following the lecture notes [84] and [85].

For a spherically symmetric perturbation of uniform density $\rho = \rho_0(1+\delta)$, the radius evolves as

$$\ddot{R} = -\frac{GM}{R^2} \quad , \quad M = \frac{4\pi}{3}\bar{\rho}_i R_i^3 , \tag{2.4}$$

where $\bar{\rho}_i$ denotes the average (unperturbed) density of the Universe at some early time t_i - when the density contrast between the perturbation and the Universe was still very small (i.e. *initially*). Multiply by $\dot{R}$ and integrate over t to obtain

$$\frac{1}{2}\dot{R}^2 - \frac{GM}{R} = E , \tag{2.5}$$

with E an integration constant. When considering the LHS it is clear the RHS denotes the total energy per unit mass for a mass element at R. The following parametrized solution obeys (2.5):

$$\begin{aligned} R &= A(1-\cos\theta) \\ t &= B(\theta - \sin\theta) \\ A^3 &= GMB^2 . \end{aligned} \tag{2.6}$$

The sphere reaches its maximum radius at $\theta = \pi$ and time $t = \pi B$, and is collapsed completely at $\theta = 2\pi$ and time $t = 2\pi B$.

The system is gravitationally bound, and thus has total energy

$$E = -\frac{3GM^2}{5R_{\max}} \tag{2.7}$$

where $R_{\max} = R(\theta = \pi) = 2A$, and virializes when it satisfies the virial theorem, which in turn mean the system is stable, and can be considered a *halo*. When $R = \frac{1}{2}R_{\max}$, the potential energy is $U = -\frac{6GM^2}{5R_{\max}}$ and the kinetic energy $T = \frac{3GM^2}{5R_{\max}}$, and the virial theorem, $U = -2T$, is satisfied. The virial radius is therefore $R_{\text{vir}} = \frac{1}{2}R_{\max}$, and since the system is now stable, so is the density - it is considered uniform throughout the entire collapsing process, and when the process stops the density also stops changing.

The density contrast between the collapsed sphere and the unperturbed Universe is then

$$\delta^{\text{coll}}_{\text{non-lin}} = \frac{\rho^{\text{coll}}_{\text{sphere}}}{\rho^{\text{coll}}_{m}} - 1 = \frac{\rho^{\text{vir}}_{\text{sphere}}}{\rho^{\text{coll}}_{m}} - 1\,, \tag{2.8}$$

where $\rho_m = \frac{1}{6\pi G t^2}$ in the model Universe[1], which is $\Omega_m = 1$ and $\Omega_\Lambda = 0$. The density of the sphere is uniform,

$$\rho^{\text{vir}}_{\text{sphere}} = \frac{3M}{4\pi R^3_{\text{vir}}} = \frac{3M}{4\pi\left(\frac{1}{2}R_{\max}\right)^3} = 8\frac{3M}{4\pi R^3_{\max}} = 8\rho^{\max}_{\text{sphere}}\,. \tag{2.9}$$

At collapse $t = 2\pi B$, whereas at maximum radius $t = \pi B$. Thus

$$\rho^{\text{coll}}_{m} = \frac{1}{6\pi G t^2_{\text{coll}}} = \frac{1}{6\pi G(2t_{\max})^2} = \frac{1}{4}\frac{1}{6\pi G t^2_{\max}} = \frac{1}{4}\rho^{\max}_{m}\,, \tag{2.10}$$

so we find

$$\delta^{\text{coll}}_{\text{non-lin}} = \frac{8\rho^{\max}_{\text{sphere}}}{\frac{1}{4}\rho^{\max}_{m}} - 1 = 32\frac{\rho^{\max}_{\text{sphere}}}{\rho^{\max}_{m}} - 1 = 32(\delta^{\max}_{\text{non-lin}} + 1) - 1\,. \tag{2.11}$$

An overdensity in this model may be written as

$$\begin{aligned}\delta &= \frac{\rho_{\text{sphere}}}{\rho_m} - 1 = 6\pi G t^2 \frac{M}{\frac{4\pi}{3}\pi R^3} - 1 = \frac{9GMt^2}{2R^3} - 1 \\ &= \frac{9GM}{2}\frac{B^2(\theta - \sin\theta)^2}{A^3(1-\cos\theta)^3} - 1 = \frac{9(\theta-\sin\theta)^2}{2(1-\cos\theta)^3} - 1\,.\end{aligned} \tag{2.12}$$

To get $\delta^{\max}_{\text{non-lin}}$, evaluate eq (2.12) at $\theta = \pi$:

$$\delta^{\max}_{\text{non-lin}} = \frac{9(\pi - \sin\pi)^2}{2(1-\cos\pi)^3} - 1 = \frac{9\pi^2}{16} - 1\,. \tag{2.13}$$

Thus the system virializes when

$$\delta^{\text{coll}}_{\text{non-lin}} = 32\frac{9\pi^2}{16} - 1 = 18\pi^2 - 1\,. \tag{2.14}$$

In terms of the present dark matter density, the virialized density is

$$\rho_{\text{vir}} = (\delta^{\text{coll}}_{\text{non-lin}} + 1)\rho^{\text{vir}}_{m} = 18\pi^2\rho_{m0}a^{-3}_{\text{vir}} = 18\pi^2\Omega_{m0}\rho_{c0}(1+z_{\text{vir}})^3\,, \tag{2.15}$$

where the 2015 Planck results [14] found $\Omega_{m0}h^2 \approx 0.1188$ and $\rho_{c0} \approx 8.62\times10^{-27}\,\text{kg}\,\text{m}^{-3}$.

From this, the radius of the virialized halo if it has a mass M:

$$M = \frac{4\pi}{3}\rho_{\text{vir}}R^3_{\text{vir}} \Rightarrow R_{\text{vir}} = \left(\frac{3M}{4\pi\rho_{\text{vir}}}\right)^{\frac{1}{3}}. \tag{2.16}$$

[1]The choice of model is due to the simple analytic form of $a(t)$ - it is matter-dominated $\Rightarrow a \propto t^{2/3} \Rightarrow \rho_{\text{m}} \propto t^{-2}$. It provides an excellent description of a flat universe at high redshifts (with non-zero Ω_Λ).

To find an expression for v in eq (2.3) while in this model, consider the speed of infalling particles at viralization:

$$v_{\rm vir} = \left.\frac{dR}{dt}\right|_{R=R_{\rm vir}} = \left.\frac{dR}{d\theta}\frac{d\theta}{dt}\right|_{\theta=\theta_{\rm vir}} = A\sin\theta\left(\frac{dt}{d\theta}\right)^{-1}\Bigg|_{\theta=\theta_{\rm vir}} = \left.A\sin\theta\frac{A}{BR(\theta)}\right|_{\theta=\theta_{\rm vir}} . \tag{2.17}$$

$v_{\rm vir}$ is reached at parameter value $\theta > \pi$ such that $R(\theta_{\rm vir}) = R_{\rm vir} = \frac{1}{2}R_{\rm max} = A \Rightarrow \theta_{\rm vir} = \frac{3\pi}{2}$. Then

$$v_{\rm vir} = -\frac{A}{B} = -\sqrt{\frac{GM}{R_{\rm vir}}} .$$

The minus sign implies radially inward motion, and is discarded as it is the magnitude that matters. With the virial radius (2.16) inserted, the virial velocity is

$$v_{\rm vir} = \sqrt{\frac{GM}{R_{\rm vir}}} = \left(\frac{4\pi\rho_{\rm vir}}{3}\right)^{1/6} G^{1/2}\, M^{1/3} . \tag{2.18}$$

Particle mass bound

Insert into eq (2.3) and find the bound on the particle mass,

$$\begin{aligned}
m &\leq \left[\frac{2^5\pi^4\hbar^3}{3}\,\rho_{\rm vir}\left(\frac{4\pi\rho_{\rm vir}}{3}\right)^{-1/2} G^{-3/2}\, M^{-1}\right]^{1/4} \\
&= \left[\left(\frac{2^{10}\pi^8\hbar^6}{3^2}\right)^{1/2}\left(\frac{3\rho_{\rm vir}}{4\pi G^3}\right)^{1/2} M^{-1}\right]^{1/4} \\
&= \left[\left(\frac{2^8\pi^7\hbar^6}{3}\right)^{1/2}\left(\frac{18\pi^2\Omega_{m0}\rho_{c0}(1+z_{\rm vir})^3}{G^3}\right)^{1/2} M^{-1}\right]^{1/4} \\
&= \left[\left(3\times(2\pi)^9\right)^{1/2}\left(\frac{\Omega_{m0}h^2\rho_{c0}\hbar^6}{G^3}\right)^{1/2} h^{-1}M^{-1}\right]^{1/4}(1+z_{\rm vir})^{3/8} \\
&= \left[3\times(2\pi)^9\times\frac{\Omega_{m0}h^2\rho_{c0}\hbar^6}{G^3}\right]^{1/8}\left(\frac{M}{h^{-1}}\right)^{-1/4}(1+z_{\rm vir})^{3/8} \\
&= \left[\frac{3\times(2\pi)^9}{(10^{12}h^{-1}\,M_\odot)^2}\times\frac{\Omega_{m0}h^2\rho_{c0}\hbar^6}{G^3}\right]^{1/8}\left(\frac{M}{10^{12}h^{-1}\,M_\odot}\right)^{-1/4}(1+z_{\rm vir})^{3/8} \\
\Rightarrow m &\lessapprox 11.2\left(\frac{M}{10^{12}h^{-1}\,M_\odot}\right)^{-1/4}(1+z_{\rm vir})^{3/8}\,{\rm eV}/c^2 .
\end{aligned} \tag{2.19}$$

The numeric factor is about 4.87 times that in [1], and is therefore less stringent. The point of this condition is to show that the particle mass m has an impact on whether or not a collapsed halo of mass M can form a BEC, which has been visualized in Figure [2.1] with $z_{\rm vir} = 2$.

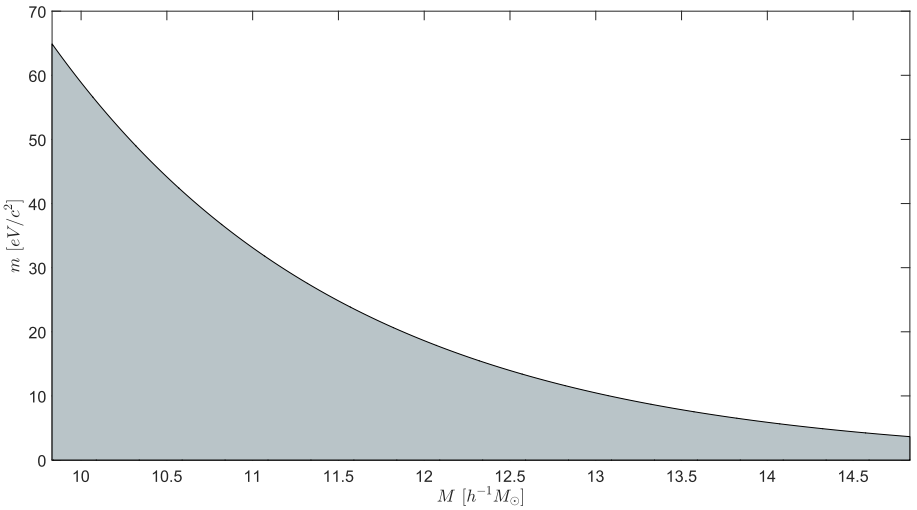

Figure 2.1: The colored area shows the particle mass m and halo mass M for which dark matter can form a BEC, assuming the condition (2.3) and $z_{\rm vir} = 2$.

2.2 The second condition

The **second condition** is that the dark matter particles thermalize (enters thermodynamic equilibrium with itself), with the temperature set by the virial velocity. For this to be the case the time-scale of thermalization must be less or at least comparable to the halo dynamical time. The former is taken to be the inverse of the self-interaction rate [86],

$$\Gamma \sim \mathcal{N} v_{\rm dis} n \sigma \tag{2.20}$$

$$\mathcal{N} \sim \frac{\rho}{m} \frac{(2\pi\hbar)^3}{\frac{4\pi}{3}(m v_{\rm dis})^3} \,. \tag{2.21}$$

The factors that goes into this are the self-interaction cross-section σ, the particle number density $n = \rho/m$, the dispersion velocity $v_{\rm dis}$, and the Bose enhancement factor $\mathcal{N}$. The needs for the three first factors are intuitive - increasing either should yield an increased rate. The last one occurs since bosons do not follow the Pauli exclusion principle - if there are N bosons in a given state, the probability of an additional boson to enter this state (over others) is "enhanced" by the factor $\mathcal{N}$.

The halo dynamical time can be thought of as a measure of the time-scale on which dynamical processes occur within the halo. A common expression for it is that of the free-fall time [87] $t_{\rm dyn} = \sqrt{3\pi/32G\rho}$, which corresponds to the time it takes for a uniform sphere of density ρ to collapse due to gravity alone. This is also the expression used in [1]. When represented by the virialized parameters (2.16), (2.17) and (2.18), the dynamical time is proportional to the time it would take to travel $R_{\rm vir}$ at constant

speed $v_{\rm vir}$. It is represented as such in this thesis to make calculations regarding the condition a little easier:

$$t_{\rm dyn} = \frac{\pi}{2^{3/2}} \frac{R_{\rm vir}}{v_{\rm vir}} \,. \tag{2.22}$$

The contition is then that the time-scale of thermalization of dark matter particles is less than, or equal to, the halo dynamical time. If this is satisfied, thermalization will occur, and the dark matter particles are able to enter BEC. Since the virialized structures are those of galactic halos, it follows that, if this condition is satisfied, the condensate is coherent throughout the halo. As stated in [1], this is important for the phonons to act coherently throughout the a galaxy such that the MONDian behaviour can occur.

As for the mathematical side, the equations (2.20), (2.21) and (2.22) yields a bound on the self-interaction cross-section σ/m. This is considered at virialization, with the dispersion velocity set by the infall velocity, which is just the virial velocity, $v_{\rm dis} = v_{\rm infall} = v_{\rm vir}$ in the non-relativistic limit, $n = \rho/m$,

$$\begin{aligned}
&\Gamma \gtrsim t_{\rm dyn}^{-1} \\
\Rightarrow \frac{\sigma}{m} &\gtrsim [\mathcal{N} v_{\rm vir} \rho_{\rm vir} t_{\rm dyn}]^{-1} = \left[\frac{\pi}{\sqrt{8}} \mathcal{N} \rho_{\rm vir} R_{\rm vir}\right]^{-1} = \left[\frac{\pi}{\sqrt{8}} \frac{\rho_{\rm vir}}{m} \frac{(2\pi\hbar)^3}{\frac{4\pi}{3}(m v_{\rm vir})^3} \rho_{\rm vir} R_{\rm vir}\right]^{-1} \\
&= \left[\frac{(2\pi\hbar)^3 \pi}{\sqrt{8}\frac{4\pi}{3}} \frac{\rho_{\rm vir}^2}{G^{3/2} M^{3/2}} m^{-4} R_{\rm vir}^{5/2}\right]^{-1} = \left[\frac{3\pi^3}{\sqrt{2}} \frac{\hbar^3}{G^{3/2}} \frac{\rho_{\rm vir}^2}{M^{3/2}} m^{-4} R_{\rm vir}^{5/2}\right]^{-1} \\
&= \left[\frac{3\pi^3}{\sqrt{2}} \frac{\hbar^3}{G^{3/2}} \frac{\rho_{\rm vir}^2}{M^{3/2}} m^{-4} \left(\frac{3M}{4\pi\rho_{\rm vir}}\right)^{5/6}\right]^{-1} = \left[\frac{3^{11/6}\pi^3}{\sqrt{2}(4\pi)^{5/6}} \frac{\hbar^3}{G^{3/2}} \rho_{\rm vir}^{7/6} m^{-4} M^{-2/3}\right]^{-1} \\
&= \left[\frac{3^{11/6}\pi^3 (18\pi^2)^{7/6}}{\sqrt{2}(4\pi)^{5/6}} \frac{\hbar^3 (\Omega_{m0}\rho_{c0})^{7/6}}{G^{3/2}(1\,{\rm eV}/c^2)^4 (10^{12} h^{-1}\, M_\odot)^{2/3}}\right]^{-1} \\
&\quad \times (1+z_{\rm vir})^{-7/2} \left(\frac{m}{1\,{\rm eV}/c^2}\right)^4 \left(\frac{M}{10^{12} h^{-1}\, M_\odot}\right)^{2/3} \\
\Rightarrow \frac{\sigma}{m} &\gtrsim 1.42\,(1+z_{\rm vir})^{-\frac{7}{2}} \left(\frac{m}{1\,{\rm eV}/c^2}\right)^4 \left(\frac{M}{10^{12} h^{-1} M_\odot}\right)^{\frac{2}{3}} {\rm cm}^2/{\rm g} \,.
\end{aligned} \tag{2.23}$$

The numerical factor is about 50 times less than that in [1], and is therefore a less stringent bound.

In line with [1], this is evaluated for halo mass $M \sim 10^{12} h^{-1} M_\odot$, at virialization $z_{\rm vir} = 2$ to find a lower bound

$$\frac{\sigma}{m} \gtrsim 0.03 \left(\frac{m}{1\,{\rm eV}/c^2}\right)^4 \frac{{\rm cm}^2}{\rm g} \,. \tag{2.24}$$

In a comparison to self-interacting dark matter (SIDM), [1] inserts a test-mass $m = 0.6\,{\rm eV}/c^2$ and checks whether or not their bound lies within the upper bound $\sim 1.25 {\rm cm}^2/{\rm g}$

found by [88]. This turns out to be the case, and subsequently is so for (2.24) in this thesis. As a little extra, the upper bound $\sim 1.25\text{cm}^2/\text{g}$ is here inserted into (2.24), and the upper bound on the particle mass $m \lesssim 2.54\,\text{eV}/c^2$. Thus eV, and possibly even sub-eV, particles are of interest. As mentioned by [1], the phenomenology of superfluid dark matter is found to be considerably different from that of SIDM, and so this result must be re-evaluated at a later point.

2.3 Critical temperature

When the dark matter condensate has thermalized, the temperature can be readily obtained by assuming equipartition of energy,

$$\frac{d}{2}k_{\text{B}}T = \frac{1}{2}m\langle v^2\rangle\,, \quad T \leq T_c\,, \tag{2.25}$$

where d represent the number of translational degrees of freedom; here $d = 3$ for the three spatial dimensions. The RHS is the average kinetic energy. As soon as $T > T_c$, all condensed particles become excited, breaking thermodynamic equilibrium, and so this description no longer holds. The critical temperature, T_c, would then be associated with a "critical" speed, v_c, which saturates (2.3),

$$k_{\text{B}}T_c = \frac{1}{3}mv_c^2\,, \tag{2.26}$$

with v_c given by (2.3),

$$v_c^2 = \left(\frac{2^5\pi^4}{3}\frac{\rho\hbar^3}{m^4}\right)^{\frac{2}{3}}\,. \tag{2.27}$$

Again evaluating at virialization, we find that

$$T_c \approx 565(1+z_{\text{vir}})^2\left(\frac{m}{1\,\text{eV}/c^2}\right)^{-\frac{5}{3}}\,\text{mK}\,. \tag{2.28}$$

It is about 100 times that in [1], which is due to the additional factor $2^5\pi^4/3$ in (2.3).

The temperature in a given halo, in units of T_c, is given by considering the velocity dispersion at virialization (divide (2.25) by (2.26)),

$$\frac{T}{T_c} = \left(\frac{v_{\text{vir}}}{v_c}\right)^2 \approx \frac{1.23\times10^{-3}}{1+z_{\text{vir}}}\left(\frac{m}{1\,\text{eV}/c^2}\right)^{\frac{8}{3}}\left(\frac{M}{10^{12}h^{-1}M_\odot}\right)^{\frac{2}{3}}\,, \tag{2.29}$$

which is a factor ~ 100 less than in [1].

Condensate fraction

For the purpose of calculating the condensate fraction, [1] now neglect interactions, and consequently the particles are considered free - they are not confined in a potential.

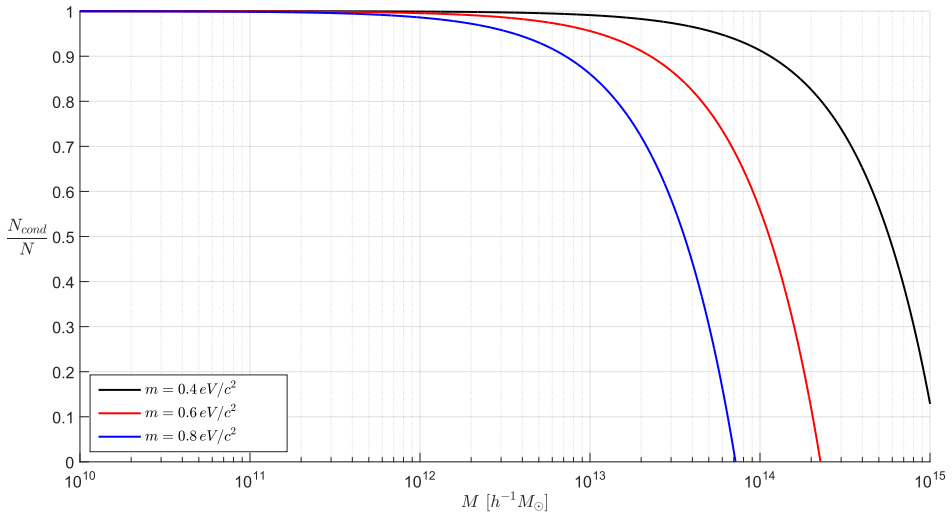

Figure 2.2: Fraction of condensed particles in halos with mass M for various particle masses m, assuming free particles and $z_{vir} = 0$.

In the temperature range $T \leq T_c$, the fraction of number of normal components to all components in the fluid is $N_{\rm nor}/N = (T/T_c)^{3/2}$, and necessarily for the condensed components

$$\frac{N_{\rm cond}}{N} = 1 - \left(\frac{T}{T_c}\right)^{\frac{3}{2}} \approx 1 - \frac{4.32 \times 10^{-5}}{(1+z_{\rm vir})^{3/2}} \left(\frac{m}{1\,{\rm eV}/c^2}\right)^4 \frac{M}{10^{12} h^{-1} M_\odot}\,, \quad T \leq T_c\,, \quad (2.30)$$

which, as expected by now, has a numerical factor smaller by ~ 100.

As mentioned in [1], the exponent 3/2 in the temperature term is only valid for free particles; a detailed reasoning behind this can be found in *e.g.* [83]. Since a halo will set up its own trapping potential - a gravitational potential - the exponent is subject to change. Figure [2.2] shows how the particle mass is a deciding factor in whether or not a collapsed object can form a condensate, here with $z_{\rm vir} = 0$ as in [1][2]. The numerical factor reduction by ~ 100 resulted in a slight shift towards smaller halo mass in Figure [2.2]. It is made clear that, for dark matter particles in the sub-eV mass range, galaxies ($M \lesssim 10^{12} h^{-1} M_\odot$) has a significant fraction of particles in the condensate whereas massive clusters ($10^{14} h^{-1} M_\odot \lesssim M \lesssim 10^{15} h^{-1} M_\odot$) can have a significant fraction, if not all, of their dark matter particles in the normal phase. This can be consider a reason behind the choice in [1] of the particle mass $m = 0.6\,{\rm eV}/c^2$ - in the sub-eV range; galaxies can condense *and* exhibit MONDian behaviour, while clusters does not condense *and* do not exhibit MONDian behaviour.

[2]Reasoning behind this change in virial redshift is unclear, and has not been provided by [1].

Chapter 3

Dark matter superfluid phase

As found in Chapter 2 in order for MONDian behaviour to occur on galactic scales, dark matter particles must form a BEC with coherence length the size of galaxies - specifically, the condensate exhibits superfluidity. In the superfluid phase, [1] argues dark matter is better described as collective excitations in the superfluid, in stead of collisionless particles. At low energies, these collective excitations are phonons (sound waves), as was mentioned in Chapter 1.

[1] claims these phonons are, in the non-relativistic limit, described by an effective field theory (EFTs are a kind of low-energy approximation to the full theory). The relativistic EFT was derived in [89], with the non-relativistic limit studied in [90].

In this chapter, the superfluid phonon EFT in the Newtonian limit is derived, based on [89] for the relativistic EFT at finite temperature, [91] for the Newtonian limit, and [90] to apply the non-relativistic limit. All this is just mentioned throughout [1] where needed. The EFT Lagrangian is exact to lowest order in derivatives, and corrections from higher-order derivatives are studied in Chapter 5.

Then, in both [1] and this thesis, the condensate properties are explored for a specific form of the superfluid effective Lagrangian chosen such that MONDian behaviour follows when dark matter superfluid phonon-baryon interactions are considered in Chapter 4. Subsequently, the halo profile is studied under the assumption of hydrostatic equilibrium, the result of which is also used in Chapter 4.

3.1 Finite temperature effective field theory for relativistic superfluids

The relevant relativistic superfluid EFT is derived following the steps, and serves as a summary of section 2, in [89]. This is subsequently taken to the Newtonian limit to fit the superfluid dark matter model.

3.1.1 Relativistic superfluids

The most general finite-temperature EFT Lagrangian is derived following the steps in [89]. It considers the long-distance degrees of freedom and the symmetries acting on them.

The two components of the fluid is parametrized by Θ, the zero-temperature relativistic superfluid field, and $\xi^I(\vec{x},t)$ for $I=1,2,3$, the comoving (or "Lagrangian") coordinates of the normal fluid component [92, 93]. The Lagrangian is constructed as a derivative expansion of the field Θ and coordinates $\xi^I(\vec{x},t)$ and are combined in a way such that the Lagrangian is compatible with the internal symmetries - they are Lorentz scalars and Poincarè invariance is thus implemented.

The superfluid state is considered as a system that carries a $U(1)$ charge - corresponding to invariance under $U(1)$ transformations (shift symmetry). Its here denoted by the field Θ, which can be thought of as the phase of the superfluid. The $U(1)$ transformation is

$$\Theta \to \Theta + a \tag{3.1}$$

for constant a - *i.e.* the dynamics of the field are invariant under this transformation.

Taking only the superfluid component into account for now, the only Lagrangian that can be constructed from Θ with (3.1) in mind is

$$\mathcal{L} = P(X)\,, \text{ where } X = \partial_\mu\Theta\partial^\mu\Theta\,, \tag{3.2}$$

where $P(X)$ is a generic scalar function. The associated Noether current is

$$j^\mu = 2P'(X)\partial^\mu\Theta, \tag{3.3}$$

and since the superfluid state has finite charge density, $\dot{\Theta} \neq 0$, one possible form expression for Θ is

$$\Theta = \mu t, \tag{3.4}$$

where μ is the chemical potential (if the spatial derivatives vanish). The spontaneous breaking of the $U(1)$ symmetry admits gapless excitations ϕ,

$$\Theta = \mu t + \phi, \tag{3.5}$$

which are the phonons.

To remind us of the task at hand, the idea is to first isolate the low-energy degrees of freedom and the symmetries acting upon them. It is then possible to construct the most general Lagrangian from the degrees of freedom which is also compatible with the symmetries, organized as a derivative expansion. The zero-temperature superfluid state was considered above, but since a fluid can inhibit superfluid properties for all temperatures less than the critical temperature T_c, the normal component must also be considered. As previously stated, the normal component has degrees of freedom parametrized by $\xi^I(\vec{x},t)$ for $I=1,2,3$, and their dynamics should be invariant under the internal symmetries

$$\xi^I \to \xi^I + a^I, \qquad\qquad a^I = \text{const.} \tag{3.6}$$

$$\xi^I \to R^I_J \xi^J, \qquad R \in SO(3) \tag{3.7}$$

$$\xi^I \to \sigma^I(\xi^J), \qquad \det\left(\frac{\partial \sigma^J}{\partial \xi^I}\right) = 1. \tag{3.8}$$

The first one is the familiar shift symmetry, and it states that the dynamics of the normal component should not change under $U(1)$ transformations. The second is that for rotations in 3-space, where R^I_J is the 3-dimensional rotation matrix in comoving space. The last one is that of volume-preserving diffeomorphism, and implies on the most basic level that particles can move independently of each other such that the normal component behaves like a fluid. Finally, Poincarè invariance is also imposed.

As for the Lorentz scalars related to the normal component, the shift symmetry (3.6) implies that the fields ξ^I enters the Lagrangian in the same fashion as Θ - with a first derivative acting on each ξ^I. Imposing Poincarè invariance forces the fields to enter the Lagrangian in the matrix form

$$B^{IJ} = (\partial_\mu \xi^I)(\partial^\mu \xi^J) \tag{3.9}$$

The rotational symmetry (3.7) forces only $SO(3)$ invariant matrices B^{IJ} to be considered, and the last condition (3.8) selects the determinants among these. The normal component Lagrangian is therefore of the form

$$\mathcal{L}_{\text{normal}} = F(B)\,, \text{ where } B \equiv \sqrt{\det\left(B^{IJ}\right)}. \tag{3.10}$$

With this, a stress-energy tensor may be calculated as a functional derivative,

$$T_{\mu\nu} = \frac{-2}{\sqrt{-g}} \frac{\delta(\sqrt{-g}\mathcal{L}_{\text{normal}})}{\delta g^{\mu\nu}}$$

where $g = \det g_{\mu\nu}$ and $g_{\mu\nu}$ is the space-time metric, which, for our purposes, will later be taken in the Newtonian gauge. Once calculated, it may be compared to that of a perfect fluid $T_{\mu\nu} = (\rho + p)u_\mu u_\nu + p g_{\mu\nu}$, and the normal fluid four-velocity is identified as

$$u^\mu = \frac{1}{6B} \varepsilon^{\mu\alpha\beta\gamma} \varepsilon_{IJK} (\partial_\alpha \xi^I)(\partial_\beta \xi^J)(\partial_\gamma \xi^K). \tag{3.11}$$

By the symmetry condition (3.8), u^μ is a vector field along which comoving coordinates do not change

$$u^\mu \partial_\mu \xi^I = 0\,,\ I = 1, 2, 3. \tag{3.12}$$

This leaves a last invariant scalar at this order in derivatives, $Y \equiv u^\mu \partial_\mu \Theta$, and, just to collect them all in one place:

$$X \equiv \partial_\mu \Theta \partial^\mu \Theta \tag{3.13}$$

$$B \equiv \sqrt{\det \partial_\mu \xi^I \partial^\mu \xi^J} \tag{3.14}$$

$$Y \equiv u^\mu \partial_\mu \Theta, \tag{3.15}$$

with u^μ is given by (3.11). Only (3.13) and (3.15) will be considered, since they will be applied in the Newtonian limit, in which $u^\mu \sim (c, \vec{v})$.

It is not included here, but [89] shows that this result does yield first and second sound modes, so this description can then be used in future work to properly investigate the effect of the second sound mode.

3.1.2 Newtonian limit

A collapsed halo is non-relativistic, thus the scalars (3.13) and (3.15) must be taken to the Newtonian limit - "non-relativistic with gravity", as will be shown. The purpose of this derivation is really just to find the normal component four-velocity in this limit. The calculations closely follows those in [91].

The Newtonian limit is defined by the requirements that *i)* particles move slowly ($v \ll c$), that is

$$\frac{dx^i}{dt} \ll c \Rightarrow \frac{dx^i}{d\tau} \ll c\,\frac{dt}{d\tau}\,, \tag{3.16}$$

ii) the gravitational field is weak and so the metric may be expressed as a perturbation from the Minkowski metric,

$$g_{\mu\nu} = \eta_{\mu\nu} + h_{\mu\nu},\ |h_{\mu\nu}| \ll 1, \tag{3.17}$$

and *iii)* the metric is static, which implies $\partial_0 g_{\mu\nu} = 0$.

The condition (3.16) means for the geodesic equation

$$\begin{aligned} \frac{d^2x^\mu}{d\tau^2} &= -\Gamma^\mu_{\alpha\beta}\,\frac{dx^\alpha}{d\tau}\,\frac{dx^\beta}{d\tau} \\ \frac{d^2x^\mu}{d\tau^2} &= -c^2\Gamma^\mu_{00}\left(\frac{dt}{d\tau}\right)^2\,, \end{aligned} \tag{3.18}$$

and the relevant Christoffel symbol Γ^μ_{00} is

$$\begin{aligned} \Gamma^\mu_{\alpha\beta} &= \frac{1}{2}g^{\mu\lambda}[\partial_\alpha g_{\beta\lambda} + \partial_\beta g_{\lambda\alpha} - \partial_\lambda g_{\alpha\beta}] \\ \Gamma^\mu_{00} &= \frac{1}{2}g^{\mu\lambda}[\partial_0 g_{\lambda 0} + \partial_0 g_{0\lambda} - \partial_\lambda g_{00}] \\ &= -\frac{1}{2}g^{\mu\lambda}\partial_\lambda g_{00}\,. \end{aligned} \tag{3.19}$$

By combining (3.17) and (3.19) to first order in $h_{\mu\nu}$ one find

$$\Gamma^\mu_{00} = -\frac{1}{2}\eta^{\mu\lambda}\partial_\lambda h_{00}, \tag{3.20}$$

and the geodesic equation

$$\frac{d^2x^\mu}{d\tau^2} = \frac{c^2}{2}\eta^{\mu\lambda}\partial_\lambda h_{00}\left(\frac{dt}{d\tau}\right)^2. \tag{3.21}$$

For the temporal component, $\mu = 0$, the third condition implies $\partial_0 h_{00} = 0$, so only the spatial components contribute. Recall that this part of $\eta^{\mu\nu}$ is the (3×3)-identity matrix, so

$$\begin{aligned} \frac{d^2x^i}{d\tau^2} &= \frac{c^2}{2}\left(\frac{dt}{d\tau}\right)^2 \partial_i h_{00} \\ \left(\frac{d\tau}{dt}\right)^2 \frac{d^2\vec{x}}{d\tau^2} &= \frac{c^2}{2}\nabla h_{00} \\ \frac{d^2\vec{x}}{dt^2} &= \frac{c^2}{2}\nabla h_{00}\,. \end{aligned} \tag{3.22}$$

By comparison to Newton's second law that connects the acceleration to the gradient of a gravitational potential Φ,

$$\frac{d^2\vec{x}}{dt^2} = -\nabla\Phi, \tag{3.23}$$

it is clear that Newtonian physics is restored if

$$h_{00} = -2\frac{\Phi}{c^2}. \tag{3.24}$$

The full metric is then,

$$g_{\mu\nu} = \begin{cases} g_{00} = -\left(1 + 2\frac{\Phi}{c^2}\right) \\ g_{0i} = 0 \\ g_{ij} = \delta_{ij} \end{cases} . \tag{3.25}$$

Since the metric (3.25) differs from the Minkowskian case (special relativity), the corresponding Lorentz factor will also differ. It can be identified through the time-like line-element

$$\begin{aligned} cd\tau &= \sqrt{-g_{\mu\nu}dx^\mu dx^\nu} \\ &= \sqrt{\left(1 + 2\frac{\Phi}{c^2}\right)c^2dt^2 - \delta_{ij}dx^i dx^j} \\ &= cdt\sqrt{1 + 2\frac{\Phi}{c^2} - \delta_{ij}\frac{dx^i dx^j}{c^2dt^2}} \\ \frac{d\tau}{dt} &= \sqrt{1 + 2\frac{\Phi}{c^2} - \frac{v^2}{c^2}}\,. \end{aligned}$$

so it is

$$\gamma_h = \frac{dt}{d\tau} = \frac{1}{\sqrt{1 + 2\frac{\Phi}{c^2} - \frac{v^2}{c^2}}}\,. \tag{3.26}$$

By the first requirement in the Newtonian limit, the term quadratic in v/c may be discarded, and the second requirement enables the expansion of γ_h to first order in $x = \Phi/c^2$,

$$\gamma_h(x) \simeq \gamma_h(x = 0) + \left.\frac{d\gamma_h}{dx}\right|_{x=0} x + \mathcal{O}(x^2)$$

$$\simeq 1 - x$$
$$\gamma_h \simeq 1 - \frac{\Phi}{c^2}\,. \tag{3.27}$$

The four-velocity, $u^\mu = (\gamma_h c, \gamma_h \vec{v})$, in the Newtonian limit, takes the form

$$u^\mu \simeq \left[\left(1 - \frac{\Phi}{c^2}\right) c, \left(1 - \frac{\Phi}{c^2}\right) \vec{v}\right]$$
$$\simeq c\left(1 - \frac{\Phi}{c^2}, \frac{\vec{v}}{c}\right), \tag{3.28}$$

where the quadratic terms $\Phi||\vec{v}||/c^2$ are discarded following the conditions of this limit.

3.1.3 Superfluid EFT in Newtonian limit

The phonons are described by the field θ which, in the non-relativistic limit, enters into the effective Lagrangian through the scalar X as [90]

$$X = \dot{\theta} - V(t, \vec{x}) - \frac{(\nabla\theta)^2}{2m}\,, \tag{3.29}$$

where $V(t, \vec{x})$ is the external trapping potential: a gravitational potential set up by the halo itself. Phonons at constant chemical potential μ are described by $\theta = \mu t + \phi$, which, according to [1], yields

$$X = \mu - m\Phi + \dot{\phi} - \frac{(\nabla\phi)^2}{2m}\,. \tag{3.30}$$

The gravitational potential $\Phi(r)$ - gravitational potential energy per unit mass - satisfies Poisson's equation and is sourced by dark matter and baryons: $\nabla^2\Phi = 4\pi G(\rho_{\rm DM} + \rho_{\rm b})$.

As for the scalar Y, [1] takes $\Theta = mc^2 t + \theta$ and subtracts the rest energy, and imposes the Newtonian limit on the four-velocity

$$\begin{aligned} Y &= u^\mu \partial_\mu \Theta - mc^2 \\ &= u^\mu \left[\frac{\partial(mc^2 t)}{c\partial t}\delta_{\mu 0} + \partial_\mu\theta\right] - mc^2 \\ &\simeq c\left(1 - \frac{\Phi}{c^2}\right) mc + c\left(1 - \frac{\Phi}{c^2}\right)\frac{\partial\theta}{c\partial t} + c\frac{\vec{v}}{c}\cdot\nabla\theta - mc^2 \\ &= \mu - m\Phi + \dot{\phi} - \vec{v}\cdot\nabla\phi\,, \end{aligned} \tag{3.31}$$

where the term $\Phi\dot{\theta}/c^2$ is negligible, and $\vec{v}$ is the normal component three-velocity.

3.2 Condensate and phonon properties

In line with (3.2) and (3.29) the phonons are described by the scalar field θ. The superfluid effective Lagrangian is for free particles ($V = 0$),

$$\mathcal{L} = P(X), \quad X = \dot{\theta} - \frac{(\nabla\theta)^2}{2m}\,, \tag{3.32}$$

To describe phonons at constant chemical potential μ, expand

$$\theta = \mu t + \phi. \tag{3.33}$$

[1] conjectures that dark matter superfluid phonons are governed by

$$P(X) = \frac{2\Lambda(2m)^{3/2}}{3\hbar^3} X\sqrt{|X|}\,, \tag{3.34}$$

which, when baryons are included, reproduces MONDian behaviour (Chapter 4). The additional factor $\hbar^{-3}$ is included to make sure (3.34) has units of pressure (energy density) - the inclusion of potential energy in (3.29) implies X has unit of energy, and since the "effective theory scale" Λ also has unit of energy. Hence $\hbar^{-3}$ is necessary to make the units add up.

3.2.1 Condensate equation of state

The purpose for now is to investigate the condensed state, so $\theta = \mu t$ for free particles. Thus $X = \mu$, and

$$P(\mu) = \frac{2\Lambda(2m)^{3/2}}{3\hbar^3}\mu^{3/2}. \tag{3.35}$$

Differentiating w.r.t. chemical potential μ yields condensed particle number density,

$$n = \frac{\partial P}{\partial \mu} = \frac{\Lambda(2m)^{3/2}}{\hbar^3}\mu^{1/2}. \tag{3.36}$$

In the non-relativistic limit, $\rho = mn$, which is reasonable for our purposes. The chemical potential may then be related to the mass density, which can be inserted back into (3.35) to yield an equation of state,

$$\begin{aligned} \mu^{1/2} &= n\Lambda^{-1}(2m)^{-3/2}\hbar^3 = \frac{\hbar^3}{m\Lambda(2m)^{3/2}}\rho \\ P &= \frac{2\Lambda(2m)^{3/2}}{3\hbar^3}\left[\frac{\hbar^3}{m\Lambda(2m)^{3/2}}\rho\right]^3 = \frac{\hbar^6}{12\Lambda^2 m^6}\rho^3\,. \end{aligned} \tag{3.37}$$

As pointed out by [1] this is a polytropic equation of state, $P = K\rho^{1+\frac{1}{n}}$ with index $n = 1/2$.

3.2.2 Phonons

In order to consider phonon excitations on top of this condensate, expand (3.34) to quadratic and higher order in phonon perturbations ϕ, $\theta = \mu t + \phi$, neglecting gravitational potential,

$$\mathcal{L} = \frac{2\Lambda(2m)^{3/2}}{3\hbar^3} X\sqrt{|X|}\,, \quad X = \mu + \dot{\phi} - \frac{(\nabla\phi)^2}{2m} = \mu + \tilde{X}(\phi)$$

$$= \frac{2\Lambda(2m)^{3/2}}{3\hbar^3}(\mu+\tilde{X})\sqrt{|\mu+\tilde{X}|}\,. \tag{3.38}$$

Consider small perturbations such that the root expression, $f(\tilde{X}) = \sqrt{|\mu+\tilde{X}|} = |\mu+\tilde{X}|^{1/2}$, can be Taylor expanded for small $\tilde{X}$, and evaluate said expansion about $\tilde{X}=0$. We will need up to the third order in derivatives, so the expansion will look as follows,

$$f(\tilde{X}) = f(0) + \frac{df}{d\tilde{X}}\bigg|_{\tilde{X}=0}\tilde{X} + \frac{1}{2}\,\frac{d^2f}{d\tilde{X}^2}\bigg|_{\tilde{X}=0}\tilde{X}^2 + \frac{1}{6}\,\frac{d^3f}{d\tilde{X}^3}\bigg|_{\tilde{X}=0}\tilde{X}^3 + \mathcal{O}(\tilde{X}^4) \tag{3.39}$$

The first term is easily found to be $\sqrt{|\mu|} = \mu^{1/2}$. As for the rest,

$$\begin{aligned}
\frac{df}{d\tilde{X}} &= \frac{df}{d|\mu+\tilde{X}|}\frac{d|\mu+\tilde{X}|}{d(\mu+\tilde{X})}\frac{d(\mu+\tilde{X})}{d\tilde{X}} = \frac{\mu+\tilde{X}}{2|\mu+\tilde{X}|^{1/2}|\mu+\tilde{X}|} \\
&= \frac{1}{2}(\mu+\tilde{X})|\mu+\tilde{X}|^{-3/2} \qquad (3.40)\\
\frac{d^2f}{d\tilde{X}^2} &= \frac{1}{2}\frac{d}{d\tilde{X}}(\mu+\tilde{X})|\mu+\tilde{X}|^{-3/2} = \frac{1}{2}(\mu+\tilde{X})\frac{d|\mu+\tilde{X}|^{-3/2}}{d\tilde{X}} + \frac{1}{2}|\mu+\tilde{X}|^{-3/2} \\
&= \frac{2|\mu+\tilde{X}|^2 - 3(\mu+\tilde{X})^2}{4|\mu+\tilde{X}|^{7/2}} = -\frac{|\mu+\tilde{X}|^2}{4|\mu+\tilde{X}|^2|\mu+\tilde{X}|^{3/2}} \\
&= -\frac{1}{4|\mu+\tilde{X}|^{3/2}} \qquad (3.41)\\
\frac{d^3f}{d\tilde{X}^3} &= -\frac{1}{4}\frac{d|\mu+\tilde{X}|^{-3/2}}{d\tilde{X}} = \frac{3(\mu+\tilde{X})}{8|\mu+\tilde{X}|^{7/2}}\,. \qquad (3.42)
\end{aligned}$$

In the second-to-last equality in (3.41) we used the fact that since $\mu, \tilde{X} \in \mathbb{R} \Rightarrow |\mu+\tilde{X}|^2 = (\mu+\tilde{X})^2$. And when evaluated at $\tilde{X}=0$,

$$\frac{df}{d\tilde{X}}\bigg|_{\tilde{X}=0} = \frac{1}{2}\mu^{-1/2} \qquad \frac{d^2f}{d\tilde{X}^2}\bigg|_{\tilde{X}=0} = -\frac{1}{4}\mu^{-3/2} \qquad \frac{d^3f}{d\tilde{X}^3}\bigg|_{\tilde{X}=0} = \frac{3}{8}\mu^{-5/2}, \tag{3.43}$$

so the expansion is

$$f(\tilde{X}) = \mu^{1/2} + \frac{1}{2}\mu^{-1/2}\tilde{X} - \frac{1}{8}\mu^{-3/2}\tilde{X}^2 + \frac{3}{16}\mu^{-5/2}\tilde{X}^3 + \mathcal{O}(\tilde{X}^4). \tag{3.44}$$

With this, the Lagrangian can be written as follows with the coefficient $C = 2\Lambda(2m)^{3/2}/3\hbar^3$,

$$\begin{aligned}
\mathcal{L} &= C(\mu+\tilde{X})\left(\mu^{1/2} + \frac{1}{2}\mu^{-1/2}\tilde{X} - \frac{1}{8}\mu^{-3/2}\tilde{X}^2 + \frac{1}{16}\mu^{-5/2}\tilde{X}^3 + \mathcal{O}(\tilde{X}^4)\right) \\
&= C\left(\mu^{3/2} + \frac{3}{2}\mu^{1/2}\tilde{X} + \frac{3}{8}\mu^{-1/2}\tilde{X}^2 - \frac{1}{16}\mu^{-3/2}\tilde{X}^3\right) + \mathcal{O}(\tilde{X}^4)\,.
\end{aligned}$$

Within the power expansion of first-order derivatives, the contributions to $\mathcal{L}_{\text{quad}}$ comes from terms containing $\tilde{X}$ and $\tilde{X}^2$

$$\begin{aligned}\mathcal{L}_{\text{quad}} &= C\left(\frac{3}{2}\mu^{1/2}\tilde{X} + \frac{3}{8}\mu^{-1/2}\tilde{X}^2\right)\\ &= C\left(-\frac{3}{2}\mu^{1/2}\frac{(\nabla\phi)^2}{2m} + \frac{3}{8}\mu^{-1/2}\dot{\phi}^2\right)\\ &= \frac{3C}{8\mu^{1/2}}\left(\dot{\phi}^2 - \frac{2\mu}{m}(\nabla\phi)^2\right)\\ &= \frac{\Lambda(2m)^{3/2}}{4\hbar^3\mu^{1/2}}\left[\dot{\phi}^2 - c_s^2(\nabla\phi)^2\right], \quad c_s = \sqrt{\frac{2\mu}{m}}\,. \end{aligned} \tag{3.45}$$

The sound speed by the usual thermodynamic expression:

$$c_s^2 = \frac{\partial P}{\partial \rho} = 3K\rho^2. \tag{3.46}$$

This may be combined with eq.s (3.36) and (3.37) to find the relation between c_s^2 and μ,

$$c_s^2 = 3K\left[\frac{2m^2\Lambda}{\hbar^3}(2m\mu)^{1/2}\right]^2 = 3\left[\frac{\hbar^6}{12\Lambda^2 m^6}\right]\left[\frac{4m^4\Lambda^2}{\hbar^6}(2m\mu)\right] = \frac{2\mu}{m}\,. \tag{3.47}$$

It can also be argued for by inserting the quadratic Lagrangian (3.45) into the Euler-Lagrange equation, which yields the equation of motion for ϕ. The Lagrangian (3.45) is only dependent on derivatives of ϕ, so

$$\begin{aligned}\frac{\partial\mathcal{L}_{\text{quad}}}{\partial\phi} - \sum_{i=t,x,y,z}\partial_i\left(\frac{\partial\mathcal{L}_{\text{quad}}}{\partial(\partial_i\phi)}\right) &= 0\\ \frac{\partial}{\partial t}\left(\frac{\partial\mathcal{L}_{\text{quad}}}{\partial(\dot{\phi})}\right) + \nabla\cdot\left(\frac{\partial\mathcal{L}_{\text{quad}}}{\partial(\nabla\phi)}\right) &= 0\\ \frac{\partial}{\partial t}\left(2\dot{\phi}\right) - \nabla\cdot\left(2c_s^2\nabla\phi\right) &= 0\\ \ddot{\phi} - c_s^2\nabla^2\phi &= 0\,,\end{aligned}$$

which is a wave equation.

Contributions to $\mathcal{L}_{\text{higher-order}}$ are from terms containing powers of $\mathcal{O}(\tilde{X}^2)$ and greater. Here, only a few terms are included, indicated by the "$\supset$" sign - it means that the terms on the RHS make up a small part of the LHS. Only terms containing $\tilde{X}^2$ and $\tilde{X}^3$ are considered, as no more is necessary in order to notice a trend,

$$\begin{aligned}\mathcal{L}_{\text{higher-order}} &\supset \alpha\left(\frac{3}{8}\mu^{-1/2}\tilde{X}^2 - \frac{1}{16}\mu^{-3/2}\tilde{X}^3\right)\\ &= C\left(\frac{3\mu^{-1/2}}{2^5m^2}(\nabla\phi)^4 + \frac{\mu^{-3/2}}{2^7m^3}(\nabla\phi)^6 - \frac{\mu^{-3/2}}{2^4}\dot{\phi}^3\right)\end{aligned}$$

$$
\begin{aligned}
&= \frac{3C}{2^7\mu^{5/2}}(c_s\nabla\phi)^4 + \frac{K}{2^{10}\mu^{9/2}}(c_s\nabla\phi)^6 - \frac{K}{2^4\mu^{3/2}}(\partial_t\phi)^3 \\
&= \frac{C}{\mu^{3/2}}\left(-2^{-4}(\partial_t\phi)^3 + 2^7 3\mu^{-1}(c_s\nabla\phi)^4 + 2^{-10}\mu^{-3}(c_s\nabla\phi)^6\right) \\
&= -\frac{\Lambda(2m)^{3/2}}{3\times 2^3\hbar^3\mu^{3/2}}(\partial_t\phi)^3 + \frac{\Lambda(2m)^{3/2}}{2^6\hbar^3\mu^{5/2}}(c_s\nabla\phi)^4 + \frac{\Lambda(2m)^{3/2}}{3\times 2^9\hbar^3\mu^{9/2}}(c_s\nabla\phi)^6 \\
&= \frac{\Lambda}{\hbar^3}\left(\frac{m}{\mu}\right)^{\frac{3}{2}}(a_3\mu^{3-3}\dot{\phi}^3 + a_4\mu^{3-4}(c_s\nabla\phi)^4 + a_6\mu^{3-6}(c_s\nabla\phi)^6) \\
&= a_n\hbar^{-3}\Lambda\left(\frac{m}{\mu}\right)^{\frac{3}{2}}\mu^{3-n}(\partial\phi)^n\,, \quad n\geq 3 \\
&= a_n\frac{\Lambda}{(\hbar c)^3}(mc^2)^{3/2}\mu^{3/2}\mu^{-n}(\partial\phi)^n \\
&= \frac{a_n}{(\hbar c)^3}[\Lambda(mc^2)^{3/2}\mu^{3/2}][\Lambda(mc^2)^{3/2}\mu^{3/2}]^{n/2}[\Lambda(mc^2)^{3/2}\mu^{3/2}]^{-n/2}\mu^{-n}(\partial\phi)^n \\
&= \frac{a_n}{(\hbar c)^3}[\Lambda(mc^2)^{3/2}\mu^{3/2}]^{1-n/2}[\Lambda^{1/2}(mc^2)^{3/4}\mu^{3/4}\mu^{-1}]^n(\partial\phi)^n \\
&= \frac{a_n}{(\hbar c)^3}[\Lambda_s^4]^{1-\frac{n}{2}}(\partial\phi_c)^n\,, \quad \phi_c = \Lambda^{1/2}(mc^2)^{3/4}\mu^{-1/4}\phi\,,
\end{aligned}
\tag{3.48}
$$

where ∂ denotes either ∂_t or $c_s\nabla$, a_n is some numeric factor, and with ϕ_c as a canonical variable (it can be used in Hamiltonian mechanics). When expressed like this, we can identify the strong coupling scale as the scale suppressing the higher order terms,

$$\Lambda_s \equiv [\Lambda(mc^2)^{3/2}\mu^{3/2}]^{1/4}\,. \tag{3.49}$$

3.3 Halo density profile

With an equation of state, we can now attempt to find the density profile of the condensate component of a halo, assuming hydrostatic equilibrium. The reason this is done is that actual dark matter halos may be inferred either from dynamical properties of its contents or by gravitational lensing of background galaxies/clusters, providing a consistency check between theory and observation.

Focusing on a static, spherically symmetric halo, pressure and acceleration are related as usual,

$$
\begin{aligned}
\frac{1}{\rho(r)}\frac{dP}{dr} = -\frac{d\Phi}{dr} &= -\frac{G}{r^2}m(r) \\
&= -\frac{G}{r^2}\int_0^r\int_0^{4\pi} d\Omega dr' r'^2\rho(r') = -\frac{4\pi G_N}{r^2}\int_0^r dr' r'^2\rho(r')\,.
\end{aligned}
\tag{3.50}
$$

Differentiate on r to obtain the Poisson equation

$$\frac{d}{dr}\left(\frac{1}{\rho}\frac{dP}{dr}\right) = -G\frac{d}{dr}\frac{m}{r^2}$$

$$
\begin{aligned}
&= \frac{2G}{r^3}m - \frac{G}{r^2}m' \\
&= -\frac{2}{r\rho}\frac{dP}{dr} - \frac{4\pi G}{r^2}\frac{d}{dr}\int_0^r dr' r'^2 \rho(r') \\
&= -\frac{2}{r\rho}\frac{dP}{dr} - 4\pi G\rho \\
\frac{d}{dr}\left(\frac{1}{\rho}\frac{dP}{dr}\right) + \frac{2}{r\rho}\frac{dP}{dr} &= -4\pi G\rho \qquad\qquad | \times r^2 \\
r^2\frac{d}{dr}\left(\frac{1}{\rho}\frac{dP}{dr}\right) + \frac{2r}{\rho}\frac{dP}{dr} &= -4\pi G\rho r^2 \\
\frac{d}{dr}\left(\frac{r^2}{\rho}\frac{dP}{dr}\right) &= -4\pi G\rho r^2 \\
\frac{1}{r^2}\frac{d}{dr}\left(\frac{r^2}{\rho}\frac{dP}{dr}\right) &= -4\pi G\rho\,. \qquad (3.51)
\end{aligned}
$$

This can be brought unto a dimensionless form: the $n = 1/2$ Lane-Emden equation. The polytrope has pressure $P = K\rho^3$, see equation (3.37). Let ρ_0 be the central density of the halo, and y a dimensionless variable. The density can now be expressed in terms of these as $\rho = \rho_0 y^{1/2}$. This brings the pressure to the form $P = K\rho_0^3 y^{3/2}$. Insert into equation (3.51) and find

$$
\begin{aligned}
\frac{1}{r^2}\frac{d}{dr}\left(\frac{r^2 K\rho_0^3}{\rho_0 y^{1/2}}\frac{dy^{3/2}}{dr}\right) &= -4\pi G\rho_0 y^{1/2} \\
\frac{K\rho_0^2}{r^2}\frac{d}{dr}\left(\frac{3r^2 y^{1/2}}{2y^{1/2}}\frac{dy}{dr}\right) &= -4\pi G\rho_0 y^{1/2} \\
\frac{1}{r^2}\frac{d}{dr}\left(r^2\frac{dy}{dr}\right) &= -\frac{8\pi G}{3K\rho_0}y^{1/2}\,. \qquad (3.52)
\end{aligned}
$$

Now, let $r = r_0 x$ where r_0 is some characteristic length and x is a dimensionless variable. Then $dr = r_0 dx$, and equation (3.52) is found to be

$$
\begin{aligned}
\frac{1}{r_0^2 x^2}\frac{d}{r_0 dx}\left(r_0^2 x^2\frac{dy}{r_0 dx}\right) &= -\frac{8\pi G}{3K\rho_0}y^{1/2} \\
\frac{1}{x^2}\frac{d}{dx}\left(x^2\frac{dy}{dx}\right) &= -\frac{8\pi G}{3K\rho_0}r_0^2 y^{1/2}\,. \qquad (3.53)
\end{aligned}
$$

Isolate the characteristic length, as the r.h.s. must be unitless,

$$
\begin{aligned}
r_0^2 &= \frac{3K\rho_0}{8\pi G} \\
r_0 &= \sqrt{\frac{3K}{8\pi G}}\rho_0^{1/2}\,. \qquad (3.54)
\end{aligned}
$$

To summarize: for a static, spherically symmetric mass of polytropic fluid with pressure $P = K\rho^3$ in hydrostatic equilibrium, the density and radius when expressed with dimensionless variables y and x,

$$\begin{aligned} \rho &= \rho_0 y^{1/2} \\ r &= \sqrt{\frac{3K}{8\pi G}}\rho_0^{1/2} x\,, \end{aligned} \tag{3.55}$$

gives the $n = 1/2$ Lane-Emden equation for the dimensionless variables,

$$\frac{1}{x^2}\frac{d}{dx}\left(x^2\frac{dy}{dx}\right) = -y^{1/2}\,. \tag{3.56}$$

This do not have an analytical solution, and must be solved numerically. The initial conditions are $y(0) = 1$, and $y'(0) = 0$. It solved on the following form using the Euler-Cromer method,

$$y'' = -\frac{2}{x}y' - y^{1/2} \tag{3.57}$$

$$y(x) \approx \cos\left(\frac{\pi}{2}\frac{x}{x_1}\right) \tag{3.58}$$

with the solution plotted in Figure 3.1 alongside the analytical approximation (3.58). The value $x_1 = 2.7526986755 \approx 2.75$ is determined as the value where the solution vanishes such that the cosine approximation vanishes also at x_1. The difference between the two is shown in Figure 3.2.

Using $x = r/r_0$ and $x_1 = R/r_0$, equation (3.58) allows equation (3.55) to be written as

$$\rho(r) \approx \rho_0\sqrt{\cos\left(\frac{\pi}{2}\frac{r}{R}\right)}\,, \tag{3.59}$$

where $R \equiv r_0 x_1$ is considered as the radial extent of the condensate component of the halo. Equation (3.59) is plotted in Figure 3.3 alongside the numerical solution, with the offset from the numerical solution shown in Figure 3.4. These also includes an ellipse in the strictly positive quadrant of the (r, ρ)-plane as comparison.

Using equations (3.55) and (3.56), the central density ρ_0 can be determined, following [94], through the average density $\bar{\rho}$

$$R = r_0 x_1 = \sqrt{\frac{3K}{8\pi G}}\rho_0^{1/2} x_1, \tag{3.60}$$

$$\begin{aligned} M &= \int_V d^3x\rho(r) = 4\pi\int_0^{x_1} r_0 dx\, r_0^2 x^2 \rho(x) = 4\pi r_0^3\rho_0\int_0^{x_1} dx\, x^2 y^{1/2} \\ &= 4\pi r_0^3\rho_0\int_0^{x_1} dx\,\left[-\frac{d}{dx}\left(x^2\frac{dy}{dx}\right)\right] = 4\pi r_0^3\rho_0\left[-x^2\frac{dy}{dx}\right]\Bigg|_{x=0}^{x=x_1} \\ \Rightarrow \bar{\rho} &\equiv \frac{M}{\frac{4}{3}\pi R^3} = \frac{4\pi r_0^3\rho_0}{\frac{4}{3}\pi r_0^3 x_1^3}\left[-x^2\frac{dy}{dx}\right]\Bigg|_{x=x_1} = -3\rho_0 x_1^{-3}x_1^2 y'(x_1) = -\frac{3\rho_0 y'(x_1)}{x_1} \end{aligned} \tag{3.61}$$

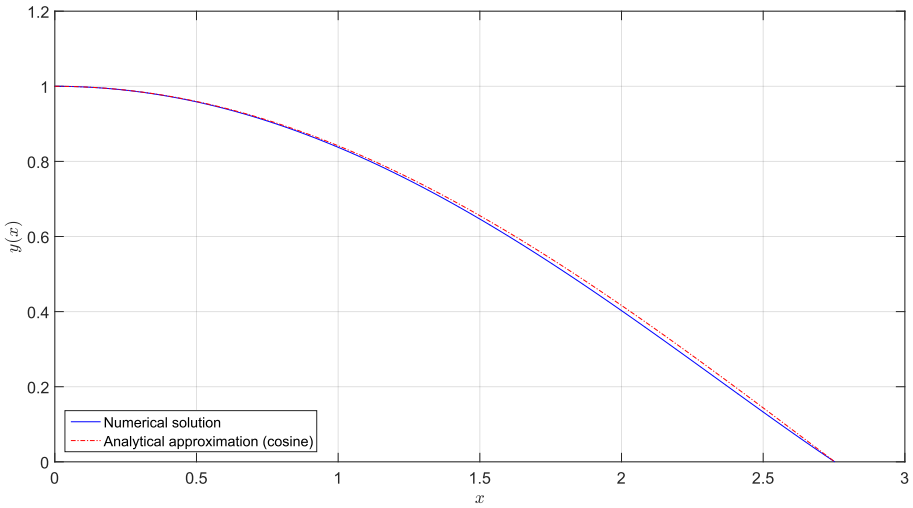

Figure 3.1: Numerical solution (blue solid line) to the $n = 1/2$ Lane-Emden equation. The red dotted line is the analytical approximation to the numerical solution, and is a cosine-function.

$$\Rightarrow \rho_0 = -\frac{\bar{\rho}}{3}\frac{x_1}{y'(x_1)} = -\frac{M}{4\pi R^3}\frac{x_1}{y'(x_1)}\,. \tag{3.62}$$

From the numerics it is found that $y'(x_1) = -0.499997663911809 \approx -1/2$, which give $y(x_1) \sim 10^{-14}$. Inserting this, $x_1 = R/r_0$ and also r_0 from (3.55) into (3.62) gives

$$\begin{aligned}
\rho_0 &= -\frac{M}{4\pi R^3}\frac{R/r_0}{-1/2} = \frac{M}{2\pi r_0 R^2} && (3.63)\\
&= \frac{M}{2\pi r_0^3 x_1^2} = \frac{M}{2\pi x_1^2}\left(\frac{8\pi G}{3K}\right)^{3/2}\rho_0^{-3/2}\\
\rho_0^5 &= \left(\frac{M}{2\pi x_1^2}\right)^2\left(\frac{8\pi G}{3K}\right)^3 && (3.64)\\
\Rightarrow \rho_0 &= \left(\frac{2^{13}\pi G^3}{\hbar^{18}x_1^4}\right)^{1/5} M^{2/5} m^{18/5}\Lambda^{6/5}\\
&= \left(\frac{2^{13}\pi G^3}{x_1^4\hbar^{18}}\right)^{1/5}(10^{12}M_\odot)^{2/5}\left(\frac{M}{10^{12}M_\odot}\right)^{2/5}(1\mathrm{eV}/c^2)^{18/5}\\
&\times\left(\frac{m}{1\mathrm{eV}/c^2}\right)^{18/5}(1\,\mathrm{meV})^{6/5}\left(\frac{\Lambda}{1\,\mathrm{meV}}\right)^{6/5}\\
&= \left(\frac{2^{13}\pi G^3(10^{12}M_\odot)^2(\mathrm{eV}/c^2)^{18}(\mathrm{meV})^6}{x_1^4\hbar^{18}}\right)^{1/5}
\end{aligned}$$

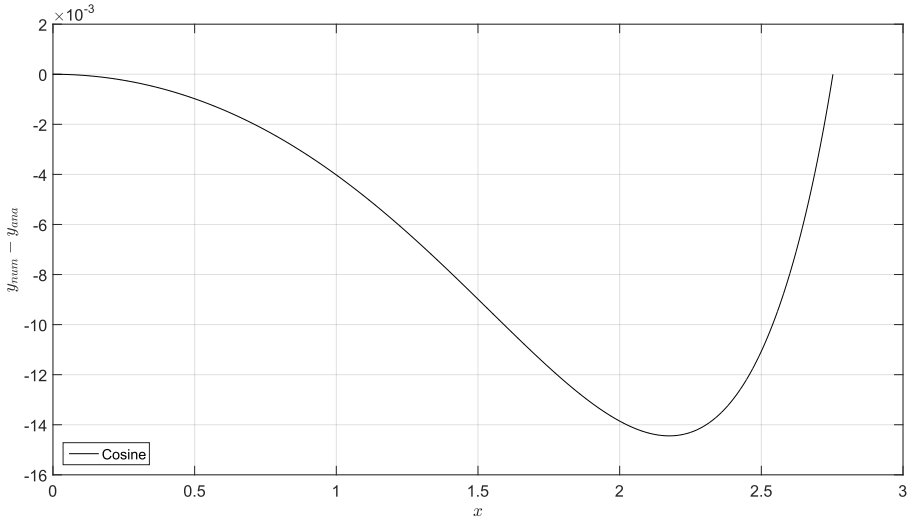

Figure 3.2: Difference between the analytical approximation and the numerical solution to the $n = 1/2$ Lane-Emden equation.

$$\times \left(\frac{M}{10^{12} M_\odot}\right)^{2/5} \left(\frac{m}{\mathrm{eV}/c^2}\right)^{18/5} \left(\frac{\Lambda}{\mathrm{meV}}\right)^{6/5}$$

$$\Rightarrow \rho_0(M,\, m,\, \Lambda) = \left(\frac{M}{10^{12} M_\odot}\right)^{2/5} \left(\frac{m}{\mathrm{eV}/c^2}\right)^{18/5} \left(\frac{\Lambda}{\mathrm{meV}}\right)^{6/5} \rho_c \,, \tag{3.65}$$

where $\rho_c = 0.6466008797382706 \times 10^{-24}\,\mathrm{g\,cm^{-3}} \approx 0.65 \times 10^{-24}\,\mathrm{g\,cm^{-3}}$ is the characteristic central density based on the normalization factors in the denominators. This is different from that in [1] only by a factor 0.65, and has repercussions for other derived quantities compared to [1]. The Milky Way halo mass is estimated [95] to be $\sim 10^{12}\, M_\odot$, and is hence used as a scale.

From the definition $R \equiv r_0 x_1$ one finds from (3.55) that the condensate radius when inserting the central density from (3.64),

$$\begin{aligned} R = r_0 x_1 &= \left(\frac{3K}{8\pi G}\right)^{1/2} x_1 \rho_0^{1/2} \\ &= \left(\frac{3K}{8\pi G}\right)^{1/2} x_1 \rho_0^{1/2} \\ &= x_1 \left(\frac{3K}{8\pi G}\right)^{1/2} \left(\frac{M}{2\pi x_1^2}\right)^{1/5} \left(\frac{8\pi G}{3K}\right)^{3/10} \\ &= x_1^{3/5} \left(\frac{3K}{8\pi G}\right)^{5/10} \left(\frac{M}{2\pi}\right)^{1/5} \left(\frac{3K}{8\pi G}\right)^{-3/10} \end{aligned}$$

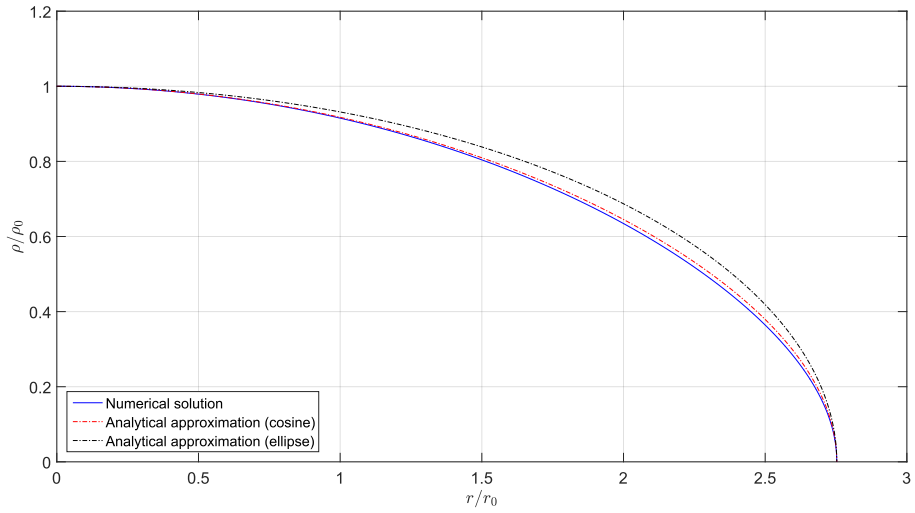

Figure 3.3: Numerically calculated density profile corresponding to the $n = 1/2$ Lane-Emden equation (blue solid line). The analytical approximations (red and black dotted lines) are the square root of a cosine and the $(x, y) = (+, +)$ quadrant ellipse respectively.

$$
\begin{aligned}
&= x_1^{3/5} \left(\frac{3K}{8\pi G}\right)^{1/5} \left(\frac{M}{2\pi}\right)^{1/5} \\
&= x_1^{3/5} \left(\frac{3K}{16\pi^2 G}\right)^{1/5} M^{1/5} \\
&= x_1^{3/5} \left(\frac{1}{64\pi^2 G}\frac{\hbar^6}{\Lambda^2 m^6}\right)^{1/5} M^{1/5} \\
&= \left[\frac{x_1^3 \hbar^6 (10^{12} M_\odot)}{64\pi^2 G (\mathrm{eV})^8\, 10^{-6}}\right]^{1/5} \left(\frac{M}{10^{12} M_\odot}\right)^{1/5} \left(\frac{m}{\mathrm{eV}/c^2}\right)^{-6/5} \left(\frac{\Lambda}{\mathrm{meV}}\right)^{-2/5} \\
\Rightarrow R(M,\, m,\, \Lambda) &= \left(\frac{M}{10^{12} M_\odot}\right)^{1/5} \left(\frac{m}{\mathrm{eV}/c^2}\right)^{-6/5} \left(\frac{\Lambda}{\mathrm{meV}}\right)^{-2/5} R_c. \qquad (3.66)
\end{aligned}
$$

Here $R_c \equiv 35.793009118045520$ kpc ≈ 35.793 kpc is the characteristic radius based on the normalization factors in the denominators. The numeric factor is about 0.8 times that in [1], which is due to the factor $\sqrt{0.65}$ that comes with the factor $\rho_0^{1/2}$ on the first line of the calculation of the radius. Finally, just as in [1], $m \sim \mathrm{eV}/c^2$ and $\Lambda \sim$ meV yields realistic condensate radius. With the fiducial values

$$m = 0.6\,\mathrm{eV}/c^2 \;\&\; \Lambda = 0.2\,\mathrm{meV}\,, \qquad (3.67)$$

which will be used from now to test the theory, the condensate radius for a halo of mass $M = 10^{12}\, M_\odot$ is about 125 kpc. This is less than the virial radius ~ 200 kpc of a halo with the same mass, as stated in [1].

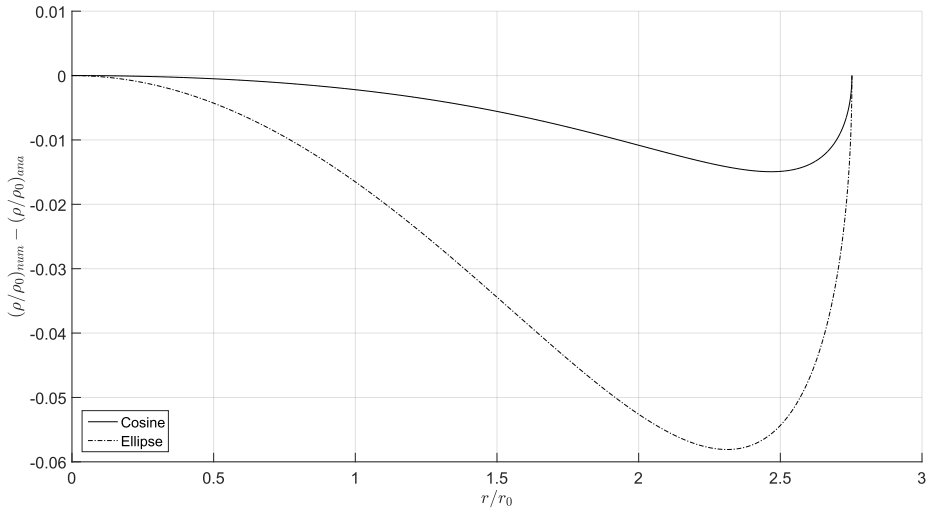

Figure 3.4: Logarithmic absolute difference between the analytical approximations and the density profile corresponding to numerical solution to the $n = 1/2$ Lane-Emden equation. The solid and dotted lines are the cosine and ellipse approximations respectively.

From the non-relativistic relation used earlier to express pressure in terms of density - see (3.37) - one finds that the density profile fixes $X(r)$,

$$
\begin{aligned}
\rho = mn = m\frac{dP}{dX} = mK\frac{d\rho^3}{dX} &= 3mK\rho^2\frac{d\rho}{dX} \\
dX &= 3mK\rho d\rho \\
X(r) = \frac{3mK}{2}\rho(r)^2 &= \frac{3mK}{2}\rho_0^2 y(r) \\
&= \left(\frac{3mK}{2}\right)^{5/5}\left(\frac{M}{2\pi x_1^2}\right)^{4/5}\left(\frac{8\pi G}{3K}\right)^{6/5} y(r) \\
&= \left(\frac{m^5 M^4 2^{18}\pi^6 G^6}{2^9\pi^4 x_1^8}\frac{1}{3K}\right)^{1/5} y(r) \\
&= \left(\frac{2^9\pi^2 G^6}{x_1^8}\, M^4\, m^5 \frac{12\Lambda^2 m^6}{3\hbar^6}\right)^{1/5} y(r) \\
&= \left(\frac{2^{11}\pi^2 G^6}{x_1^8\hbar^6} M^4 m^{11}\Lambda^2\right)^{1/5} y(r) \\
&= \left(\frac{2^{11}\pi^2 G^6 (10^{12} M_\odot)^4 (\mathrm{eV}/c^2)^{11}(\mathrm{meV})^2}{x_1^8\hbar^6}\right)^{1/5}
\end{aligned}
$$

$$\times \left(\frac{M}{10^{12}M_\odot}\right)^{4/5}\left(\frac{mc^2}{\text{eV}}\right)^{11/5}\left(\frac{\Lambda}{\text{meV}}\right)^{2/5} y(r)$$

$$X(r;\, M,\, m,\, \Lambda) = X_c\left(\frac{M}{10^{12}M_\odot}\right)^{4/5}\left(\frac{m}{\text{eV}/c^2}\right)^{11/5}\left(\frac{\Lambda}{\text{meV}}\right)^{2/5} y(r)\,. \tag{3.68}$$

Here $X_c = 48.14231453320181 \times 10^{-6}\,\text{eV}$ is the characteristic energy scale based on the normalizations in the denominators, and $y(r)$ is the solution for the $n = 1/2$ Lane-Emden equation - see (3.56).

As stated in (3.38),

$$X = \mu + \tilde{X} = \frac{3mK}{2}\rho^2 = \frac{\hbar^6}{8\Lambda^2 m^5}\rho^2\,, \tag{3.69}$$

and since only the condensate is considered in this case, the phonon excitations $\tilde{X}$ are set to be zero. This give a chemical potential that varies with radius. However, phonons will be considered at a later time, so the chemical potential may be fixed as $\mu \equiv \max\{X(r)\} = X(0)$:

$$\mu \equiv \frac{3mK}{2}\rho_0^2 = \frac{(\hbar c)^6}{8\Lambda^2 m^2 (mc^2)^3}\rho_0^2\,. \tag{3.70}$$

The factors of c are kept since the strong coupling scale (3.49) depends on the particle rest energy:

$$\begin{aligned}
\Lambda_s &= \left[\Lambda(mc^2)^{3/2}\mu^{3/2}\right]^{1/4} = \left[\Lambda(mc^2)^{3/2}\right]^{1/4}\left(\frac{3mK}{2}\rho_0^2\right)^{3/8} \\
&= \left[\Lambda(mc^2)^{3/2}\right]^{2/8}\left[\frac{(\hbar c)^6}{8\Lambda^2 m^2(mc^2)^3}\left(\frac{M}{10^{12}M_\odot}\right)^{4/5}\left(\frac{mc^2}{\text{eV}}\right)^{36/5}\left(\frac{\Lambda}{\text{meV}}\right)^{12/5}\rho_c^2\right]^{3/8} \\
&= \left[\left(\frac{(\hbar c)^{18}c^{12}\rho_c^6}{2^9\Lambda^4(mc^2)^{12}}\right)\left(\frac{M}{10^{12}M_\odot}\right)^{12/5}\left(\frac{mc^2}{\text{eV}}\right)^{108/5}\left(\frac{\Lambda}{\text{meV}}\right)^{36/5}\right]^{1/8} \\
\Lambda_s &= (\Lambda_s)_c\left(\frac{M}{10^{12}M_\odot}\right)^{3/10}\left(\frac{mc^2}{\text{eV}}\right)^{6/5}\left(\frac{\Lambda}{\text{meV}}\right)^{2/5}, \quad (\Lambda_s)_c \equiv \left[\frac{(\hbar c)^{18}c^{12}\rho_c^6}{2^9\times 10^{-12}(\text{eV})^{16}}\right]^{1/8}.
\end{aligned} \tag{3.71}$$

The subscript c means the usual, and the numerical value of the characteristic strong coupling energy scale is $(\Lambda_s)_c = 0.9889767067172432\,\text{meV} \sim \text{meV}$, and so is of same order as Λ.

Chapter 4

Including Baryons: Phonon Mediated Force

The structure of this chapter differs a little from [1].

The purpose of this chapter is to include baryons to the theory in order to obtain a suitable acceleration. This is done first in the zero-temperature limit, then non-zero temperatures are considered.

In both [1] and this thesis, the acceleration of baryons due to the superfluid phonons is found to depend on the radial gradient of the phonon field, hereby referred to as the "phonon gradient".

The phonon gradient depends on whether or not the scalar X is of positive or negative value. [1] explores both cases, and their stability is determined through an alternative Poisson's equation - the argument in the Laplacian operator depends on X, not on just Φ.

This is done differently in this thesis, mainly by not using an alternative Poisson's equation. The sign of X is first determined in order to obtain an acceleration comparable to that of MOND. Then the stability of the quadratic order Lagrangian for phonon perturbations is probed w.r.t the sign of X.

The baryon distribution is considered a static, spherically symmetric localized source for simplicity, which entails that the baryon distribution $M_{\mathrm{b}}(r)$ has uniform density ρ_{b} throughout the volume $V(r)$ that it spans.

Finally, the section in [1] regarding the sound speed is here moved to Chapter 5.

4.1 Zero-temperature analysis

The EFT Lagrangian in question is on the form $\mathcal{L} = \mathcal{L}_{T=0} + \mathcal{L}_{\mathrm{coupling}}$, where

$$\mathcal{L}_{T=0} = \frac{2\Lambda(2m)^{3/2}}{3\hbar^3} X\sqrt{|X|} \tag{4.1}$$

$$\mathcal{L}_{\mathrm{coupling}} = -\frac{\alpha\Lambda}{M_{\mathrm{Pl}}\hbar}\theta\rho_{\mathrm{b}}\,, \tag{4.2}$$

of which (4.2) is of interest as it considers interactions between superfluid phonons, described by θ, and the density distribution of baryonic matter, described by ρ_{b}. As stated by [1], the interaction (4.2) represents the breaking of the global $U(1)$ symmetry of the condensed state due to the presence of the baryons.

4.1.1 Determining the acceleration of baryons

An acceleration on the baryon distribution due to the superfluid phonons can be determined by treating the EFT Lagrangian $\mathcal{L} = \mathcal{L}_{T=0} + \mathcal{L}_{\mathrm{coupling}}$ in the classical sense, $\mathcal{L} = \mathcal{T} - \mathcal{V}$, which yields a "force density"

$$\vec{\mathcal{F}} = -\nabla\mathcal{V}\,. \tag{4.3}$$

By identifying $\mathcal{V} = -\mathcal{L}_{\mathrm{coupling}}$ we find

$$\begin{aligned}\vec{\mathcal{F}} &= \alpha\frac{\Lambda}{M_{\mathrm{Pl}}\hbar}\nabla(\theta\rho_{\mathrm{b}}) \\ &= \alpha\frac{\Lambda}{M_{\mathrm{Pl}}\hbar}(\nabla\theta)\rho_{\mathrm{b}}\,.\end{aligned} \tag{4.4}$$

As we are also using the static spherically-symmetric approximation $\theta = \theta(r) = \mu t + \phi(r)$, eq (4.4) is

$$\begin{aligned}\vec{\mathcal{F}} &= \alpha\frac{\Lambda}{M_{\mathrm{Pl}}\hbar}(\nabla\phi)\rho_{\mathrm{b}} \\ &= \alpha\frac{\Lambda}{M_{\mathrm{Pl}}\hbar}(\partial_r\phi)\rho_{\mathrm{b}}\vec{e}_r\,.\end{aligned} \tag{4.5}$$

The scalar force $\mathcal{F} = ||\vec{\mathcal{F}}||$ is then

$$\mathcal{F}_\phi = \rho_{\mathrm{b}}a_\phi\,, \tag{4.6}$$

where the scalar acceleration is identified as

$$\begin{aligned}a_\phi &= \frac{\alpha\Lambda}{M_{\mathrm{Pl}}\hbar}||\nabla\phi|| \\ &= \frac{\alpha\Lambda}{M_{\mathrm{Pl}}\hbar}(\partial_r\phi)\,.\end{aligned} \tag{4.7}$$

As per eq (4.7) we need to find an expression for $(\partial_r\phi)$, the phonon gradient, to determine the acceleration. Recall the zero-temperature phonon Lagrangian is on the form $\mathcal{L} = \mathcal{L}_0 + \mathcal{L}_{\mathrm{coupling}}$,

$$\mathcal{L} = \frac{2\Lambda(2m)^{3/2}}{3\hbar^3}X\sqrt{|X|} - \alpha\frac{\Lambda}{M_{\mathrm{Pl}}}\frac{\theta}{\hbar}\rho_b. \tag{4.8}$$

In the static, spherically symmetric approximation, $\theta = \mu t + \phi(r)$, the equation of motion of the phonon field is found through the Euler-Lagrange equation,

$$\frac{\partial\mathcal{L}}{\partial\phi} - \nabla\cdot\frac{\partial\mathcal{L}}{\partial(\nabla\phi)} = 0. \tag{4.9}$$

The scalar X is

$$\begin{aligned} X &= \dot{\theta} - m\Phi - \frac{(\nabla\theta)^2}{2m} \\ &= \mu - m\Phi - \frac{(\nabla\phi)^2}{2m} \\ &= \hat{\mu} - \frac{(\nabla\phi)^2}{2m}\,,\ \hat{\mu} = \mu - m\Phi\,. \end{aligned} \tag{4.10}$$

With this, the terms of (4.9) are,

$$\begin{aligned} \frac{\partial\mathcal{L}}{\partial\phi} &= \frac{2\Lambda(2m)^{3/2}}{3\hbar^3}\frac{\partial X\sqrt{|X|}}{\partial\phi} - \alpha\frac{\Lambda}{M_{\rm Pl}\hbar}\frac{\partial\theta}{\partial\phi}\rho_b(r) \\ &= -\alpha\frac{\Lambda}{M_{\rm Pl}\hbar}\rho_b \end{aligned} \tag{4.11}$$

$$\begin{aligned} \nabla\cdot\frac{\partial\mathcal{L}}{\partial(\nabla\phi)} &= \nabla\cdot\left(\frac{2\Lambda(2m)^{3/2}}{3\hbar^3}\frac{\partial X\sqrt{|X|}}{\partial(\nabla\phi)} - \alpha\frac{\Lambda}{M_{\rm Pl}\hbar}\frac{\partial\theta}{\partial(\nabla\phi)}\rho_b(r)\right) \\ &= \frac{2\Lambda(2m)^{3/2}}{3\hbar^3}\nabla\cdot\left(\frac{\partial\sqrt{|X|^3}}{\partial(\nabla\phi)}\right) \\ &= \frac{2\Lambda(2m)^{3/2}}{3\hbar^3}\nabla\cdot\left(\frac{\partial\sqrt{|X|^3}}{\partial X}\frac{\partial X}{\partial(\nabla\phi)}\right) \\ &= -\frac{\Lambda(2m)^{3/2}}{m\hbar^3}\nabla\cdot\left(\sqrt{|X|}\nabla\phi\right)\,. \end{aligned} \tag{4.12}$$

The identity $|X|^2 = X^2$ was used, and in the last equality

$$\begin{aligned} \frac{\partial\sqrt{|X|^3}}{\partial X} &= \frac{\partial\sqrt{|X|^3}}{\partial|X|}\frac{\partial|X|}{\partial X} = \frac{3|X|^{1/2}}{2}\frac{X}{|X|} = \frac{3X}{2|X|^{1/2}} \\ &= \frac{3X^{1/2}}{2|X|^{1/2}}X^{1/2} = \frac{3}{2}\mathrm{sgn}(X)^{1/2}X^{1/2} = \frac{3|X|^{1/2}}{2}\,. \end{aligned}$$

The equation of motion is then

$$\begin{aligned} \frac{2\Lambda(2m)^{1/2}}{\hbar^3}\nabla\cdot\left(\sqrt{|X|}\nabla\phi\right) &= \alpha\frac{\Lambda}{M_{\rm Pl}\hbar}\rho_b(r) \\ \nabla\cdot\left(\sqrt{2m|X|}\nabla\phi\right) &= \frac{\alpha\hbar^2}{2M_{\rm Pl}}\rho_b(r)\,. \end{aligned} \tag{4.13}$$

This is integrated in spherical coordinates, and as this is in a spherically symmetric approximation, then

$$\frac{1}{r^2}\frac{d}{dr}\left(r^2\sqrt{2m|X|}\nabla\phi\right) = \alpha\frac{\hbar^2}{2M_{\rm Pl}}\rho_b(r)$$

$$\frac{d}{dr}\left(r^2\sqrt{2m|X|}\nabla\phi\right) = \alpha\frac{\hbar^2}{8\pi M_{\rm Pl}}4\pi r^2\rho_b(r)$$
$$\sqrt{2m|X|}\nabla\phi = \alpha\frac{\hbar^2}{8\pi M_{\rm Pl}}\frac{M_b(r)}{r^2} \equiv \kappa(r)\,. \tag{4.14}$$

This implies a second-order polynomial for $(\nabla\phi)^2$. First insert for X:

$$\begin{aligned} X &= \hat{\mu}(r) - \frac{(\nabla\phi)^2}{2m} \\ \Rightarrow 2m|X| &= 2m\,\mathrm{sgn}(X)X \\ &= \mathrm{sgn}(X)\left[2m\hat{\mu} - (\nabla\phi)^2\right]\,. \end{aligned}$$

Let $z = (\nabla\phi)^2 = ||\nabla\phi||^2 = (\nabla\phi)\cdot(\nabla\phi) = (\partial_r\phi)^2$, and take both sides of equation (4.14) to the second power:

$$\begin{aligned} 2m|X|z &= \kappa(r)^2 \\ \mathrm{sgn}(X)\left[2m\hat{\mu} - z\right]z &= \kappa^2 \\ z^2 - 2m\hat{\mu}z + \mathrm{sgn}(X)\kappa^2 &= 0 \\ \Rightarrow z &= \frac{2m\hat{\mu} \pm \sqrt{4m^2\hat{\mu}^2 - 4\mathrm{sgn}(X)\kappa^2}}{2} \\ (\partial_r\phi)^2 &= m\hat{\mu} \pm \sqrt{m^2\hat{\mu}^2 - \mathrm{sgn}(X)\kappa^2} \end{aligned} \tag{4.15}$$

With the phonon gradient (4.15), the acceleration is

$$a_\phi = \frac{\alpha\Lambda}{M_{\rm Pl}\hbar}\left[m\hat{\mu} \pm \sqrt{m^2\hat{\mu}^2 - \mathrm{sgn}(X)\kappa^2}\right]^{1/2}\,.$$

The function $\kappa \propto r^{-2}$, so $a_\phi \propto r^{-1}$ is recovered if there exists a limit such that $(\partial_r\phi)^2 \simeq \sqrt{\kappa^2}$; thus $a_\phi \propto r^{-1}$ and is comparable to MONDian acceleration. This is achievable only in the case $X < 0$, for $\kappa^2 \gg m^2\hat{\mu}^2$, hence $(\partial_r\phi) \simeq \sqrt{\kappa}$ and the acceleration

$$\begin{aligned} a_\phi &= \frac{\alpha\Lambda}{M_{\rm Pl}\hbar}(\partial_r\phi) \\ &\simeq \frac{\alpha\Lambda}{M_{\rm Pl}\hbar}\sqrt{\kappa} \\ &= \frac{\alpha\Lambda}{M_{\rm Pl}\hbar}\sqrt{\frac{\alpha\hbar^2}{8\pi M_{\rm Pl}}\frac{M_b(r)}{r^2}} \\ &= \sqrt{\frac{\alpha^2\Lambda^2}{M_{\rm Pl}^2\hbar^2}\frac{\alpha\hbar^2}{8\pi G_{\rm N}M_{\rm Pl}}\frac{G_{\rm N}M_b(r)}{r^2}} \\ &= \sqrt{\frac{\alpha^3\Lambda^2}{(\hbar c)M_{\rm Pl}}a_{\rm N}}\,. \end{aligned} \tag{4.16}$$

By comparing this to the MONDian acceleration

$$a_\phi = \sqrt{\frac{\alpha^3\Lambda^2}{(\hbar c)M_{\rm Pl}}a_{\rm N}}\,, \quad a_{\rm MOND} = \sqrt{a_0 a_{\rm N}}\,, \tag{4.17}$$

the coupling parameter α can be fixed to the scale Λ,

$$\begin{aligned}
\frac{\alpha^3\Lambda^2}{(\hbar c)M_{\rm Pl}} &= a_0 && (4.18)\\
\alpha^3\Lambda^2 &= a_0(\hbar c)M_{\rm Pl} \\
\alpha &= [a_0(\hbar c)M_{\rm Pl}]^{1/3}\Lambda^{-2/3} \\
&= \left[\frac{a_0(\hbar c)M_{\rm Pl}}{(1\,\text{meV})^2}\right]^{1/3}\left(\frac{\Lambda}{1\,\text{meV}}\right)^{-2/3} && (4.19)\\
\alpha &= b_0\left(\frac{\Lambda}{1\,\text{meV}}\right)^{-2/3}\,,
\end{aligned}$$

where $b_0 = 0.811717960744417 \approx 0.82$, with $a_0 = 10^{-10}$ ms^{-2} as in [1]. The fiducial value $\Lambda = 0.2$ meV yields $\alpha \approx 2.5$ in galaxies.

4.1.2 Stability of phonon perturbations

This was only briefly mentioned in [1] in order to explain the origin of an instability in their alternate Poisson's equation. In this paper, the quadratic order Lagrangian for phonon perturbations is derived. It is found to depend on the sign of the scalar $\bar{X}$, which corresponds to the scalar X in the absence of phonon perturbations. As in [1], the consequences of the dependence on sgn($\bar{X}$) are discussed.

When checking the behaviour of quadratic order phonon perturbations $\varphi(r,\theta,\chi) = \phi(r,\theta,\chi) - \bar{\phi}(r)$, in which case only (4.1) is of interest as it is the only contributor. Denote the prefactor of (4.1) by C, then

$$\mathcal{L}_{T=0} = CXf(X) \tag{4.20}$$

where $f(X) = \sqrt{|X|}$, and

$$X = \hat{\mu} + \dot{\phi} - \frac{(\nabla\phi)^2}{2m}\,. \tag{4.21}$$

Insert for ϕ the perturbation $\phi(\vec{r},t) = \varphi(\vec{r},t) + \bar{\phi}(r)$,

$$\begin{aligned}
X &= \hat{\mu} + \dot{\varphi} - \frac{[\nabla(\varphi+\bar{\phi})]^2}{2m} \\
&= \hat{\mu} + \dot{\varphi} - \frac{(\nabla\varphi)^2 + (\nabla\bar{\phi})^2 + 2(\nabla\varphi)\cdot(\nabla\bar{\phi})}{2m} \\
&= \hat{\mu} - \frac{(\nabla\bar{\phi})^2}{2m} + \dot{\varphi} - \frac{(\nabla\varphi)^2}{2m} - \frac{2(\nabla\varphi)\cdot(\nabla\bar{\phi})}{2m} \\
&= \bar{X}(r) + \gamma(\vec{r},t)\,,
\end{aligned} \tag{4.22}$$

where $\bar{X}$ is identified as the phonon energy in the absence of perturbations and γ the perturbed phonon energy. Eq (4.22) may be inserted into eq (4.20), and $f(X) \to f(\gamma) = \sqrt{|\bar{X}+\gamma|}$ may be expanded for small γ, in the same manner as eq (3.39), though only terms up to $\mathcal{O}(\gamma^2)$ are needed, yielding the same result,

$$f(\gamma) = |\bar{X}|^{1/2} + \frac{\operatorname{sgn}(\bar{X})}{2|\bar{X}|^{1/2}}\gamma - \frac{1}{8|\bar{X}|^{3/2}}\gamma^2 + \mathcal{O}(\gamma^3)\,. \tag{4.23}$$

The Lagrangian is therefore

$$\begin{aligned}\mathcal{L}_{T=0} &= C(\bar{X}+\gamma)\left[|\bar{X}|^{1/2} + \frac{\operatorname{sgn}(\bar{X})}{2|\bar{X}|^{1/2}}\gamma - \frac{1}{8|\bar{X}|^{3/2}}\gamma^2 + \mathcal{O}(\gamma^3)\right] \\ &= C\left[(\bar{X}+\gamma)|\bar{X}|^{1/2} + \frac{\operatorname{sgn}(\bar{X})}{2|\bar{X}|^{1/2}}(\bar{X}+\gamma)\gamma - \frac{1}{8|\bar{X}|^{3/2}}(\bar{X}+\gamma)\gamma^2 + (\bar{X}+\gamma)\mathcal{O}(\gamma^3)\right].\end{aligned} \tag{4.24}$$

We only keep terms proportional to γ and γ^2, as the terms of γ are $\dot{\varphi}$, $(\nabla\varphi)^2/2m$ and $2(\nabla\varphi)\cdot(\nabla\bar{\phi})/2m$. Thus

$$\begin{aligned}\mathcal{L}_{T=0} &\supset C\left[|\bar{X}|^{1/2}\gamma + \frac{\operatorname{sgn}(\bar{X})}{2|\bar{X}|^{1/2}}\bar{X}\gamma + \frac{\operatorname{sgn}(\bar{X})}{2|\bar{X}|^{1/2}}\gamma^2 - \frac{1}{8|\bar{X}|^{3/2}}\bar{X}\gamma^2\right] \\ &= C\left\{\left[|\bar{X}|^{1/2} + \frac{\operatorname{sgn}(\bar{X})}{2|\bar{X}|^{1/2}}\bar{X}\right]\left[\dot{\varphi} - \frac{(\nabla\varphi)^2}{2m} - \frac{2(\nabla\varphi)\cdot(\nabla\bar{\phi})}{2m}\right]\right. \\ &\quad \left. + \left[\frac{\operatorname{sgn}(\bar{X})}{2|\bar{X}|^{1/2}} - \frac{1}{8|\bar{X}|^{3/2}}\bar{X}\right]\left[\dot{\varphi} - \frac{(\nabla\varphi)^2}{2m} - \frac{2(\nabla\varphi)\cdot(\nabla\bar{\phi})}{2m}\right]^2\right\}.\end{aligned}$$

The prefactors may be expressed as

$$\begin{aligned}|\bar{X}|^{1/2} + \frac{\operatorname{sgn}(\bar{X})}{2|\bar{X}|^{1/2}}\bar{X} &= \frac{|\bar{X}|}{|\bar{X}|^{1/2}} + \frac{\operatorname{sgn}(\bar{X})}{2|\bar{X}|^{1/2}}\bar{X} \\ &= \frac{\operatorname{sgn}(\bar{X})}{|\bar{X}|^{1/2}}\bar{X} + \frac{\operatorname{sgn}(\bar{X})}{2|\bar{X}|^{1/2}}\bar{X} \\ &= \frac{3\operatorname{sgn}(\bar{X})}{2|\bar{X}|^{1/2}}\bar{X} \\ &= q\bar{X}, \\ \frac{\operatorname{sgn}(\bar{X})}{2|\bar{X}|^{1/2}} - \frac{1}{8|\bar{X}|^{3/2}}\bar{X} &= \frac{\operatorname{sgn}(\bar{X})}{2|\bar{X}|^{1/2}} - \frac{1}{8|\bar{X}|^{1/2}}\frac{\bar{X}}{|\bar{X}|} \\ &= \frac{\operatorname{sgn}(\bar{X})}{8|\bar{X}|^{1/2}} - \frac{\operatorname{sgn}(\bar{X})}{8|\bar{X}|^{1/2}} \\ &= \frac{3\operatorname{sgn}(\bar{X})}{8|\bar{X}|^{1/2}} \\ &= \frac{q}{4}\,.\end{aligned}$$

As for the perturbations, in the first term we only need to keep $-(\nabla\varphi)^2/2m$. The second when written out as terms on the form

$$(a + b^2 + cd)^2 = a^2 + 2ab^2 + 2acd + b^4 + 2b^2cd + (cd)^2\,,$$

of which the terms contributing to $\mathcal{L}_{\text{quad}}$ are

$$\begin{aligned} a^2 &= \dot{\varphi}^2 \\ 2acd &= -2\dot{\varphi}\frac{2(\nabla\varphi)\cdot(\nabla\bar{\phi})}{2m} \\ (cd)^2 &= \left[\frac{2(\nabla\varphi)\cdot(\nabla\bar{\phi})}{2m}\right]^2 . \end{aligned}$$

When inserted this yields

$$\mathcal{L}_{\text{quad}} = Cq\left\{-\bar{X}\frac{(\nabla\varphi)^2}{2m} + \frac{1}{4}\left[\dot{\varphi}^2 - 2\dot{\varphi}\frac{2(\nabla\varphi)\cdot(\nabla\bar{\phi})}{2m} + \left(\frac{2(\nabla\varphi)\cdot(\nabla\bar{\phi})}{2m}\right)^2\right]\right\}. \quad (4.25)$$

The gradient of any differentiable function f is in spherical coordinates (r, θ, χ) given as

$$\nabla f = \frac{\partial f}{\partial r}\hat{e}_r + \frac{1}{r}\frac{\partial f}{\partial\theta}\hat{e}_\theta + \frac{1}{r\sin\theta}\frac{\partial f}{\partial\chi}\hat{e}_\chi\,,$$

so the inner product of any two gradients ∇f and ∇g is

$$(\nabla f)\cdot(\nabla g) = \frac{\partial f}{\partial r}\frac{\partial g}{\partial r} + \frac{1}{r^2}\frac{\partial f}{\partial\theta}\frac{\partial g}{\partial\theta} + \frac{1}{r^2\sin^2\theta}\frac{\partial f}{\partial\chi}\frac{\partial g}{\partial\chi}\,.$$

Let $f = \varphi$, and $g = \bar{\phi}$, and denote the radial derivative with just ∂_r, then

$$\begin{aligned} (\nabla\varphi)\cdot(\nabla\bar{\phi}) &= \frac{\partial\varphi}{\partial r}\frac{\partial\bar{\phi}}{\partial r} \\ &= (\partial_r\varphi)(\partial_r\bar{\phi})\,, \end{aligned} \quad (4.26)$$

since $\bar{\phi}$ is spherically-symmetric. As for the term in (4.25) proportional to $(\nabla\varphi)^2 = (\nabla\varphi)\cdot(\nabla\varphi)$,

$$\begin{aligned} (\nabla\varphi)\cdot(\nabla\varphi) &= \left(\frac{\partial\varphi}{\partial r}\right)^2 + \frac{1}{r^2}\left(\frac{\partial\varphi}{\partial\theta}\right)^2 + \frac{1}{r^2\sin^2\theta}\left(\frac{\partial\varphi}{\partial\chi}\right)^2 \\ &= (\partial_r\varphi)^2 + \frac{1}{r^2}(\partial_\Omega\varphi)^2 \end{aligned} \quad (4.27)$$

where ∂_Ω denotes the gradient along the angular directions:

$$\begin{aligned} (\partial_\Omega\varphi)^2 &= (\partial_\Omega\varphi)\cdot(\partial_\Omega\varphi) \\ &= \left(\frac{\partial\varphi}{\partial\theta}\right)^2 + \frac{1}{\sin^2\theta}\left(\frac{\partial\varphi}{\partial\chi}\right)^2 . \end{aligned}$$

Thus (4.25) is

$$\begin{aligned}\mathcal{L}_{\text{quad}} &= \frac{Cq}{4}\left\{-\frac{2\bar{X}}{m}\left[(\partial_r\varphi)^2+\frac{1}{r^2}(\partial_\Omega\varphi)^2\right]+\dot{\varphi}^2-2\frac{(\partial_r\bar{\phi})}{m}\dot{\varphi}(\partial_r\varphi)+\frac{(\partial_r\varphi)^2(\partial_r\bar{\phi})^2}{m^2}\right\}\\ &= \frac{Cq}{4}\left\{\dot{\varphi}^2-2\frac{(\partial_r\bar{\phi})}{m}\dot{\varphi}(\partial_r\varphi)-\frac{2(\partial_r\varphi)^2}{m}\left[\bar{X}-\frac{(\partial_r\bar{\phi})^2}{2m}\right]-\frac{2\bar{X}}{mr^2}(\partial_\Omega\varphi)^2\right\}\\ \mathcal{L}_{\text{quad}} &= \operatorname{sgn}(\bar{X})\frac{\Lambda(2m)^{3/2}}{4\hbar^3|\bar{X}|^{1/2}}\left\{\dot{\varphi}^2-2\frac{(\partial_r\bar{\phi})}{m}\dot{\varphi}(\partial_r\varphi)-\frac{2(\partial_r\varphi)^2}{m}\left[\bar{X}-\frac{(\partial_r\bar{\phi})^2}{2m^2}\right]-\frac{2\bar{X}}{mr^2}(\partial_\Omega\varphi)^2\right\}.\end{aligned} \tag{4.28}$$

At first glance, positive $\bar{X}$ yields correct sign for the kinetic term $\propto \dot{\varphi}^2$. However, for MONDian behaviour to occur, $\kappa^2 \gg m^2\hat{\mu}^2$ which for positive $\bar{X}$ has complex phonon gradient - see (4.15). This is not the case for negative $\bar{X}$ - as shown in (4.16) - though the kinetic term has the wrong sign, which indicates the presence of an instability[1].

4.2 Finite-temperature effects

The only difference between [1] and this thesis is the inclusion of more calculations, which are more accurate.

At non-zero temperatures the Lagrangian is built from the the three scalars X, B, and Y described in Chapter 3. The analysis is done in the normal component's rest frame, $\vec{v} = \vec{0}$.

[1] provides an example on how to fix the faulty sign of the kinetic term of (4.28) by supplementing the zero-temperature Lagrangian (4.1) with

$$\Delta\mathcal{L} = M^2Y^2 = M^2(\hat{\mu}+\dot{\phi})^2\,. \tag{4.29}$$

This contributes to the quadratic Lagrangian an amount $M^2\dot{\varphi}^2$, and thus fixes the sign if

$$\begin{aligned}M^2\dot{\varphi}^2 &> \frac{\Lambda(2m)^{3/2}}{4\hbar^3|\bar{X}|^{1/2}}\dot{\varphi}^2\\ M^2 &> \frac{\Lambda(2m)^{3/2}}{4\hbar^3|\bar{X}|^{1/2}} = \frac{\Lambda m^2}{\hbar^3\sqrt{2m|\bar{X}|}}.\end{aligned}$$

If MONDian behaviour is to be reproduced, eq. (4.15) for $\bar{X} > 0$ must be inserted into $2m\bar{X} = 2m\hat{\mu} - (\nabla\bar{\phi})^2$, and this must be taken in the limit $\kappa(r) \gg m\hat{\mu}$, in which case

$$|2m\bar{X}| = |2m\hat{\mu} - (\nabla\bar{\phi})^2| = |2m\hat{\mu} - m\hat{\mu} \pm \sqrt{(m\hat{\mu})^2+\kappa(r)^2}| \approx |\pm\kappa(r)| = \kappa(r)\,.$$

[1] As an example, consider the state of a system to be an unstable equilibrium; if the state is perturbed, it will not return to its original configuration. In other words: if a needle is balanced on its tip on a surface in a uniform gravitational field, giving it a small push in any direction parallel to the surface will make the needle fall over until it lies parallel to the surface.

The constraint on M becomes

$$\begin{aligned}
M^2 &> \frac{(1\,\mathrm{meV})}{\hbar^3|2m\bar{X}|^{1/2}}\left(\frac{\Lambda}{1\,\mathrm{meV}}\right)m^2 \\
&\gtrsim \frac{(1\,\mathrm{meV})}{\hbar^3\kappa(r)^{1/2}}\left(\frac{\Lambda}{1\,\mathrm{meV}}\right)m^2 \\
&\gtrsim \frac{(1\,\mathrm{meV})}{\hbar^3}\sqrt{\frac{8\pi M_{\mathrm{Pl}}}{\alpha\hbar^2}}M_{\mathrm{b}}^{-1/2}\left(\frac{\Lambda}{1\,\mathrm{meV}}\right)rm^2 \\
&\gtrsim \frac{(1\,\mathrm{meV})(10\,\mathrm{kpc})(10^{11}\,M_\odot)^{-1/2}}{\hbar^3}\sqrt{\frac{8\pi M_{\mathrm{Pl}}}{\alpha\hbar^2}}\left(\frac{M_{\mathrm{b}}}{10^{11}\,M_\odot}\right)^{-1/2}\left(\frac{\Lambda}{1\,\mathrm{meV}}\right)\left(\frac{r}{10\,\mathrm{kpc}}\right)m^2 \\
&\gtrsim \frac{(1\,\mathrm{meV})(10\,\mathrm{kpc})}{\hbar^4}\sqrt{\frac{8\pi M_{\mathrm{Pl}}}{10^{11}\,\alpha M_\odot}}\left(\frac{M_{\mathrm{b}}}{10^{11}\,M_\odot}\right)^{-1/2}\left(\frac{\Lambda}{1\,\mathrm{meV}}\right)\left(\frac{r}{10\,\mathrm{kpc}}\right)m^2 \\
&\gtrsim \frac{(1\,\mathrm{meV})(10\,\mathrm{kpc})}{\hbar^4}\sqrt{\frac{8\pi M_{\mathrm{Pl}}}{10^{11}M_\odot b_0}}\left(\frac{M_{\mathrm{b}}}{10^{11}\,M_\odot}\right)^{-1/2}\left(\frac{\Lambda}{1\,\mathrm{meV}}\right)^{4/3}\left(\frac{r}{10\,\mathrm{kpc}}\right)m^2 \\
&\gtrsim \frac{1.7856\times10^{55}}{\mathrm{kg\,J\,m^3}}\left(\frac{10^{11}\,M_\odot}{M_{\mathrm{b}}}\right)^{1/4}\left(\frac{\Lambda}{1\,\mathrm{meV}}\right)^{2/3}\left(\frac{r}{10\,\mathrm{kpc}}\right)^{1/2}m \\
&\gtrsim \left[3.1416\times10^{-20}\,\mathrm{J\,m^3}\right]^{-1}\left(\frac{10^{11}\,M_\odot}{M_{\mathrm{b}}}\right)^{1/4}\left(\frac{\Lambda}{1\,\mathrm{meV}}\right)^{2/3}\left(\frac{r}{10\,\mathrm{kpc}}\right)^{1/2}\left(\frac{m}{1\,\mathrm{eV}/c^2}\right) \\
M &\gtrsim \left(\frac{10^{11}\,M_\odot}{M_{\mathrm{b}}}\right)^{1/4}\left(\frac{\Lambda}{1\,\mathrm{meV}}\right)^{2/3}\left(\frac{r}{10\,\mathrm{kpc}}\right)^{1/2}\left(\frac{m}{1\,\mathrm{eV}/c^2}\right)\frac{0.443}{\mathrm{eV}^{1/2}\,\mathrm{m}^{3/2}}\,,
\end{aligned} \tag{4.30}$$

of which the numerical factor is about the same as in [1]. However the particle mass is scaled as shown, and the dependence of α on Λ is implemented; the latter changing $M \sim \Lambda^{1/2}$ (in [1]) to $M \sim \Lambda^{2/3}$ here.

By supplementing (4.1) with (4.30), the condensate pressure (3.35) also get a contribution $\Delta P = M^2\mu^2$, which would alter the condensate equation of state (3.37). The scaling of the baryonic mass to the estimated [96] total baryonic mass $\sim 10^{11}\,M_\odot$, will also be a fiducial value $M_{\mathrm{b}} = 3\times10^{11}\,M_\odot$.

4.2.1 Toy theory

As is the case in this thesis, the finite-temperature theory that [1] actually goes for is the *ad hoc* addition of $-\beta Y$ into the absolute-valued root expression in the zero-temperature Lagrangian,

$$\begin{aligned}
\mathcal{L}_{T=0} \to \mathcal{L}_{T\neq0} &= \frac{2\Lambda(2m)^{3/2}}{3\hbar^3}X\sqrt{|X-\beta Y|} \\
&= \frac{2\Lambda(2m)^{3/2}}{3\hbar^3}X\sqrt{|X-\beta(\hat{\mu}+\dot{\phi})|}\,,
\end{aligned} \tag{4.31}$$

where this is also taken in the normal fluid rest frame. The dimensionless parameter β is taken to vary with T/T_c in some way. It is determined later in this Chapter that

$$\beta \geq \frac{3}{2} \tag{4.32}$$

reproduces MONDian behaviour with stable perturbations, in which case the absolute value-function has a negative argument. As such, the case (4.32) will be considered throughout this thesis, as with [1], and the fiducial value $\beta = 2$ is used for calculations.

Now consider the dark matter density profile in the absence of baryons. Setting phonons and gravitational potential to zero, $X \to \mu$ and $Y \to \mu$, the condensate pressure is

$$\begin{aligned} P(\mu, T) &= \frac{2\Lambda(2m)^{3/2}}{3\hbar^3}\mu\sqrt{|\mu - \beta\mu|} \\ &= \frac{2\Lambda(2m)^{3/2}}{3\hbar^3}\mu^{3/2}\sqrt{|1-\beta|} \\ &= \frac{2\Lambda\sqrt{\beta-1}}{3\hbar^3}(2m\mu)^{3/2}\,, \end{aligned} \tag{4.33}$$

and it is exactly the same tot he zero-temperature case, except for the replacement $\Lambda \to \Lambda\sqrt{\beta-1}$. This is carried through the rest of the zero-temperature analysis - for instance, the halo radius (3.66) is now

$$R(T) = \left(\frac{M_{\rm DM}}{10^{12}\,M_\odot}\right)^{1/5}\left(\frac{m}{1\,{\rm eV}/c^2}\right)^{-6/5}\left(\frac{\Lambda}{1\,{\rm meV}}\right)^{-2/5}\frac{R_c}{(\beta-1)^{1/5}}. \tag{4.34}$$

Note that the choice $\beta = 2$ leaves the pressure and halo radius unchanged w.r.t. the zero-temperature scenario.

Phonon equation of motion

The arguments in absolute value-functions are negative, so the full EFT Lagrangian is then

$$\mathcal{L} = \frac{2\Lambda(2m)^{3/2}}{3\hbar^3}X\sqrt{\beta(\dot\theta - m\Phi) - X} - \frac{\alpha\Lambda}{M_{\rm Pl}\hbar}\theta\rho_{\rm b}\,. \tag{4.35}$$

As in the zero-temperature analysis, the equation of motion is found under the static spherically-symmetric approximation $\theta = \mu t + \phi(r)$ for $X = \dot\theta - m\Phi - (\nabla\theta)^2/2m$ by solving the Euler-Lagrange equation,

$$\frac{\partial\mathcal{L}}{\partial\phi} - \nabla\cdot\frac{\partial\mathcal{L}}{\partial(\nabla\phi)} = 0 \tag{4.36}$$

$$\begin{aligned} \frac{\partial\mathcal{L}}{\partial\phi} &= -\frac{\alpha\Lambda}{M_{\rm Pl}\hbar}\rho_{\rm b} \\ \frac{\partial\mathcal{L}}{\partial(\nabla\phi)} &= C\frac{\partial}{\partial(\nabla\phi)}X\sqrt{\beta(\dot\theta - m\Phi) - X} \end{aligned} \tag{4.37}$$

$$
\begin{aligned}
&= C\frac{\partial}{\partial(\nabla\phi)}X\sqrt{\beta\hat{\mu}-X} \\
&= C\frac{\partial\sqrt{\beta\hat{\mu}X^2-X^3}}{\partial(\nabla\phi)} \\
&= C\frac{\partial\sqrt{\beta\hat{\mu}X^2-X^3}}{\partial X}\frac{\partial X}{\partial(\nabla\phi)} \\
&= -C\frac{2\beta\hat{\mu}X-3X^2}{\sqrt{\beta\hat{\mu}X^2-X^3}}\frac{(\nabla\phi)}{2m} \\
&= -\frac{C}{2m}\frac{2\beta\hat{\mu}-3X}{\sqrt{\beta\hat{\mu}-X}}\nabla\phi \\
&= -\frac{C}{2m}\frac{2\beta\hat{\mu}-3\hat{\mu}-(\nabla\phi)^2/2m}{\sqrt{\beta\hat{\mu}-\hat{\mu}-(\nabla\phi)^2/2m}}\nabla\phi \\
&= -\frac{3C}{2m}\frac{(\nabla\phi)^2/2m+\left(\frac{2\beta}{3}-1\right)\hat{\mu}}{\sqrt{(\nabla\phi)^2/2m+(\beta-1)\hat{\mu}}}\nabla\phi \\
&= -\frac{3C}{2m}f(||\nabla\phi||^2,\beta)\nabla\phi\,, \qquad (4.38)
\end{aligned}
$$

and the equation of motion for ϕ is

$$
\begin{aligned}
\nabla\cdot\frac{\partial\mathcal{L}}{\partial(\nabla\phi)} &= \frac{\partial\mathcal{L}}{\partial\phi} \\
\nabla\cdot\left(-\frac{3C}{2m}f(||\nabla\phi||^2,\beta)\nabla\phi\right) &= -\frac{\alpha\Lambda}{M_{\rm Pl}\hbar}\rho_{\rm b} \\
\nabla\cdot[f(||\nabla\phi||^2,\beta)\nabla\phi] &= \frac{\alpha\Lambda}{M_{\rm Pl}\hbar}\frac{2m}{3C}\rho_{\rm b} = \frac{\alpha\hbar^2}{2\sqrt{2m}M_{\rm Pl}}\rho_{\rm b} \\
\nabla\cdot[\sqrt{2m}f(||\nabla\phi||^2,\beta)\nabla\phi] &= \frac{\alpha\hbar^2}{2M_{\rm Pl}}\rho_{\rm b} \\
\sqrt{2m}f(||\nabla\phi||^2,\beta)||\nabla\phi|| &= \frac{\alpha\hbar^2}{8\pi M_{\rm Pl}}\frac{M_{\rm b}}{r^2}\equiv\kappa(r) \\
\sqrt{2m}\frac{(\nabla\phi)^2/2m+\left(\frac{2\beta}{3}-1\right)\hat{\mu}}{\sqrt{(\nabla\phi)^2/2m+(\beta-1)\hat{\mu}}}||\nabla\phi|| &= \kappa \\
\frac{(\nabla\phi)^2+2m\left(\frac{2\beta}{3}-1\right)\hat{\mu}}{\sqrt{(\nabla\phi)^2+2m\,(\beta-1)\,\hat{\mu}}}||\nabla\phi|| &= \kappa\,.
\end{aligned}
$$

The phonon gradient is taken to only vary radially $||\nabla\phi|| = \partial_r\phi$, so instead express the eqution of motion as

$$
\frac{(\partial_r\phi)^2+2m\left(\frac{2\beta}{3}-1\right)\hat{\mu}}{\sqrt{(\partial_r\phi)^2+2m\,(\beta-1)\,\hat{\mu}}}(\partial_r\phi) = \kappa\,. \qquad (4.39)
$$

This implies a cubic equation for $(\partial_r\phi)^2$ which will be solved numerically to obtain the ϕ-mediated acceleration shortly.

First consider two extremal cases; *i*) sufficiently close to the baryon source, such that $(\partial_r\phi)^2 \gg m\hat{\mu}$, the equation of motion takes the form

$$\begin{aligned}\frac{(\partial_r\phi)^2}{\sqrt{(\partial_r\phi)^2}}(\partial_r\phi) &\simeq \kappa \\ (\partial_r\phi) &\simeq \sqrt{\kappa}\end{aligned}$$

where the solution scales as $1/r$ and the MONDian profile form the zero-temperature analysis is recovered, and *ii*) in the absence of baryons, such that $(\partial_r\phi)^2 \ll m\hat{\mu}$, the equation of motion takes the form

$$\begin{aligned}\frac{2m\left(\frac{2\beta}{3}-1\right)\hat{\mu}}{\sqrt{2m\left(\beta-1\right)\hat{\mu}}}(\partial_r\phi) &\simeq \kappa \\ (\partial_r\phi) &\simeq \frac{\sqrt{2m\left(\beta-1\right)\hat{\mu}}}{2m\left(\frac{2\beta}{3}-1\right)\hat{\mu}}\sqrt{\kappa} \\ &\simeq \frac{3}{\sqrt{2m\hat{\mu}}}\frac{\sqrt{\beta-1}}{2\beta-3}\kappa\end{aligned}$$

where the solution now scales as $1/r^2$ since $\hat{\mu}$ is kept approximately constant. This is different from [1] in that the factor $3/(2\beta-3)$ is also in the square root. The transition between these two behaviours is at the radius $r_\star$, defined by the radius at which $m\hat{\mu} = \kappa(r_\star)$ where $\hat{\mu}$ is approximated constant with a value defined by the central density (3.70) and (3.64),

$$\begin{aligned}m\hat{\mu} &\simeq \kappa(r_\star) \\ \frac{\hbar^6}{8\Lambda^2 m^4}\rho_0^2 &\simeq \frac{\alpha\hbar^2}{8\pi M_{\rm Pl}}\frac{M_{\rm b}}{r_\star^2} \\ r_\star^2 &\simeq \frac{\alpha}{\pi M_{\rm Pl}\hbar^4}\rho_0^{-2} M_{\rm b}\Lambda^2 m^4 \\ &\simeq \frac{b_0}{\pi M_{\rm Pl}\hbar^4}\left[\left(\frac{2^{13}\pi G^3}{\hbar^{18}x_1^4}\right)^{1/5} M^{2/5} m^{18/5}\Lambda^{6/5}\right]^{-2}\left(\frac{\Lambda}{1\,\text{meV}}\right)^{-2/3} M_{\rm b}\,\Lambda^2\,m^4 \\ &\simeq \frac{b_0(\text{meV})^{2/3}}{\pi M_{\rm Pl}\hbar^4}\left(\frac{2^{13}\pi G^3}{\hbar^{18}x_1^4}\right)^{-2/5} M^{-4/5}\,m^{-36/5}\,\Lambda^{-12/5}\,\Lambda^{-2/3}\,M_{\rm b}\,\Lambda^2\,m^4 \\ &\simeq \frac{b_0(\text{meV})^{2/3}}{\pi M_{\rm Pl}\hbar^4}\left(\frac{2^{13}\pi G^3}{\hbar^{18}x_1^4}\right)^{-2/5} M_{\rm b}^{1/5}\left(\frac{M}{M_{\rm b}}\right)^{-4/5} m^{-16/5}\,\Lambda^{-16/15} \\ &\simeq \frac{b_0(\text{meV})^{2/3}}{\pi M_{\rm Pl}\hbar^4}\left(\frac{2^{13}\pi G^3}{\hbar^{18}x_1^4}\right)^{-2/5}\left(10^{12}\,M_\odot\right)^{1/5}(\text{eV}/c^2)^{-16/5}(\text{meV})^{-16/15} \\ &\quad\left(\frac{M_{\rm b}}{10^{12}\,M_\odot}\right)^{1/5}\left(\frac{M}{M_{\rm b}}\right)^{-4/5}\left(\frac{m}{\text{eV}/c^2}\right)^{-16/5}\left(\frac{\Lambda}{\text{meV}}\right)^{-16/15}\end{aligned}$$

$$r_\star \simeq \left(\frac{M_\mathrm{b}}{10^{12}\,M_\odot}\right)^{1/10}\left(\frac{M}{M_\mathrm{b}}\right)^{-2/5}\left(\frac{m}{\mathrm{eV}/c^2}\right)^{-8/5}\left(\frac{\Lambda}{\mathrm{meV}}\right)^{-8/15} 25.721\,\mathrm{kpc}\,. \tag{4.40}$$

With fiducial values $M_\mathrm{b} = 3\times10^{11}\,M_\odot$, $m = 0.6\,\mathrm{eV}/c^2$, $\Lambda = 0.2\,\mathrm{meV}$, with dark matter-to-baryon ratio set by cosmology $M/M_\mathrm{b} = \Omega_\mathrm{DM}/\Omega_\mathrm{b} \simeq 6$, the transition radius is $r_\star \simeq 59.4952\,\mathrm{kpc}$, which is greater than the upper bound on the Milky Way halo radius [97] at 24.5 kpc (this corresponds to a diameter of ~ 160000 light-years). This implies that the phonon gradient is $(\partial_r\phi) \simeq \sqrt{\kappa}$ and the acceleration is subsequently MONDian at least throughout the stellar disk. To summarize, assuming $\beta \geq 3/2$, the expected phonon-gradient behaviour is

$$\partial_r\phi \simeq \begin{cases} \sqrt{\kappa}\,, & r \ll r_\star \\ \frac{3}{\sqrt{2m\hat{\mu}}}\frac{\sqrt{\beta-1}}{2\beta-3}\kappa\,, & r \gg r_\star \end{cases} \tag{4.41}$$

with $r_\star$ set by (4.40).

The equation of motion for ϕ, eq. (4.39), implies a cubic equation for $z = (\partial_r\phi)^2$,

$$z^3 + 2sz^2 + \left[s^2 - \kappa^2\right] z - t\kappa^2 = 0\,, \tag{4.42}$$

which is guaranteed to have at least one real solution at all radii except $r = 0$. The parameters in the coefficients are

$$\begin{aligned} s &= 2m\left(\frac{2\beta}{3} - 1\right)\hat{\mu} \\ t &= 2m\,(\beta-1)\,\hat{\mu} \\ \kappa &= \frac{\alpha\hbar^2}{8\pi M_\mathrm{Pl}}\frac{M_\mathrm{b}}{r^2}\,. \end{aligned}$$

This is solved numerically with $\beta = 2$ and all the fiducial values mentioned under (4.40), with the result shown in Figure (4.1). As can be seen, the two accelerations are on top of each other, with a smaller difference than in [1].

Their ratio may be calculated by expressing (4.39) as equation for $\mathcal{A} \equiv a_\phi/a_\mathrm{MOND}$. This is done by first multiplying in $\alpha\Lambda/M_\mathrm{Pl}\hbar$ such (4.39) is now an equation for a_ϕ, then scaling the equation by a_MOND The equation for $\mathcal{A}^2$ in the likes of (4.42) is

$$\mathcal{A}^6 + 2\tilde{s}\mathcal{A}^4 + \left[\tilde{s}^2 - \tilde{\kappa}^2\right]\mathcal{A}^2 - \tilde{t}\tilde{\kappa}^2 = 0\,, \tag{4.43}$$

where the parameters in the coefficients are

$$\begin{aligned} \tilde{s} &= \left(\frac{\alpha\Lambda}{M_\mathrm{Pl}\hbar}\frac{1}{a_\mathrm{MOND}}\right)^2 s \\ \tilde{t} &= \left(\frac{\alpha\Lambda}{M_\mathrm{Pl}\hbar}\frac{1}{a_\mathrm{MOND}}\right)^2 t \end{aligned}$$

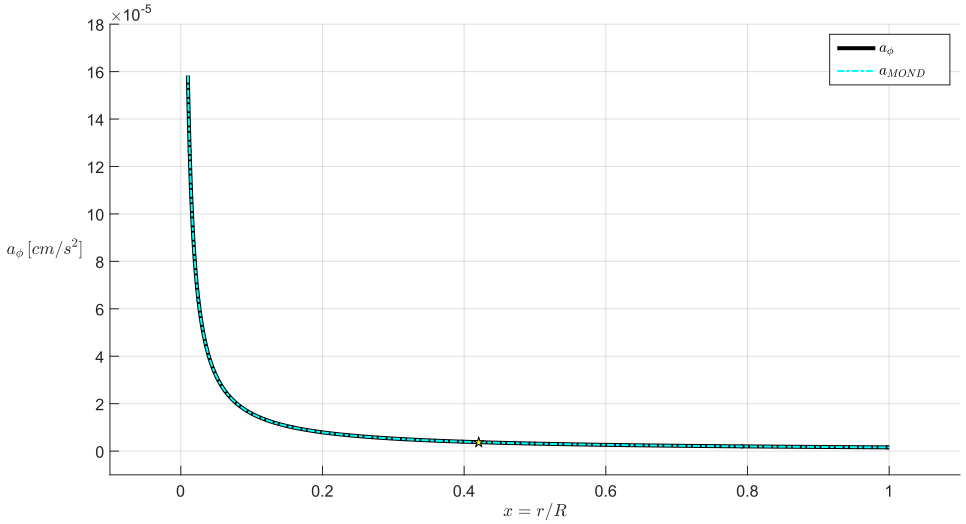

Figure 4.1: The ϕ-mediated acceleration plotted with fiducial values alongside the MONDian expression on a test baryonic particle. The yellow star represents the transition radius $r_\star$.

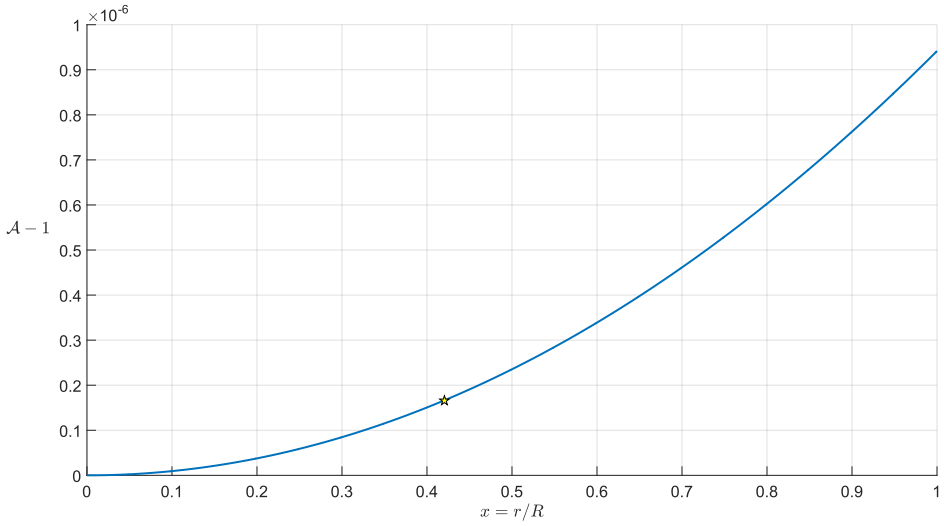

Figure 4.2: The ratio between ϕ-mediated acceleration with fiducial values and MONDian acceleration on a test baryonic particle. The yellow star represents the transition radius $r_\star$.

$$\tilde{\kappa} = \left(\frac{\alpha\Lambda}{M_{\rm Pl}\hbar}\frac{1}{a_{\rm MOND}}\right)^2 \kappa\,.$$

It is solved numerically with fiducial values, and the result is shown in Figure (4.2). As can be seen, they are indistinguishable down to 10^{-5} ratio, so MONDian dynamics do apply - *e.g.* "asymptotic" velocity, BTFR, and so on. This, too, shows smaller difference than in [1].

Comparing to gravitational acceleration

The acceleration due to the phonon interaction on a test baryonic particle should be compared to that of dark matter through Newtonian gravity. The former is defined in (4.7), and the latter is defined by Poisson's equation sourced by dark matter alone: the acceleration of a test baryonic particle due to dark matter in the Newtonian picture is $\vec{a}_{\rm DM} = -\nabla\Phi$, therefore Poisson's equation may be expressed as

$$\nabla\cdot\vec{a}_{\rm DM} = -4\pi G\rho_{\rm DM}\,. \tag{4.44}$$

The density is found by the usual thermodynamic identity, where in the pressure the replacement $\Lambda \to \Lambda\sqrt{\beta-1}$ is applied to (3.34),

$$\begin{aligned}
\rho_{\rm DM} &= m\frac{dP}{dX}\\
&= \frac{2m\Lambda\sqrt{\beta-1}(2m)^{3/2}}{3\hbar^3}\frac{d\,X|X|^{1/2}}{dX}\\
&= \frac{2m\Lambda\sqrt{\beta-1}(2m)^{3/2}}{3\hbar^3}\left(|X|^{1/2}+\frac{X^2}{2|X|^{3/2}}\right)\\
&= \frac{2m\Lambda\sqrt{\beta-1}(2m)^{3/2}}{3\hbar^3}\left(\frac{X^2}{|X|^{3/2}}+\frac{X^2}{2|X|^{3/2}}\right)\\
&= \frac{2m\Lambda\sqrt{\beta-1}(2m)^{3/2}}{3\hbar^3}\frac{3X^2}{2|X|^{3/2}}\\
&= \frac{m\Lambda\sqrt{\beta-1}(2m)^{3/2}}{\hbar^3}\frac{X^2}{|X|^{3/2}}\\
&= \frac{m\Lambda\sqrt{\beta-1}(2m)^{3/2}}{\hbar^3}|X|^{1/2}\\
&= \frac{2m^2\Lambda\sqrt{\beta-1}}{\hbar^3}|2mX|^{1/2}\,,
\end{aligned}$$

where the identity $X^2 = |X|^2$ was used.

Since X varies with $\partial_r\phi$, its behaviour at radii much less and much greater than $r_\star$ makes the acceleration easier to analyze analytically. Take first the domain $r \ll r_\star$ such that $(\partial_r\phi)^2 \gg m\hat{\mu}$ and $\partial_r\phi \simeq \sqrt{\kappa}$. Here $|2mX| \simeq (\partial_r\phi)^2$ and

$$\rho_{\rm DM} \simeq \frac{2m^2\Lambda\sqrt{\beta-1}}{\hbar^3}\sqrt{\kappa}\,. \tag{4.45}$$

The scalar acceleration $a_{\rm DM} = ||\vec{a}_{\rm DM}||$, eq. (4.44), is then

$$\begin{aligned}
\frac{1}{r^2}\frac{d\left[r^2 a_{\rm DM}\right]}{dr} &= \frac{8\pi G m^2 \Lambda\sqrt{\beta-1}}{\hbar^3}\sqrt{\kappa} \\
\frac{d\left[r^2 a_{\rm DM}\right]}{dr} &= \frac{8\pi G m^2 \Lambda\sqrt{\beta-1}}{\hbar^3}\sqrt{\kappa(r) r^2}\, r \\
r^2 a_{\rm DM} &= \frac{8\pi G m^2 \Lambda\sqrt{\beta-1}}{\hbar^3}\sqrt{\kappa(r) r^2}\,\frac{r^2}{2} \\
a_{\rm DM} &= \frac{4\pi G m^2 \Lambda\sqrt{\beta-1}}{\hbar^3}\sqrt{\kappa(r) r^2}\,, \qquad (4.46)
\end{aligned}$$

and is thus independent[2] of radius. The dark matter-to-ϕ acceleration ratio is therefore

$$\begin{aligned}
\frac{a_{\rm DM}}{a_\phi} &= \frac{\frac{4\pi G m^2 \Lambda\sqrt{\beta-1}}{\hbar^3}\sqrt{\kappa(r) r^2}}{\frac{\alpha\Lambda}{M_{\rm Pl}\hbar}\sqrt{\kappa(r)}} \\
&= \frac{4\pi G m^2 M_{\rm Pl}\sqrt{\beta-1}}{\alpha\hbar^2}\, r \\
&\simeq 0.1179\,\frac{r}{r_\star}\,, \quad r \ll r_\star \qquad (4.47)
\end{aligned}$$

with fiducial values inserted. The numerical factor is within the same order of magnitude as [1] - it is six times smaller here. It is clear that the gravitational acceleration due to dark matter is subdominant in the MONDian regime, and becomes comparable to a_ϕ at $r \sim r_\star$.

In the other regime, $(\partial_r\phi)^2 \ll m\hat{\mu}$ so $X \simeq \hat{\mu}$ and the equation of state that follows from the calculations in Chapter 3. In [1] $a_{\rm DM}$ is approximated by the scale of radial derivative $|\partial_r X|/m \sim X/mR$, and their a_ϕ has that factor $3/(2\beta-3)$ in the square root. In this thesis, $a_{\rm DM}$ is derived from the the calculations in Chapter 3, and a_ϕ is as it has been presented.

The calculation is exactly as in Chapter (3) and the dark matter density is therefore given by (3.59),

$$\rho_{\rm DM} \simeq \rho_0\sqrt{\cos\left(\frac{\pi}{2}\frac{r}{R}\right)}\,. \qquad (4.48)$$

Through hydrostatic equilibrium, the acceleration is easy to find,

$$\begin{aligned}
\frac{1}{\rho_{\rm DM}}\frac{dP}{dr} &= -\frac{d\Phi}{dr} \\
3K\rho_{\rm DM}\frac{d\rho_{\rm DM}}{dr} &= -\frac{d\Phi}{dr} \\
\frac{d}{dr}\left(-\frac{3K}{2}\rho_{\rm DM}\right) &= \frac{d}{dr}\Phi
\end{aligned}$$

[2]Integration would yield a constant term, further yielding an extra term $a_{\rm DM} \supset Cr^{-2}$. This is the baryon contribution to Newtonian gravity, and since baryons are neglect, so is also this Cr^{-2} term.

and by the arguments in radial derivatives it is clear that $\Phi(r) = -3K\rho_{\mathrm{DM}}(r)^2/2$ where K is now the proportionality factor of (3.37), again with the replacement $\Lambda \to \Lambda\sqrt{\beta-1}$. The acceleration is then

$$\begin{aligned}
\vec{a}_{\mathrm{DM}} &= -\nabla\Phi \\
a_{\mathrm{DM}} &= \frac{3K}{2}\left|\frac{d\rho_{\mathrm{DM}}(r)^2}{dr}\right| \\
&= \frac{3K\rho_0^2}{2}\left|\frac{d}{dr}\left[\cos\left(\frac{\pi}{2}\frac{r}{R}\right)\right]\right| \\
&= \frac{3\pi K\rho_0^2}{4R}\left|\sin\left(\frac{\pi}{2}\frac{r}{R}\right)\right| ,
\end{aligned}$$

Keep in mind that the density (4.48) is discontinuous at $r \geq R$ which implies that a_{DM} is undefined at these radii. However, if the case $r \gg r_\star$ implies the limit $r \to R$, the sine-function approaches the numeric value 1. Recall that for large radii

$$\begin{aligned}
\partial_r\phi &= \frac{3}{\sqrt{2m\hat{\mu}}}\frac{\sqrt{\beta-1}}{2\beta-3}\kappa \\
&= \frac{3}{\sqrt{2m\hat{\mu}}}\kappa ,
\end{aligned}$$

where $\beta = 2$ has been inserted. The acceleration ratio is

$$\begin{aligned}
\frac{a_{\mathrm{DM}}}{a_\phi} &\simeq \frac{\frac{3\pi K\rho_0^2}{4R}}{\frac{\alpha\Lambda}{M_{\mathrm{Pl}}\hbar}\frac{3}{\sqrt{2m\hat{\mu}}}\kappa} \\
&\simeq \frac{\frac{3\pi\rho_0^2}{4R}\frac{\hbar^6}{12\Lambda^2m^6}}{\frac{\alpha\Lambda}{M_{\mathrm{Pl}}\hbar}\frac{3}{\sqrt{2m\hat{\mu}}}\kappa} \\
&\simeq \frac{1}{16}\left(\frac{\hbar}{m}\right)^6\frac{\pi\rho_0^2}{R\Lambda^2}\frac{M_{\mathrm{Pl}}\hbar\sqrt{2m\hat{\mu}}}{3\alpha\Lambda}\frac{8\pi M_{\mathrm{Pl}}}{\alpha\hbar^2}\frac{r^2}{M_{\mathrm{b}}} \\
&\simeq \frac{1}{6}\left(\frac{\hbar}{m}\right)^6\frac{\pi^2\rho_0^2M_{\mathrm{Pl}}^2\sqrt{2m\hat{\mu}}}{\alpha^2\Lambda^3R\hbar M_{\mathrm{b}}}r_\star^2\left(\frac{r}{r_\star}\right)^2 \\
&\simeq 0.0334\left(\frac{r}{r_\star}\right)^2 , \quad r \gg r_\star
\end{aligned} \tag{4.49}$$

with fiducial values. This is two order of magnitude less than in [1], though this has been calculated with the central density found in Chapter 3.3 - finite-temperature effects and baryon interactions may change the central density significantly. The two accelerations are comparable at radii $r \sim 10r_\star \approx 600\,\mathrm{kpc}$, which is far outside the extent of the halo $R \sim 140\,\mathrm{kpc}$. Consequently, the gravitational acceleration is not dominant for $r \gg r_\star$, in opposition to [1].

Stability of phonon perturbations

The stability of the phonon background should be checked - eq. (4.31) is expanded to quadratic order in first-derivatives for the perturbations $\varphi = \phi - \bar{\phi}$. By insertion of $\phi(r) \to \phi(r,t) = \varphi(r,t) + \bar{\phi}(r)$, the scalar X becomes

$$\begin{aligned} X &= \dot{\theta} - m\Phi - \frac{(\nabla\theta)^2}{2m} \\ &= \mu + \dot{\phi} - m\Phi - \frac{(\nabla\phi)^2}{2m} \\ &= \hat{\mu} + \dot{\varphi} - \frac{(\nabla\varphi + \nabla\bar{\phi})^2}{2m} \\ &= \hat{\mu} + \dot{\varphi} - \frac{(\nabla\varphi)^2}{2m} - \frac{(\nabla\bar{\phi})^2}{2m} - \frac{(\nabla\varphi)\cdot(\nabla\bar{\phi})}{m} \\ &= \bar{X} + \gamma_1 \,, \end{aligned} \tag{4.50}$$

where

$$\bar{X} \equiv \hat{\mu} - \frac{(\nabla\bar{\phi})^2}{2m} \tag{4.51}$$

$$\gamma_1 \equiv \dot{\varphi} - \frac{(\nabla\varphi)^2}{2m} - \frac{(\nabla\varphi)\cdot(\nabla\bar{\phi})}{m} \,. \tag{4.52}$$

Throughout the calculation, let $\bar{q} \equiv (\nabla\bar{\phi})^2/2m$ for aesthetics. Thus

$$\mathcal{L} = C\left(\bar{X} + \gamma_1\right)\sqrt{|\bar{X} + \gamma_1 - \beta\left(\hat{\mu} + \dot{\varphi}\right)|} \tag{4.53}$$

and since the arguments absolute values are taken to be negative,

$$\begin{aligned} |\bar{X} + \gamma_1 - \beta\left(\hat{\mu} + \dot{\varphi}\right)| &= -\left[\bar{X} + \gamma_1 - \beta\left(\hat{\mu} + \dot{\varphi}\right)\right] \\ &= \beta\hat{\mu} + \beta\dot{\varphi} - \bar{X} - \gamma_1 \\ &= \left[\beta\hat{\mu} - \hat{\mu} + \bar{q}\right] + \left[\beta\dot{\varphi} - \dot{\varphi} + \frac{(\nabla\varphi)^2}{2m} + \frac{(\nabla\varphi)\cdot(\nabla\bar{\phi})}{m}\right] \\ &= \bar{Z} + \gamma_2 \,, \end{aligned} \tag{4.54}$$

where

$$\bar{Z} \equiv (\beta - 1)\,\hat{\mu} + \bar{q} \tag{4.55}$$

$$\gamma_2 \equiv (\beta - 1)\,\dot{\varphi} + \frac{(\nabla\varphi)^2}{2m} + \frac{(\nabla\varphi)\cdot(\nabla\bar{\phi})}{m} \,. \tag{4.56}$$

The Lagrangian is then expressed as

$$\mathcal{L} = C\left(\bar{X} + \gamma_1\right)\sqrt{\bar{Z} + \gamma_2} \tag{4.57}$$

where the square root is expanded to second order in perturbations γ_2, and has the same result as in the zero-temperature case,

$$\sqrt{\bar{Z}+\gamma_2} = \bar{Z}^{1/2} + \frac{1}{2\bar{Z}^{1/2}}\gamma_2 - \frac{1}{8\bar{Z}^{3/2}}\gamma_2^2 + \mathcal{O}(\gamma_2^3)\,,$$

so eq. (4.57) has terms

$$\begin{aligned}\mathcal{L} &\supset C\left(\bar{X}+\gamma_1\right)\left[\bar{Z}^{1/2} + \frac{1}{2\bar{Z}^{1/2}}\gamma_2 - \frac{1}{8\bar{Z}^{3/2}}\gamma_2^2\right] \\ &= \frac{C}{\bar{Z}^{3/2}}\left\{\bar{X}\bar{Z}^2 + \frac{\bar{X}\bar{Z}}{2}\gamma_2 - \frac{\bar{X}}{8}\gamma_2^2 + \bar{Z}^2\gamma_1 + \frac{\bar{Z}}{2}\gamma_1\gamma_2 - \frac{1}{8}\gamma_1\gamma_2^2\right\}. \qquad (4.58)\end{aligned}$$

From (4.52) and (4.56) it is clear that the only contributors to $\mathcal{L}_{\text{quad}}$ are the terms proportional to γ_1, γ_2, $\gamma_1\gamma_2$ and γ_2^2,

$$\begin{aligned}\mathcal{L} &\supset \frac{C}{\bar{Z}^{3/2}}\left\{\frac{\bar{X}\bar{Z}}{2}\gamma_2 - \frac{\bar{X}}{8}\gamma_2^2 + \bar{Z}^2\gamma_1 + \frac{\bar{Z}}{2}\gamma_1\gamma_2\right\} \\ &= \frac{C}{\bar{Z}^{3/2}}\left\{\frac{\bar{X}\bar{Z}}{2}\left[(\beta-1)\,\dot{\varphi} + \frac{(\nabla\varphi)^2}{2m} + \frac{(\nabla\varphi)\cdot(\nabla\bar{\phi})}{m}\right]\right. \\ &\quad + \bar{Z}^2\left[\dot{\varphi} - \frac{(\nabla\varphi)^2}{2m} - \frac{(\nabla\varphi)\cdot(\nabla\bar{\phi})}{m}\right] \\ &\quad + \frac{\bar{Z}}{2}\left[\dot{\varphi} - \frac{(\nabla\varphi)^2}{2m} - \frac{(\nabla\varphi)\cdot(\nabla\bar{\phi})}{m}\right]\left[(\beta-1)\,\dot{\varphi} + \frac{(\nabla\varphi)^2}{2m} + \frac{(\nabla\varphi)\cdot(\nabla\bar{\phi})}{m}\right] \\ &\quad \left. - \frac{\bar{X}}{8}\left[(\beta-1)\,\dot{\varphi} + \frac{(\nabla\varphi)^2}{2m} + \frac{(\nabla\varphi)\cdot(\nabla\bar{\phi})}{m}\right]^2\right\}.\end{aligned}$$

In both the terms proportional to $\bar{X}\bar{Z}/2$ and $\bar{Z}^2$ only $(\nabla\varphi)^2/2m$ is kept, and the contribution is

$$\begin{aligned}\mathcal{L}_{\text{quad}} &\supset \frac{C}{\bar{Z}^{3/2}}\left\{\left[\frac{1}{2}\bar{X}\bar{Z} - \bar{Z}^2\right]\frac{(\nabla\varphi)^2}{2m}\right\} \\ &= \frac{C}{\bar{Z}^{3/2}}\left\{\left[\frac{1}{2}\bar{X}\bar{Z} - \bar{Z}^2\right]\left(\frac{(\partial_r\varphi)^2}{2m} + \frac{(\partial_\Omega\varphi)^2}{2mr^2}\right)\right\} \\ &= -\frac{C}{\bar{Z}^{3/2}}\left\{\left[\bar{Z}^2 - \frac{1}{2}\bar{X}\bar{Z}\right]\frac{(\partial_r\varphi)^2}{2m} + \left[\bar{Z} - \frac{1}{2}\bar{X}\right]\frac{\bar{Z}(\partial_\Omega\varphi)^2}{2mr^2}\right\}. \qquad (4.59)\end{aligned}$$

In the term proportional to $\bar{Z}/2$ the contribution is

$$\begin{aligned}\mathcal{L}_{\text{quad}} &\supset \frac{C}{\bar{Z}^{3/2}}\left\{\frac{1}{2}\bar{Z}\left[(\beta-1)\dot{\varphi}^2 - \frac{(\partial_r\bar{\phi})^2}{m}\frac{(\partial_r\varphi)^2}{m} + \frac{(\partial_r\bar{\phi})}{m}\dot{\varphi}(\partial_r\varphi) - (\beta-1)\frac{(\partial_r\bar{\phi})}{m}\dot{\varphi}(\partial_r\varphi)\right]\right\} \\ &= \frac{C}{\bar{Z}^{3/2}}\left\{\frac{1}{2}\bar{Z}\left[(\beta-1)\dot{\varphi}^2 - 4\frac{(\partial_r\bar{\phi})^2}{2m}\frac{(\partial_r\varphi)^2}{2m} - (\beta-2)\frac{(\partial_r\bar{\phi})}{m}\dot{\varphi}(\partial_r\varphi)\right]\right\}. \qquad (4.60)\end{aligned}$$

As for the last term, the contribution is

$$\mathcal{L}_{\text{quad}} \supset \frac{C}{\bar{Z}^{3/2}} \left\{ -\frac{1}{8}\bar{X} \left[(\beta-1)^2\dot{\varphi}^2 + 4\frac{(\partial_r\bar{\phi})^2}{2m}\frac{(\partial_r\varphi)^2}{2m} + 2(\beta-1)\frac{(\partial_r\bar{\phi})}{m}\dot{\varphi}(\partial_r\varphi) \right] \right\} . \tag{4.61}$$

The quadratic Lagrangian is then

$$\begin{aligned} \mathcal{L}_{\text{quad}} = \frac{C}{\bar{Z}^{3/2}} \Bigg\{ & \left[\bar{Z} - \frac{\beta-1}{4}\bar{X} \right] \frac{(\beta-1)\dot{\varphi}^2}{2} \\ & - \left[(\beta-2)\bar{Z} + \frac{\beta-1}{2}\bar{X} \right] \frac{(\partial_r\bar{\phi})}{2m}\dot{\varphi}(\partial_r\varphi) \\ & - \left[\left(2\bar{Z} + \frac{1}{2}\bar{X} \right) \frac{(\partial_r\bar{\phi})^2}{2m} + \left(\bar{Z} - \frac{1}{2}\bar{X} \right) \bar{Z} \right] \frac{(\partial_r\varphi)^2}{2m} \\ & - \left[\bar{Z} - \frac{1}{2}\bar{X} \right] \frac{\bar{Z}(\partial_\Omega\varphi)^2}{2mr^2} \Bigg\} . \end{aligned} \tag{4.62}$$

The expressions in square brackets may be calculated as well. Starting with the angular term,

$$\begin{aligned} \bar{Z} - \frac{1}{2}\bar{X} &= (\beta-1)\hat{\mu} + \bar{q} - \frac{1}{2}\hat{\mu} + \frac{1}{2}\bar{q} \\ &= \left(\beta - \frac{3}{2} \right) \hat{\mu} + \frac{3}{2}\bar{q} , \end{aligned}$$

then the radial term,

$$\begin{aligned} & 2\bar{Z}\bar{q} + \frac{1}{2}\bar{X}\bar{q} + \left(\bar{Z} - \frac{1}{2}\bar{X} \right) \bar{Z} \\ & \quad = 2(\beta-1)\hat{\mu}\bar{q} + 2\bar{q}^2 + \frac{1}{2}\hat{\mu}\bar{q} - \frac{1}{2}\bar{q}^2 + \left[\left(\beta - \frac{3}{2} \right) \hat{\mu} + \frac{3}{2}\bar{q} \right] [(\beta-1)\hat{\mu} + \bar{q}] \\ & \quad = \left(2\beta - \frac{3}{2} \right) \hat{\mu}\bar{q} + \frac{3}{2}\bar{q}^2 + (\beta-1) \left(\beta - \frac{3}{2} \right) \hat{\mu}^2 + \frac{3}{2}\bar{q}^2 + \left(\beta - \frac{3}{2} \right) \hat{\mu}\bar{q} + \frac{3}{2}(\beta-1)\hat{\mu}\bar{q} \\ & \quad = (\beta-1) \left(\beta - \frac{3}{2} \right) \hat{\mu}^2 + 3\bar{q}^2 + \frac{9}{2}(\beta-1)\hat{\mu}\bar{q} , \end{aligned}$$

the temporal-radial mixing term,

$$\begin{aligned} (\beta-2)\bar{Z} + \frac{\beta-1}{2}\bar{X} &= (\beta-2)(\beta-1)\hat{\mu} + (\beta-2)\bar{q} + \frac{\beta-1}{2}\hat{\mu} - \frac{\beta-1}{2}\bar{q} \\ &= (\beta-1) \left(\beta - \frac{3}{2} \right) \hat{\mu} + \frac{\beta-3}{2}\bar{q} , \end{aligned}$$

and finally the kinetic term,

$$\bar{Z} - \frac{\beta-1}{4}\bar{X} = (\beta-1)\hat{\mu} + \bar{q} - \frac{\beta-1}{4}\hat{\mu} + \frac{\beta-1}{4}\bar{q}$$

$$= \frac{3(\beta-1)}{4}\hat{\mu} + \frac{\beta+3}{4}\bar{q}\,.$$

With the factor $2(2m)/3$ multiplied in from C, the quadratic Lagrangian is then

$$\begin{aligned}\mathcal{L}_{\text{quad}} = \frac{\Lambda(2m)^{1/2}}{\bar{Z}^{3/2}\hbar^3}\Bigg\{&\left[(\beta-1)\hat{\mu} + \left(\frac{\beta}{3}+1\right)\bar{q}\right]\frac{m(\beta-1)\dot{\varphi}^2}{2} \\ &- \left[(\beta-1)\left(\frac{2\beta}{3}-1\right)\hat{\mu} + \left(\frac{\beta}{3}-1\right)\frac{(\nabla\bar{\phi})^2}{2m}\right](\partial_r\bar{\phi})\dot{\varphi}(\partial_r\varphi) \\ &- \left[(\beta-1)\left(\frac{2\beta}{3}-1\right)\hat{\mu}^2 + \frac{3(\nabla\bar{\phi})^2}{2m}(\beta-1)\hat{\mu} + \frac{(\nabla\bar{\phi})^4}{2m^2}\right](\partial_r\varphi)^2 \\ &- \left[\left(\frac{2\beta}{3}-1\right)\hat{\mu} + \frac{(\nabla\bar{\phi})^2}{2m}\right]\frac{\bar{Z}(\partial_\Omega\varphi)^2}{r^2}\Bigg\}\,. \end{aligned} \tag{4.63}$$

It is clear that the kinetic term $\propto \dot{\varphi}^2$ is healthy if $\beta > 1$, and the radial and angular terms $\propto (\partial_r\varphi)^2$ and $\propto (\partial_\Omega\varphi)^2$ are healthy if $\beta \geq 3/2$. Therefore, the bound $\beta \geq 3/2$ guarantees a healthy Lagrangian.

Chapter 5

Validity of EFT and the Solar System

The purpose here is to check whether or not the theory holds any ground with respect to the superfluid stability criterion (1.7) and contributions to the EFT from higher-order derivatives.

The structure of the chapter follows that in [1], though with more calculations at higher precision. Some numerical factors are found to be smaller than in [1]. Also the section on sound speed is included in the beginning.

5.1 Superfluid stability

As discussed in Chapter 1, a superfluid is stable as long as its velocity is strictly less than the sound speed. Consequntly these are derived in order to check whether or not Landau's stability criterion (1.7) holds.

Sound speed

The speed of sound is calculated by the traditional formula $c_s^2 = dP/d\rho$, where the equation of state is given by (3.37) and goes as $P = K\rho^3$. Thus, with density given by (4.45) and the replacement $\Lambda \to \Lambda\sqrt{\beta - 1}$, the speed of sound is

$$\begin{aligned} c_s^2 &= 3\frac{\hbar^6}{12\Lambda^2(\beta-1)m^6}\frac{4m^4\Lambda^2(\beta-1)}{\hbar^6}|2m\bar{X}| \\ &= \frac{|2m\bar{X}|}{m^2} \\ c_s &= \frac{|2m\bar{X}|^{1/2}}{m}\,. \end{aligned}$$

In the MONDian regime, $(\nabla\bar{\phi})^2 \gg m\hat{\mu}$, so $2m\bar{X} \simeq (\nabla\bar{\phi})^2 = (\partial_r\bar{\phi})^2$, and the sound speed

$$c_s = \frac{|\nabla\bar{\phi}|}{m}\,. \tag{5.1}$$

[1] uses the zero-temperature, no-baryon sound speed $c_s = \sqrt{2\mu/m}$, while this thesis uses (5.1). The result is nonetheless similar in the regard that stability is broken.

Second sound, which was briefly mentioned in Chapters 1 and 3, is here brought up: the MOND force between baryons are mediated by the phonons (first sound), so this is where effects of second sound could be important.

The criterion

In the theory presented here, the superfluid is the Bose-Einstein condensed of dark matter particles in the halo, and baryons are the obstacles. Therefore, the Landau critical velocity is the sound speed (5.1), presented here with the bar removed

$$v_{\text{crit}} \stackrel{!}{=} c_s^{\text{MOND}} = \frac{|\nabla\phi|}{m}\,,$$

where ϕ is the field that describes the phonons. Consequently, the theory presented is invalid if the superfluid velocity is less than this sound speed - no phonons are generated, and MONDian behaviour cannot occur.

Going from a relativistic Lagrangian to the one in (3.34) is the subject of Chapter 6, which succeeds this chapter. The relativistic field introduced is expressed in terms of amplitude ρ and phase $\chi = (\theta + mc^2t)/\hbar$. The superfluid velocity is then

$$v_s = \frac{\hbar}{m}||\nabla\chi|| = \frac{||\nabla\theta||}{m}\,. \tag{5.2}$$

With the scalar θ given in (3.33) inserted, it is clear that the superfluid velocity and the phonon sound speed are *exactly* equal:

$$v_s = \frac{||\nabla\theta||}{m} = \frac{||\nabla\phi||}{m} \stackrel{!}{=} c_s\,. \tag{5.3}$$

Therefore, the stability criterion (1.7) dictates that phonons will be generated.

With regards to second sound, if it propagates at $c_s/\sqrt{3}$, the stability criterion is still broken. However, whether or not it has any lasting impact on the theory needs to be studied.

5.2 Higher-order derivatives

The EFT was made in terms of first-derivatives in order to account for the global $U(1)$ symmetry - see Chapter 3. This is, however, not limited to first-derivatives, since n-th derivatives are also consistent with the symmetry, and the EFT is effectivle a sum of all orders of derivatives [98]. In order to have only first-order derivatives on the relevant scales, the higher order contributions must be negligible on those scales.

Higher-order contributions are negligible provided that the ratio between those of order n and $n-1$ are negligible. The strong coupling scale identified in (3.49) suppresses

higher-order contributions, hence[1]

$$\frac{\hbar c}{\Lambda_s}\frac{\partial_r^2\phi}{\partial_r\phi} \sim \frac{\hbar c}{\Lambda_s r} \ll 1\,, \tag{5.4}$$

since the ratio of derivatives of orders n to $n-1$ scales as r^{-1}.

With the fiducial values, the strong coupling scale (3.71) is $\simeq 1\,\mathrm{meV}$, hence higher-order derivatives are suppressed if

$$\begin{aligned} r &\gg \frac{\hbar c}{1\,\mathrm{meV}} \\ &\gg 0.2\,\mathrm{mm}\,, \end{aligned} \tag{5.5}$$

Which is clearly the case on the astrophysical scales the EFT is relevant, as found in [1].

5.3 Local breakdown of coherence

If the superfluid velocity, eq. (5.2) exceeds the BEC critical velocity, eq. (2.27), coherence will be lost and dark matter particles become excited. Thus a condition for no loss of coherence is obtained,

$$\begin{aligned} v_s &\ll v_c \\ \frac{(\partial_r\phi)}{m} &\ll \left(\frac{2^5\pi^4}{3}\frac{\rho\hbar^3}{m^4}\right)^{\frac{1}{3}}\,. \end{aligned} \tag{5.6}$$

This is applied to the MONDian regime where the density ρ is given by. (4.45) with $\beta = 2$ and $(\partial_r\phi)/2m \gg \mu \Rightarrow X \simeq (\partial_r\phi)/2m$, and the phonon gradient is $(\partial_r\phi) \simeq \sqrt{\kappa}$. The two velocities are

$$\begin{aligned} v_c &\simeq \left(\frac{2^5\pi^4}{3}\frac{\hbar^3}{m^4}\frac{2m^2\Lambda}{\hbar^3}\sqrt{\kappa}\right)^{\frac{1}{3}} \\ &= \left(\frac{2^6\pi^4}{3}\frac{\Lambda}{m^2}\sqrt{\frac{\alpha\hbar^2}{8\pi M_{\mathrm{Pl}}}\frac{M_{\mathrm{b}}(r)}{r^2}}\right)^{1/3} \\ &= \left(\frac{2^6\pi^4 b_0^{1/2}}{3}\frac{(1\,\mathrm{meV})(10^{11}\,M_\odot)^{1/2}}{(1\,\mathrm{eV}/c^2)^2(1\,\mathrm{kpc})}\sqrt{\frac{\hbar^2}{8\pi M_{\mathrm{Pl}}}}\right)^{1/3} \\ &\times \left(\frac{m}{1\,\mathrm{eV}/c^2}\right)^{-2/3}\left(\frac{M_{\mathrm{b}}(r)}{10^{11}\,M_\odot}\right)^{1/6}\left(\frac{\Lambda}{1\,\mathrm{meV}}\right)^{2/9}\left(\frac{1\,\mathrm{kpc}}{r}\right)^{1/3} \\ v_s &\simeq \frac{\sqrt{\kappa}}{m} \end{aligned} \tag{5.7}$$

[1] The addition of the $\hbar c$ factor is necessary to have the units make sense.

$$
\begin{aligned}
=&\frac{1}{m}\sqrt{\frac{\alpha\hbar^2}{8\pi M_{\rm Pl}}\frac{M_{\rm b}(r)}{r^2}} \\
=&\frac{(10^{11}b_0\,M_\odot)^{1/2}}{(1\,{\rm eV}/c^2)(1\,{\rm kpc})}\sqrt{\frac{\hbar^2}{8\pi M_{\rm Pl}}} \\
&\times\left(\frac{m}{1\,{\rm eV}/c^2}\right)^{-1}\left(\frac{M_{\rm b}(r)}{10^{11}\,M_\odot}\right)^{1/2}\left(\frac{\Lambda}{1\,{\rm meV}}\right)^{-1/3}\frac{1\,{\rm kpc}}{r}\,,
\end{aligned}
\tag{5.8}
$$

where c is the speed of light. The numeric factor of (5.7) is $7.66\times10^7\,{\rm m\,s^{-1}}$, and that of (5.8) is $2.4\times10^6\,{\rm m\,s^{-1}}$.

Due to the difference in power dependence on the radius from the origin, the condition (5.6) can be expressed as a bound on the radius from the galactic center,

$$
v_c \simeq 0.2554c\left(\frac{m}{1\,{\rm eV}/c^2}\right)^{-2/3}\left(\frac{M_{\rm b}(r)}{10^{11}\,M_\odot}\right)^{1/6}\left(\frac{\Lambda}{1\,{\rm meV}}\right)^{2/9}\left(\frac{1\,{\rm kpc}}{r}\right)^{1/3} \tag{5.9}
$$

$$
v_s \simeq 0.008c\left(\frac{m}{1\,{\rm eV}/c^2}\right)^{-1}\left(\frac{M_{\rm b}(r)}{10^{11}\,M_\odot}\right)^{1/2}\left(\frac{\Lambda}{1\,{\rm meV}}\right)^{-1/3}\frac{1\,{\rm kpc}}{r} \tag{5.10}
$$

$$
r \gg 0.005\left(\frac{m}{1\,{\rm eV}/c^2}\right)^{-1/2}\left(\frac{M_{\rm b}(r)}{10^{11}\,M_\odot}\right)^{1/2}\left(\frac{\Lambda}{1\,{\rm meV}}\right)^{-5/6}{\rm kpc}\,. \tag{5.11}
$$

The numeric factor in (5.9) is greater than in [1] by one order of magnitude, where the increase w.r.t. is expected due to the additional factor $(2^5\pi^4/3)^{1/3}\approx10$. Hence the superfluid can reach higher velocities than in [1]

The condensate therefore remains coherent down to the central regions. The numeric factor in (5.11) is one order of magnitude less than that which is presented in [1] - $0.005/0.2 = 1/40$. This is due to the increased critical velocity (5.9).

It is important point out that this critical velocity is the same as in Chapter 2. That case was analyzed in the context of *non-interacting* dark matter particles. Also, the numeric factor in (5.9) implies that coherence break down when the superfluid velocity is of order $0.1c$ - *i.e.* lightly relativistic. This suggests that this test must be properly reconsidered taking into account these points - something [1] did not mention.

MOND and the Solar System

As mentioned by [1], MOND has problems within the Solar System - the additional acceleration a_ϕ gives an unacceptably large correction to Newtonian gravity. In other words: the observed dynamics within the Solar System does not fit with predictions from MOND. The condition of coherence (5.11) can be applied to the Solar System; if coherence is broken, dark matter exists in the normal phase, and MONDain behaviour will not occur.

The local superfluid velocity in the vicinity of the Sun is given by replacing $M_{\rm b} = M_\odot$ in (5.10)

$$
v_s \simeq 0.008c\left(\frac{m}{1\,{\rm eV}/c^2}\right)^{-1}\left(\frac{M_\odot}{10^{11}\,M_\odot}\right)^{1/2}\left(\frac{\Lambda}{1\,{\rm meV}}\right)^{-1/3}\frac{1\,{\rm kpc}}{r}
$$

$$\simeq 2.53c \times 10^{-8} \left(\frac{m}{1\,\mathrm{eV}/c^2}\right)^{-1} \left(\frac{\Lambda}{1\,\mathrm{meV}}\right)^{-1/3} \frac{1\,\mathrm{kpc}}{r}\,, \tag{5.12}$$

where r now represents the distance from the sun. The critical velocity is here found by evaluating (5.9) at $r \sim 8$ kpc (the distance of the sun from the galactic center) with $M_b = 3 \times 10^{11}\, M_\odot$:

$$\begin{aligned} v_c &\simeq 0.2554c \left(\frac{m}{1\,\mathrm{eV}/c^2}\right)^{-2/3} \left(\frac{3 \times 10^{11}\, M_\odot}{10^{11}\, M_\odot}\right)^{1/6} \left(\frac{\Lambda}{1\,\mathrm{meV}}\right)^{2/9} \left(\frac{1\,\mathrm{kpc}}{8\,\mathrm{kpc}}\right)^{1/3} \\ &\simeq \frac{0.2554(3)^{1/6}c}{2} \left(\frac{m}{1\,\mathrm{eV}/c^2}\right)^{-2/3} \left(\frac{\Lambda}{1\,\mathrm{meV}}\right)^{2/9}\,. \end{aligned} \tag{5.13}$$

The superfluid remains coherent down to

$$\begin{aligned} \frac{r}{1\,\mathrm{kpc}} &\gg \frac{2.53c \times 10^{-8}}{0.2554c \times (3)^{1/6}/2} \left(\frac{m}{1\,\mathrm{eV}/c^2}\right)^{-1/3} \left(\frac{\Lambda}{1\,\mathrm{meV}}\right)^{-5/9} \\ r &\gg 1.6497 \times 10^{-7} \left(\frac{m}{1\,\mathrm{eV}/c^2}\right)^{-1/3} \left(\frac{\Lambda}{1\,\mathrm{meV}}\right)^{-5/9} \mathrm{kpc} \\ r &\gg 34.028 \left(\frac{m}{1\,\mathrm{eV}/c^2}\right)^{-1/3} \left(\frac{\Lambda}{1\,\mathrm{meV}}\right)^{-5/9} \mathrm{AU}\,. \end{aligned} \tag{5.14}$$

This is also one order of magnitude less than in [1]. For reference, the numeric value ≈ 34 AU lies just beyond the orbit of Neptune [99]. With fiducial values inserted the boundary is $r \gg 98.65$ AU, which lies beyond the termination shock [100] - the first point at which the solar wind collides with interstellar medium.

Thus the result is in agreement with [1] - coherence of the condensate is broken within the Solar System, so dark matter particles are excited into the normal phase. MONDian behaviour does not occur, and standard Newtonian gravity applies.

Since the dark matter particles are in the normal phase and has mass range coinciding with axions, standard axion detection experiments can be used to directly detect dark matter particles - [1] lists [101] as an example.

Chapter 6

A relativistic completion

A relativistic theory, in the weak-coupling regime, is proposed by [1], of which the Lagrangian is built from a self-interacting complex scalar field with a global $U(1)$ symmetry. It is taken in the non-relativistic, weak-field regime, the MOND limit (which is identified) and the superfluid Lagrangian (3.34) is recovered.

This thesis provides the full calculation, done in SI-units.

6.1 The theory

As mentioned by [1], a superfluid in the weak-coupling regime can be described by a self-interacting complex scalar field with a global $U(1)$ symmetry. With this in mind, the dynamics of the field can be determined from a Klein-Gordon Lagrangian,

$$\mathcal{L}_{\mathrm{KG}} = -\frac{1}{2}\left[|\partial_\mu \Phi|^2 + V\left(|\Phi|^2\right)\right] ,$$

where $V\left(|\Phi|^2\right)$ is the self-interaction potential.

Initially [1] proposes a simple self-interaction potential, the free-particle potential $\sim |\Phi|^2$ and an additional hexic term $\sim |\Phi|^6$,

$$V\left(|\Phi|^2\right) = \frac{m^2c^2}{\hbar^2}|\Phi|^2 + \lambda|\Phi|^6 ,$$

which does reproduce (3.34) in the appropriate limit, though the MOND regime is not stable. *This* calculation is not included here.

Instead [1] opts for a Lagrangian built from a combination of free-particle Klein-Gordon Lagrangians,

$$\mathcal{L}_{\mathrm{KG}} = -\frac{1}{2}\left[|\partial_\mu \Phi|^2 + \frac{m^2c^2}{\hbar^2}|\Phi|^2\right] , \tag{6.1}$$

of different powers. Specifically, it is (6.1) with a term cubic in $\mathcal{L}_{\mathrm{KG}}$ added to it:

$$\mathcal{L} = -\frac{1}{2}\left[|\partial_\mu \Phi|^2 + \frac{m^2c^2}{\hbar^2}|\Phi|^2\right] - \frac{\Lambda^4}{6\left(\Lambda_{\mathrm{c}}^2 + |\Phi|^2\right)^6}\left[|\partial_\mu \Phi|^2 + \frac{m^2c^2}{\hbar^2}|\Phi|^2\right]^3 . \tag{6.2}$$

This has terms hexic in $|\Phi|$, which implies three-body interactions (as opposed to the two-body interaction a quartic term implies). The fraction of the cubic KG term is included to ensure the theory reduces to (3.34) in the non-relativistic, weak-field and MOND limits; the latter of which is explained later. Accordingly, the scale Λ_c is included to admit a $\Phi = 0$ vacuum.

This is taken in the non-relativistic regime, with the field Φ expressed in terms of amplitude and phase:

$$\Phi(\vec{r},\, t) = \rho(\vec{r}) e^{i\chi(\vec{r},\, t)}\,,\ \chi(\vec{r},\, t) = \frac{\theta(\vec{r},\, t) + mc^2 t}{\hbar}\,, \tag{6.3}$$

thus $|\Phi|^2 = \rho^2$. However, ρ is not to be considered as mass density, since, according to (6.1), the units/dimensions of $|\Phi|^2$ is that of [Energy][Length]$^{-1}$. Hence (6.3) could instead be considered a "polar coordinate" representation of the complex quantity that is the scalar field Φ, keeping in mind ρ and χ are not physical coordinates.

The inner products are done over the metric (3.25) in which $\Phi_{\rm G}$ now denote the gravitational potential[1]. Thus the kinetic term is

$$\begin{aligned} |\partial_\mu \Phi|^2 &= (\partial_\mu \Phi)^* (\partial^\mu \Phi) = g^{\mu\nu} (\partial_\mu \Phi)^* (\partial_\nu \Phi) \\ &= g^{00} (\partial_0 \Phi)^* (\partial_0 \Phi) + g^{ab} (\partial_a \Phi)^* (\partial_b \Phi)\,. \end{aligned}$$

The contravariant time-time component for the metric is determined by the condition that $g^{\mu\nu} g_{\mu\nu} \stackrel{!}{=} 4$:

$$g^{\mu\nu} g_{\mu\nu} = g^{00} g_{00} + g^{ab} g_{ab} = -g^{00} \left[1 + \frac{2\Phi_{\rm G}}{c^2}\right] + 3 \stackrel{!}{=} 4\,.$$

Thus g^{00} is simply $(g_{00})^{-1}$. In the weak-field limit is the case $\Phi_{\rm G} \ll c^2$, so g^{00} may be Taylor expanded for small $\Phi_{\rm G}/c^2$:

$$g^{00} = -\left[1 + \frac{2\Phi_{\rm G}}{c^2}\right]^{-1} = -\left[1 - \frac{2\Phi_{\rm G}}{c^2} + \mathcal{O}\left(\left[\frac{\Phi_{\rm G}}{c^2}\right]^2\right)\right] \simeq -\left[1 - \frac{2\Phi_{\rm G}}{c^2}\right]\,.$$

In the non-relativistic, weak-field limit, the field Φ is given by (6.3), and the kinetic term is then

$$|\partial_\mu \Phi|^2 = -\left[1 - \frac{2\Phi_{\rm G}}{c^2}\right] \left(\frac{1}{c}\frac{\partial}{\partial t} \rho e^{-i\chi}\right) \left(\frac{1}{c}\frac{\partial}{\partial t} \rho e^{i\chi}\right) + \left[\nabla\left(\rho e^{-i\chi}\right)\right] \cdot \left[\nabla\left(\rho e^{i\chi}\right)\right]\,,$$

where the differentials are

$$\frac{\partial}{\partial t} \rho e^{\pm i\chi} = \pm i \rho e^{\pm i\chi} \frac{\partial \chi}{\partial t} \qquad \nabla\left(\rho e^{\pm i\chi}\right) = (\nabla \rho)\, e^{\pm i\chi} + \rho\left(\nabla e^{\pm i\chi}\right)$$

[1] Since gravity is included, the partial derivatives should be replaced with covariant derivatives. Luckily, this is unnecessary here as the covariant derivative of a scalar field is equal to its partial derivative.

$$= e^{\pm i\chi}\left[(\nabla\rho) \pm i\rho\,(\nabla\chi)\right]$$

$$\frac{\partial\chi}{\partial t} = \frac{\dot{\theta} + mc^2}{\hbar} \qquad \nabla\chi = \frac{(\nabla\theta)}{\hbar}\,.$$

This inserted yields for the Lagrangian (6.1)

$$\begin{aligned}
\mathcal{L}_{\mathrm{KG}} &= -\frac{1}{2}\left\{-\left[1-\frac{2\Phi_{\mathrm{G}}}{c^2}\right]\frac{\rho^2}{c^2}\left(\frac{\partial\chi}{\partial t}\right)^2 + (\nabla\rho)^2 + \rho^2\,(\nabla\chi)^2 + \frac{m^2c^2}{\hbar^2}\,\rho^2\right\} \\
&= -\frac{1}{2}\left\{(\nabla\rho)^2 + \frac{\rho^2}{\hbar^2}\left[(\nabla\theta)^2 + m^2c^2\right] - \left[1-\frac{2\Phi_{\mathrm{G}}}{c^2}\right]\frac{\rho^2}{\hbar^2c^2}\left[\dot{\theta}^2 + (mc^2)^2 + 2mc^2\dot{\theta}\right]\right\} \\
&= -\frac{1}{2}\left\{(\nabla\rho)^2 + \frac{\rho^2}{\hbar^2}\left((\nabla\theta)^2 + m^2c^2 - \left[1-\frac{2\Phi_{\mathrm{G}}}{c^2}\right]\left[\frac{\dot{\theta}^2 + m^2c^4 + 2mc^2\dot{\theta}}{c^2}\right]\right)\right\} \\
&= -\frac{1}{2}\left\{(\nabla\rho)^2 + \frac{\rho^2}{\hbar^2}\left[(\nabla\theta)^2 + m^2c^2 - \left(m^2c^2 + 2m\dot{\theta} - 2m^2\Phi_{\mathrm{G}}\right)\right]\right\} \\
&= -\frac{1}{2}\left\{(\nabla\rho)^2 + \frac{2m\rho^2}{\hbar^2}\left[\frac{(\nabla\theta)^2}{2m} + m\Phi_{\mathrm{G}} - \dot{\theta}\right]\right\} \\
&= -\frac{1}{2}\left\{(\nabla\rho)^2 - \frac{2m\rho^2}{\hbar^2}\left[\dot{\theta} - m\Phi_{\mathrm{G}} - \frac{(\nabla\theta)^2}{2m}\right]\right\} \\
&= -\frac{1}{2}\left\{(\nabla\rho)^2 - \frac{2mX\rho^2}{\hbar^2}\right\}, \qquad (6.4)
\end{aligned}$$

where the scalar X from Chapter 3 has been identified, and the terms $\dot{\theta}^2/c^2$, $2\Phi_{\mathrm{G}}\dot{\theta}^2/c^4$ and $4m\dot{\theta}\Phi_{\mathrm{G}}/c^2$ are neglected following the applied limits. Hence the full Lagrangian is

$$\mathcal{L} = -\frac{1}{2}\left[(\nabla\rho)^2 - \frac{2mX\rho^2}{\hbar^2}\right] - \frac{\Lambda^4}{6\left(\Lambda_{\mathrm{c}}^2 + \rho^2\right)^6}\left[(\nabla\rho)^2 - \frac{2mX\rho^2}{\hbar^2}\right]^3. \qquad (6.5)$$

To leading order in derivatives, contributions from $(\nabla\rho)^2$ can be ignored. The equation for ρ is found by the Euler-Lagrange equation, which here reduces to

$$\begin{aligned}
\frac{\partial\mathcal{L}}{\partial\rho} = \frac{\partial}{\partial\rho}\left\{-\frac{1}{2}\left[-\frac{2mX\rho^2}{\hbar^2}\right] - \frac{\Lambda^4}{6\left(\Lambda_{\mathrm{c}}^2 + \rho^2\right)^6}\left[-\frac{2mX\rho^2}{\hbar^2}\right]^3\right\} &\stackrel{!}{=} 0 \\
\frac{2mX\rho}{\hbar^2} + \frac{8\Lambda^4m^3X^3}{6\hbar^6}\frac{\partial}{\partial\rho}\left\{\frac{\rho^6}{(\Lambda_c^2+\rho^2)^6}\right\} &= 0 \\
\frac{2mX\rho}{\hbar^2} + \frac{8\Lambda^4m^3X^3}{6\hbar^6}\left\{\frac{6\rho^5}{(\Lambda_c^2+\rho^2)^6} - \frac{12\rho^7}{(\Lambda_c^2+\rho^2)^7}\right\} &= 0 \\
\frac{2mX\rho}{\hbar^2}(\Lambda_c^2+\rho^2)^7 + \frac{\Lambda^4(2mX)^3\rho^5}{\hbar^6}[(\Lambda_c^2+\rho^2) - 2\rho^2] &= 0 \\
2mX\rho\left\{(\Lambda_c^2+\rho^2)^7 + \frac{\Lambda^4(2mX)^2\rho^4(\Lambda_c^2-\rho^2)}{\hbar^4}\right\} &= 0\,. \qquad (6.6)
\end{aligned}$$

The MOND limit $\rho \gg \Lambda_c$ is now applied, and subsequently justified by the result. The equation (6.6) is solved for ρ^2:

$$\begin{aligned}(\rho^2)^7 - \frac{\Lambda^4(2mX)^2(\rho^2)^3}{\hbar^4} &= 0 \\ (\rho^2)^4 &= \frac{\Lambda^4(2mX)^2}{\hbar^4} \\ \rho^2 &= \frac{\Lambda[(2mX)^2]^{1/4}}{\hbar} = \frac{\Lambda|2mX|^{1/2}}{\hbar}\,. \end{aligned} \tag{6.7}$$

The use of absolute values is necessary since, as shown in Chapter 4, the sign of X must be negative[2] to obtain a stable MOND regime in galaxies.

Now, (6.7) is inserted into (6.4) under the MOND limit, ignoring $(\nabla\rho)^2$,

$$\begin{aligned}\mathcal{L} &= -\frac{1}{2}\left[-\frac{2mX\rho^2}{\hbar^2}\right] - \frac{\Lambda^4}{6\,(\rho^2)^6}\left[-\frac{2mX\rho^2}{\hbar^2}\right]^3 \\ &= \frac{1}{2}\frac{2mX}{\hbar^2}\,\rho^2 + \frac{1}{6}\frac{\Lambda^4(2mX)^3}{\hbar^6(\rho^2)^3} \\ &= \frac{1}{2}\frac{\Lambda(2m)^{3/2}}{\hbar^3}X\sqrt{|X|} + \frac{1}{6}\frac{\Lambda^4(2mX)^3}{\hbar^6[\Lambda^3|2mX|^{3/2}/\hbar^3]} \\ &= \frac{1}{2}\frac{\Lambda(2m)^{3/2}}{\hbar^3}X\sqrt{|X|} + \frac{1}{6}\frac{\Lambda(2m)^{3/2}}{\hbar^3}\left(\frac{X}{|X|^{1/2}}\right)^3\,. \end{aligned}$$

The cubed fraction in the last term is

$$\begin{aligned}\left(\frac{X}{|X|^{1/2}}\right)^3 = \left(\frac{\mathrm{sgn}(X)|X|}{|X|^{1/2}}\right)^3 &= \left(\mathrm{sgn}(X)|X|^{1/2}\right)^3 = \mathrm{sgn}(X)^3|X|^{3/2} \\ &= \mathrm{sgn}(X)|X||X|^{1/2} = X|X|^{1/2}\,. \end{aligned}$$

The second-to-last equality used the fact that the sign of a real quantity when raised to an odd power is unchanged. Thus

$$\mathcal{L} = \frac{2\Lambda(2m)^{3/2}}{3\hbar^3}X\sqrt{|X|}\,, \tag{6.8}$$

and the action (6.2) in the non-relativistic, weak-field, MOND limit recovers the action (3.34) conjectured back in Chapter 3.

The scalar acceleration a_ϕ

As claimed, the conjectured MOND action (3.34) is reproduced from (6.6) assuming $\rho \gg \Lambda_c$, though [1] lists a less stringent bound $\rho \gtrsim \Lambda_c$, the so-called "MOND limit". This is further bolstered by realising that *if* the MOND limit corresponds to $\rho \gtrsim \Lambda_c$

[2] X^2 yields a positive value regardless of the sign of X, but $(X^2)^{1/4} = X^{1/2}$ does depend on the sign. Hence the absolute value function must be applied.

then (6.7) implies a direct relation between the scalar acceleration a_ϕ and Λ_c, since $2m|X| \simeq (\partial_r\phi)^2$ in the MONDian regime and $a_\phi \propto (\partial_r\phi)$, as discussed in Chapter 4.

The MOND limit thus yields

$$\begin{aligned} \rho^2 &\gtrsim \Lambda_c^2 \\ \frac{\Lambda|2mX|^{1/2}}{\hbar} &\gtrsim \Lambda_c^2 \\ |2mX| &\gtrsim \frac{\hbar^2\Lambda_c^4}{\Lambda^2} \\ (\partial_r\phi)^2 &\gtrsim \frac{\hbar^2\Lambda_c^4}{\Lambda^2}\,, \end{aligned}$$

where the acceleration (4.7) is inserted for $(\partial_r\phi)$,

$$\begin{aligned} \left(\frac{M_{\rm Pl}\hbar}{\alpha\Lambda}\,a_\phi\right)^2 &\gtrsim \frac{\hbar^2\Lambda_c^4}{\Lambda^2} \\ a_\phi &\gtrsim \frac{\alpha\Lambda_c^2}{M_{\rm Pl}}\,, \end{aligned}$$

and (4.18) is inserted for $\alpha/M_{\rm Pl}$:

$$a_\phi \gtrsim \hbar c\left(\frac{\Lambda_c}{\alpha\Lambda}\right)^2 a_0\,. \tag{6.9}$$

The content of (6.9) is that the RHS represents the breakdown acceleration scale of MOND, given Λ_c.

This is a bit different than in [1], namely in the extra factor $\hbar c\Lambda_c/\Lambda$ with respect to [1]. It was found that $|\Phi|^2$ must have units of [Energy][Length]$^{-1}$, and so must also the units of Λ_c^2. This means that the units of Λ_c^2 and Λ differ, whereas in [1] they have the same unit. The extra factor $\hbar c$ makes sure the units on both sides are equal.

The real point of having a_ϕ bounded by Λ_c is that, observationally, as mentioned in [1], MOND works well for accelerations down to $\sim a_0/10$. For instance, the fiducial value for Λ can also be inserted:

$$a_\phi \gtrsim \frac{\Lambda_c^2}{1.2893\,\mathrm{eV\,m^{-1}}}\,a_0\,, \tag{6.10}$$

which can be used to infer a value on Λ_c^2 such that MOND breaks down for accelerations $\lesssim a_0/10$. This implies $\Lambda_c^2 \simeq 0.12893\,\mathrm{eV\,m^{-1}}$, so MOND is valid provided

$$a_\phi \gtrsim \frac{a_0}{10}\,. \tag{6.11}$$

[1] also suggest that Λ_c can be fixed such that the breakdown occurs at the acceleration scales of the Milky Way dwarf spheroidals, which have caused some problems for MOND [57, 58]

Additional terms in $\mathcal{L}$

It is claimed [1] that a quartic term $\propto g\mathcal{L}_{\rm KG}^2$ may added to (6.2), provided MOND is recovered for vanishing coefficient g after the non-relativistic and weak-field limits have been applied, and that the corresponding condensate Lagrangian has correct sign for finite g. This can be further generalized to any $k_n\mathcal{L}_{\rm KG}^n$ addition.

This is only briefly mentioned here, though [1] does delve into calculations briefly.

6.2 Future considerations

The next step would be to implement finite-temperature effects, since this was deemed necessary in Chapter 4. To find a relativistic Lagrangian that reduces to (4.31), it must properly accommodate the new degrees of freedom that comes with the normal component of the fluid, with respect to their internal symmetries (as was done in Chapter 3).

In order to actually get MOND in galaxies, the scalar field that describes the phonons must couple to the baryon distribution. When considered in terms of particle physics and quantum field theory, this is reminiscent of the *Yukawa interaction*.

Yukawa interaction

In this theory, fermions interact through the exchange of virtual bosons [28]. More specifically, there is a force between two fermions, mediated by a meson. The similarity with superfluid dark matter is obvious: a MOND force is mediated between baryons by the Goldstone bosons of the superfluid.

Though phenomenologically different, the mathematics of the Yukawa interaction could possibly provide a starting point for the implementations of baryons within the context of this chapter.

Intriguingly, the force between fermions can be described by the *Yukawa potential* [28] (here presented within the context of quantum field theory, thus also in natural units):

$$V(r) = -\frac{g^2}{4\pi}\,\frac{e^{-m_\phi r}}{r}\,,$$

where g is a coupling parameter, and m_ϕ is the mass of the force mediating boson. The corresponding force is then

$$F(r) = -\frac{dV(r)}{dr} = -\frac{g^2}{4\pi}\left[\frac{m_\phi e^{-m_\phi r}}{r} + \frac{e^{-m_\phi r}}{r^2}\right].$$

This has one term[3] $\sim r^{-1}$, precisely that which is needed to analytically reproduce the BTFR.

[3] Sans the exponential in the numerator. As of now, this is mentioned *purely* as an example.

Chapter 7

Cosmology

The superfluid dark matter is considered in cosmological context. Dark matter is found to condense on cosmological scales, and as such the equation of state is investigated. A way to recover superfluid dark matter in form of non-relativistic dust, a temperature dependence on Λ is suggested by [1]. It is here compared on cosmological and galactic scales, and is found to be satisfactory.

Not done in [1] is the evolution of the condensate mass density in the expanding universe, but is done here.

Subsequently baryons are included, and to obtain dark matter as cosmological dust, the value of the superfluid phonon-baryon coupling parameter must be different than in galaxies. It is presented in [1] as dependent on temperature. It is here compared on cosmological and galactic scales, and is found to not be satisfactory as it is off by one order of magnitude. Consequently, the critical acceleration depends on on temperature.

As in all other chapters in this thesis, calculations are done in SI units.

7.1 Cosmological dark matter condensate

As found in Chapter 2, as in [1], the particle mass being in the sub-eV/c^2 range, axions (or at least axion like) and must have been produced by a displacement mechanism early in the universe. Unfortunately not reproduced here, [1] found that this must have happened when the corresponding baryon-photon temperature was at $T_i \sim 50$ TeV, here presented in natural units, around the weak scale as pointed out by [1]:

$$T_i \overset{\text{nat.}}{=} \sqrt{mM_{\text{Pl}}} \overset{\text{SI}}{=} \frac{\sqrt{mM_{\text{Pl}}}c^2}{k_{\text{B}}} \sim 10^{17}\,\text{K}\,,$$

where the fiducial particle mass has been inserted. What is meant by how this is related to the weak scale is that, when the temperature of the universe exceeds $\sim 10^{15}$ K, the electromagnetic and weak nuclear forces combine into the electroweak force according to [1].

The density redshifts cosmologically as $1/a^3$, and the velocity $1/a$, then considering the first dark matter condensation condition (2.3) it is clear it is independent of cosmic

time. Consequently, if it is satisfied at any time, it is satisfied at all times: as soon as it is generated cosmologically - dark matter enters, and remains in, the condensed state.

Not derived here, [1] found the temperature of the cosmological condensate to be

$$T/T_c \sim 10^{-28}\,, \tag{7.1}$$

to within a factor $m^{5/3}$ (which would be in natural units). The temperature in collapsed structures is given by (2.29), and (to within a factor $m^{8/3}$) is $\sim 10^{-7}$ for dwarf galaxies ($M \sim 10^6 h^{-1} M_\odot$) and $\sim 10^{-3}$ for massive galaxies ($M \sim 10^{12} h^{-1} M_\odot$). Therefore, the cosmological superfluid is very well approximated as a $T = 0$ superfluid.

7.2 Equation of state

Since cosmological dark matter is at a temperature much less than that needed for condensation to occur, it is well approximated by a $T = 0$ superfluid. Also, the equation of state $P = K\rho^3$ was found in Chapter 3.

Cosmologically, the equation of state of any fluid is given by $P = w\rho c^2$, where $w = 0$ for non-relativistic dust (CDM and baryons) and $w = 1/3$ for relativistic particles. Assuming the universe expands adiabatically, the time-evolution of the mass density is given by

$$\dot{\rho} = -3\,\frac{\dot{a}}{a}\left(\rho + \frac{P}{c^2}\right) = -3\,\frac{\dot{a}}{a}\,\rho\,(1+w)\,. \tag{7.2}$$

For cosmological superfluid dark matter, the parameter w varies quadratically with the cosmic mass density, the pressure given by (3.37)

$$w = \frac{P}{\rho} = \frac{\hbar^6}{12\Lambda_0^2 m^6}\frac{\rho^2}{c^2} = \frac{K\rho^2}{c^2} = \frac{1}{3}\frac{c_s^2}{c^2}\,, \tag{7.3}$$

where Λ_0 denotes the cosmological value for the theory scale parameter, and an additional factor c^2 in the denominator is added to make w unitless. The sound speed $c_s^2 = 3K\rho^2$ found in (3.46) has been recognized, and it does seems that a relativistic sound speed $c_s \sim c$ reproduces a relativistic equation of state, while $c_s \ll c$ reproduces the non-relativistic dust equation of state.

It is interesting that $\sqrt{w}c = c_s/\sqrt{3}$, which is *precisely* the propagation rate of second sound as mentioned in Chapter 1. Whether or not this is anything else than a coincidence is unclear.

Temperature-dependent theory scale Λ

The non-relativistic dust description of dark matter, "cold dark matter", is cosmologically preferable due to its successes on cosmological scale - see Chapter 1. With the equation of state (7.3), this can be achieved by having the theory scale Λ depend on temperature. Its cosmological value is denoted Λ_0, and a bound on it can be obtained by constraining $w \sim 0$.

This is achieved in [1] by having Λ depend on the temperature, subject to the constraint that the superfluid component behaves like CDM at least throughout the matter-dominated era - *i.e.*

$$\Lambda_0 \gg \frac{\hbar^3 \rho_{\rm eq}}{m^3 c} \approx 0.3688 \left(\frac{m}{\mathrm{eV}/c^2}\right)^{-1} \mathrm{eV}$$
$$\Lambda_0 \gg 1.7074\,\mathrm{eV}\,, \tag{7.4}$$

where $\rho_{\rm eq} \simeq 8.556 \times 10^{-17}$ and with the fiducial particle mass inserted. Thus the scale is at least three orders of magnitude large cosmologically than in galaxies, $\Lambda = 0.2\,\mathrm{meV}$. It is suggested in [1] to fix Λ in terms of temperature,

$$\Lambda(T) = \frac{\Lambda_0}{1 + \kappa_\Lambda (T/T_c)^{1/4}}\,, \tag{7.5}$$

where $\kappa_\Lambda \sim 10^4$ and T_c the BEC critical temperature.

As a check (without regards to the particle mass factor), compare the cosmological temperature (7.1) to that found in galaxies of mass $M \sim 10^{12} h^{-1}\, M_\odot$ found in (2.29). Cosmologically, the temperature term is of order $\sim 10^4 \times 10^{-28/4} = 10^{-3}$ and therefore negligible, and Λ takes its cosmological value Λ_0. For galactic temperatures given by (2.29), the temperature term is of order $\sim 10^4 \times 10^{-3/4} = 10^{3+1/4} \approx 10^3 \times 10^{1/4} \sim 10^3$, and Λ in galaxies is $\sim 10^{-3}\Lambda_0$, as it needs to.

Another way to ensure $w \sim 0$ is to consider the last equality in (7.3) in terms of the superfluid sound speed for dark matter only. This was done in Chapter 3 where it was found that $c_s^2 = 2\mu/m$, which leads to $\mu \ll 3mc^2/2$ and is thus of order the particle rest energy.

Evolution of the condensate density

Here I will solve the adiabatic equation (7.2) for the condensate density, with the pressure $P = K\rho^3 c^2$ where K is the proportionality constant of (7.3). The purpose is to check the deviation form the familiar $\rho_{\rm dust}(a) \propto a^{-3}$, while not considering the imposed temperature dependence of Λ for now. Equation (7.2) is solved for the density by integrating[1] from the present values, denoted by a subscripted "0", to some arbitrary values in some other time,

$$\dot\rho = -3\,\frac{\dot a}{a}\,\rho\left(1 + K\rho^2\right)$$
$$\int_{\rho_0}^{\rho} \frac{d\hat\rho}{\hat\rho(1 + K\hat\rho^2)} = -3\int_{a_0}^{a} \frac{d\hat a}{\hat a}$$
$$\left[\ln\left(\hat\rho\right) - \frac{1}{2}\,\ln\left(1 + K\hat\rho^2\right)\right]\Bigg|_{\hat\rho=\rho_0}^{\hat\rho=\rho} = -3\left[\ln(\hat a)\right]\Bigg|_{\hat a=a_0}^{\hat a=a}$$
$$\frac{\rho}{\rho_0}\sqrt{\frac{1 + K\rho_0^2}{1 + K\rho^2}} = \left(\frac{a}{a_0}\right)^{-3}\,.$$

[1] Integration variables are denoted with a "hat".

Setting $a_0 = 1$ and taking both sides to the second power, $\rho(a)$ can be obtained:

$$\begin{aligned}
\rho^2(1 + K\rho_0^2) &= \rho_0^2(1 + K\rho^2)a^{-6} \\
\rho^2(1 + K\rho_0^2) - \rho^2 K\rho_0^2 a^{-6} &= \rho_0^2 a^{-6} \\
\rho^2(1 + K\rho_0^2 - K\rho_0^2 a^{-6}) &= \rho_0^2 a^{-6} \\
\rho(a) &= \frac{\rho_0 a^{-3}}{\sqrt{1 + K\rho_0^2 - K\rho_0^2 a^{-6}}} \\
&= \frac{\rho_0}{\sqrt{(1 + K\rho_0^2)a^6 - K\rho_0^2}} \,. \qquad (7.6)
\end{aligned}$$

As expected the superfluid behaves as dust if the condition (7.4) is satisfied - $\rho \propto a^{-3}$. However, the temperature dependence of Λ must, in some way, vary such that a divergence at

$$a_d^6 = \frac{K\rho_0^2}{1 + K\rho_0^2} \qquad (7.7)$$

is avoided. This could provide an extra condition on the temperature dependence of Λ.

Finally, if there for some cosmic time the denominator is *not* comparable to a^3, the dark matter superfluid should be treated as its own contributor to the universe energy density. This leads to an additional term in the Friedmann equations, and therefore has an impact on the evolution of the scale factor a throughout cosmic time.

7.3 Coupling to baryons

The evolution of the cosmological superfluid is carried through its phase $\theta = \theta(t)$, where t represents cosmic time. The governing equation is the Euler-Lagrange equation for θ.

In an expanding universe, the metric is that of the Friedmann-Lemaître-Robertson-Walker kind, which, in matrix representation, is

$$g_{\mu\nu} = \mathrm{diag}(-1, a^2, a^2, a^2) \,, \qquad (7.8)$$

where $a = a(t)$ is the scale factor of the universe.

To find the equation of motion for the superfluid phase, consider the action

$$S = \int d^4x \sqrt{-g}\mathcal{L}$$

where the factor $\sqrt{-g}$, $g \equiv \det(g_{\mu\nu})$, is necessary to ensure correct transformation properties [91]. Redefine the integrand,

$$S = \int d^4x \, \mathcal{L}' \,, \qquad (7.9)$$

where $\mathcal{L}' = \sqrt{-g}\mathcal{L}$, then the Euler-Lagrange equation for θ follows from the principle of least action[2]. The variation is not done here, but the result for is the Euler-Lagrange

[2]When any system discribed by the integrand in (7.9) evolves from any time t_1 to any other given time t_2, it does so such that the action S is an extremal value (out of all possible values) [28].

equation for θ with the Lagrangian $\mathcal{L}' = \sqrt{-g}\mathcal{L}$ as the argument:

$$\frac{d}{dt}\left(\frac{\partial(\sqrt{-g}\mathcal{L})}{\partial\dot{\theta}}\right) = \frac{\partial(\sqrt{-g}\mathcal{L})}{\partial\theta}\,. \tag{7.10}$$

With the Lagrangian including baryons $\mathcal{L} = \mathcal{L}_{T=0} + \mathcal{L}_{\text{coupling}}$ given by (4.1) and (4.2) respectively is inserted, and

$$\frac{d}{dt}\left(\frac{\Lambda_0(2m)^{3/2}}{\hbar^3}\,a^3\dot{\theta}^{1/2}\right) = -\frac{\alpha_0\Lambda_0}{M_{\text{Pl}}\hbar}\,a^3\rho_{\text{b}}\,. \tag{7.11}$$

The RHS is constant, since $\rho_{\text{b}} \propto a^{-3}$ cosmologically,

$$\begin{aligned}\frac{(2m)^{3/2}}{\hbar^3}\,a^3\dot{\theta}^{1/2} &= -\frac{\alpha_0}{M_{\text{Pl}}\hbar}\,a^3\rho_{\text{b}}t + C\\ \frac{(2m)^{3/2}}{\hbar^3}\,\dot{\theta}^{1/2} &= -\frac{\alpha_0}{M_{\text{Pl}}\hbar}\,\rho_{\text{b}}t + \frac{C}{a^3}\,,\end{aligned}$$

where C is an integration constant. The LHS can be expressed by the mass density since $\rho = mn = m(dP/dX)$ with $X = \dot{\theta}$,

$$\begin{aligned}\rho = mn = m\frac{dP}{dX} = m\frac{dP}{d\dot{\theta}} = m\frac{d}{d\dot{\theta}}\left(\frac{2\Lambda_0(2m)^{3/2}}{3\hbar^3}\,\dot{\theta}^{3/2}\right) = m\,\frac{\Lambda_0(2m)^{3/2}}{\hbar^3}\,\dot{\theta}^{1/2} \qquad (7.12)\\ \Rightarrow \frac{(2m)^{3/2}}{\hbar^3}\,\dot{\theta}^{1/2} = \frac{\rho}{m\Lambda_0}\,.\end{aligned}$$

Then

$$\rho = -\frac{\alpha_0\Lambda_0}{M_{\text{Pl}}\hbar}\,m\,\rho_{\text{b}}\,t + \rho_{\text{dust}}\,,\ \text{where}\ \rho_{\text{dust}} = \frac{m\Lambda_0 C}{a^3}\,. \tag{7.13}$$

In the limit of vanishing baryon density, the density (7.13) must reduce to the density used in the previous Chapter, hence the latter term is identified as the dust contribution as discussed earlier. Note also that when $\dot{\theta} \sim mc^2$ implies that (7.12) reduces to $\rho \sim \Lambda_0 m^3 c/\hbar^3$, which is precisely the transition region between a relativistic and non-relativistic equation of state.

It should be noted that with (7.12) inserted into (7.11) yields a LHS $\sim d(a^3\rho)/dt = 3a^2\dot{a} + a^3\dot{\rho}$, and so (7.11) or (7.13) should be compared to the adiabatic equation (7.2).

Temperature-dependent interaction parameter α

Ultimately, we want the superfluid to behave as dust on cosmological scales. The conditions for this can be obtained by having the second term in eq. (7.13) dominate the first. This is done in [1] throughout the matter-dominated era, in which $t \propto a^{3/2}$ and the baryon contribution $\rho_{\text{b}}t$ redshifts as $a^{-3/2}$ while the dust contribution ρ_{dust} redshifts as a^{-3}. This dust domination is carried through all the way to today, in which case the present time is the age of the universe $t_0 = 13.8\,\text{Gyrs} = 4.352 \times 10^{17}\,s$,

$$\frac{\alpha_0\Lambda_0}{M_{\text{Pl}}\hbar}\,m\,\rho_{\text{b}}\,t_0 \leq \rho_{\text{dust}}\,.$$

This can be expressed as a boundary on the cosmological value of α, denoted by a subscripted "0",

$$\begin{aligned}\alpha_0 &\leq \frac{\rho_{\rm dust}}{\rho_{\rm b}}\,\frac{M_{\rm Pl}\hbar}{m\Lambda_0 t_0}\\ &\ll \frac{6M_{\rm Pl}c}{\rho_{\rm eq}\hbar^2 t_0}\,m^2\end{aligned} \tag{7.14}$$

where we have used the cosmological Λ_0 in (7.4) and the dust-to-baryon ratio is $\rho_{\rm dust}/\rho_{\rm b} = 6$. Thus

$$\alpha_0 \ll \frac{m^2}{1.8857\times10^{-67}\,{\rm kg}^2} = \frac{m^2}{1.6688\times10^4\,({\rm eV}/c^2)^2} = 6\times10^{-5}\left(\frac{m}{1\,{\rm eV}/c^2}\right)^2 . \tag{7.15}$$

Compared to the value found for galaxies, $\alpha \approx 2.5 \sim 1$, a temperature dependence of α is suggested in [1],

$$\alpha(T) = \alpha_0\left[1+\kappa_\alpha(T/T_c)^{1/4}\right]\ ,\ \kappa_\alpha \sim 10^4\,. \tag{7.16}$$

As done with Λ_0, compare the cosmological temperature (7.1) to that found in galaxies of mass $M \sim 10^{12}h^{-1}\,M_\odot$ found in (2.29) to within factors of particle mass. Cosmologically, the temperature term is of order $\sim 10^4\times10^{-28/4} = 10^{-3}$ and therefore negligible, and α takes its cosmological value α_0. For galactic temperatures given by (2.29), the temperature term is of order $\sim 10^4\times10^{-3/4}\sim10^3$, and α in galaxies is $\sim 10^3\alpha_0$, which is off by one order of magnitude.

In contrast to [1] the cosmological α_0 is not the same, though this may be fixed by setting $\kappa_\alpha \sim 10^5$ or greater. This theses will nonetheless use (7.16) as in [1].

Consequently the parameter $\alpha\Lambda$, with their temperature dependence given by (7.5) and (7.16), is nearly temperature independent on cosmological and galactic scales.

Velocity-dependent critical acceleration

An immediate consequence of the temperature dependence of α and Λ is that the MOND critical acceleration (4.18) is also dependent on temperature. As pointed out in [1]

$$a_0(T) \sim \alpha(T)(\alpha\Lambda)^2\,. \tag{7.17}$$

Thus by the condition (7.15), and the definition (4.18), the critical acceleration takes a different value on cosmological scales than in galaxies:

$$a_0^{\rm cosmo} \ll 10^{-4}a_0^{\rm galaxy}\,. \tag{7.18}$$

For galaxies, this temperature dependence implies that the galactic a_0 varies with the virial velocity of the halo, since the temperature is set by the virial velocity: $T = T_{\rm vir} = mv_{\rm vir}^2/2k_{\rm B}$. Specifically, a_0 decreases with the velocity, and therefore also the mass. [1] mentions that low-surface-brightness galaxies (LSBs) - low brightness dwarf galaxies with most of their baryonic matter in neutral gaseous hydrogen - have been observed to favor lower values of a_0 [102].

Chapter 8

Other consequences

This chapter takes up consequences of superfluid dark matter pertaining to Bose-Einstein condensate theory and astrophysics. Some new points regarding Bose-Einstein condensate theory is brought, while others points in general are either a explained little or kept as a summary if nothing is added with respect to [1].

8.1 Bose-Einstein condensate theory

The Gross-Pitaevskii equation

A BEC is a quantum state, and its attributes must therefore be studied in the context of quantum mechanics. The wave-function ϕ (which is normalized to the particle number density) of a BEC state is that which solves a non-linear form of the Schrödinger equation; the non-linearity comes from an inter-particle interaction term which contributes to the energy of the state. Usually this is done by the *Gross-Pitaevskii* equation, here given in the time-independent form,

$$-\frac{\hbar^2}{2m}\nabla^2\psi(\vec{r}) + V(\vec{r})\psi(\vec{r}) + U_0|\psi(\vec{r})|^2\psi(\vec{r}) = \mu\psi(\vec{r})\,, \tag{8.1}$$

in which the interactions are considered to be between two bodies, and are modeled as a contact interaction. In the G-P equation, U_0 is the *effective interaction* - a measure of the strength of the interaction - μ is the chemical potential, and V is the external potential energy.

The presented model [1], as was shown in Chapter 6, must have significant three-body interactions in order to obtain the wanted result. Therefore, the interaction term in the corresponding Gross-Pitaevskii equation must accommodate this. The potential term in the equation is that of gravitational potential energy, of which the potential itself also abide by Poisson's equation. This three-body interaction may also yield a different collective excitation spectrum, which means the sound speed would be different than what is traditionally calculated - see [83].

The Thomas-Fermi approximation

The non-linearity comes from the two-body interactions between particles in the condensed state, which are modeled as a contact interaction and goes as N^2. Thus for large particle number, the kinetic contribution may be neglected in what is called the *Thomas-Fermi approximation*. The resulting particle distribution is then, here in the context of standard condensate theory (two-body interactions),

$$|\psi|^2 = n = \frac{\mu - V}{U_0}\,, \tag{8.2}$$

In the context superfluid dark matter, here without baryons, the interaction contribution to the G-P equation is that of three-body interactions. Hence the G-P equation must accommodate this, while $V = m\Phi$ is the gravitational potential energy set up by the halo. The T-F approximation is very well applicable, since halos of this size have most of their particles in the condensed phase: The total number of particles in a halo of mass $M \sim 10^{12}\, M_\odot$ is $N \sim M/m \sim 10^{78}$, where $m \sim 10^{-36}$ kg is the fiducial particle mass.

Dark-bright solitons

This part is briefly mentioned in [1], and is also here, though with some background on *solitons*.

Solitons are exact, solitary wave solutions to the non-linear G-P equation that maintains its shape throughout propagation. They come in variations of two overlying kinds.

One kind is that of *dark* solitons, which have density minima. As an example consider a uniform medium in one dimension with a Gaussian depression with a minimum at some point x_0: it is a dark soliton if it propagates while keeping its Gaussian shape throughout.

The other is *bright* solitons, which have density maxima. As an example, consider a standard Gaussian with a maximum at some point x_0: it is a bright soliton if it propagates while keeping its Gaussian shape throughout. A more intuitive example would be the particle number density itself, in which case it would be a bright soliton with zero rate of propagation. The book [83] goes further in-depth than this thesis.

With respect to solitons, [1] mentions so-called *dark-bright* solitons - a form of interference pattern that have been observed in counterflowing BECs at supercritical velocities [103]. The interest is whether or not they can be used to explain the shell structure seen around elliptical galaxies - [104] for a study on this for NGC7600 in the context of CDM.

Vortices

When condensates rotate, or are confined in a rotating external potential, they pick up angular momentum provided the angular frequency of the rotation is above some critical value. This critical value marks the lowest angular frequency for which it is energetically favorable for the condensate to enter a state with angular momentum

vs. staying in the ground state. In simpler terms: the rotation must be high enough to excite the condensate into a state with angular momentum (this does not excite individual particles into the normal phase). However, the angular momentum is carried by vortices in the condensate plane of rotation. This is also due to an energy preference: it is preferable for the condensate to have N_v vortices of a single quanta of angular momentum, as opposed to a single vortex with N_v quanta of angular momentum - see[1] [83].

The critical angular frequency is, as in [1], given in [105]

$$\omega_\mathrm{crit} = \frac{\hbar}{mR^2} \ln\left(\frac{R}{\xi}\right) \tag{8.3}$$

Disregarding the logarithmic factor, [1] applies this for halo radius $R \sim 100$ kpc and particle mass $m \sim \mathrm{eV}/c^2$ which yields $\omega_\mathrm{crit} \sim 10^{-41}\,\mathrm{s}^{-1}$, and they use $\omega \sim 10^{-18}\,\mathrm{s}^{-1}$ for a halo with mass density $\rho \sim 10^{-25}\,\mathrm{g\,cm}^{-3}$. Thus $\omega \gg \omega_\mathrm{crit}$ and vortex generation occurs.

In fact, [105] has the vortex number density in the plane be $n_\mathrm{v} = 2m\omega/h$, and thus the total number of vortices

$$N_\mathrm{v} = \frac{2\pi m R^2}{h}\,\omega = \frac{\omega}{\omega_\mathrm{crit}}\,, \tag{8.4}$$

which, with the values above, yields $N_\mathrm{v} \sim 10^{23}$ neglecting the logarithmic factor in (8.3).

As discussed in *e.g.* [83], when many vortices are present, they tend to settle in a lattice configuration. Given certain conditions, the lattice can mimic rigid-body rotation, and have collective modes (sound- and shear waves) propagate through them. Whether or not this has any effect on a galaxy is not clear at this point, but could be of interest for further investigation of the dark matter superfluid theory.

Vortices also tend to move toward the outer regions of the rotating condensate, when the system is acted upon by a mechanism that dissipates angular momentum. This could, *e.g*, occur during fly-by events due to dynamical friction.

Superfluid surface tension

This was mentioned in context of "Tri-axial halos" in [1]. These are halos in which their extent in the three axes are not equal - they have *ellipticity* [106].

Superfluids have surface tension, and so the superfluid core tends to be isotropic Thus the ellipticity must be sourced by the normal component. This could, as [1] claims, provide bounds on the self-interaction cross-section between dark matter particles in the normal phase, which is only mentioned here in passing.

An other property pertaining to surface tension is that of *surface modes*. As a most basic interpretation, they are analogous to normal waves in water. Mechanism that generate these modes, and whether or not they are significant, could be considered in future work.

[1] This is done in terms of *quantized circulation* about the axis of rotation. However, in terms of vortex states, circulation and angular momentum are (somewhat) related.

Finite sound speed

In the MOND regime, the sound speed varies inversely with distance from a baryon source. For an already collapsed halo the MOND behaviour can be obtained by having a static, spherically symmetric effective potential that accounts for this. For a halo in the process of collapse, this may not be the case and other methods to accommodate this must be employed when considering (small-scale?) structure formation.

Again, the property *second sound* is mentioned, though only as a reminder seeing as its effect on the theory presented is still uncertain.

8.2 Astrophysics

General Relativity

The only exploration that [1] did into general relativity was a comparison to gravitational lensing in the weak-field, quasi-static regime within the context of TeVeS [69].

In TeVeS, there is no dark matter, and to obtain proper gravitational lensing the baryon distribution must couple to a scalar field, which itself couples to a time-like vector field. Within the weak-field, quasi-static regime, the gravitational potential Φ is sourced by only baryons.

In the superfluid dark matter framework, the theory provides a scalar field in the superfluid phase θ, as well as the time-like vector field that is the dark matter normal component four-velocity u^μ. In the appropriate regime, the gravitational potential is then sourced by both dark matter and baryons.

Superfluid dark matter can then be thought of as providing the necessary scalar and vector fields that make TeVeS yield correct inferred mass density with respect to gravitational lensing.

Mergers - *e.g.* the "Bullet" and "Counter-Bullet"

It is brought up [1] how infall velocity v_{infall} for merging galaxies with respect to the phonon sound speed c_s can affect the following events.

If $v_{\text{infall}} \gtrsim c_s$ the halos will be driven out of equilibrium, and dark matter particles are excited into the normal phase. Thus, dynamical friction leads to a rapid halo merger.

If $v_{\text{infall}} \lesssim c_s$ the superfluid cores will pass through each other, and the dynamical friction between the halos is reduced due to the superfluid cores. Thus, halo merger will take longer, possibly resulting in multiple encounters.

The "Bullet" and "Counter-Bullet"

The "Bullet" Cluster consists of two colliding galaxy clusters, and has been studied with regards to dark matter - see *e.g.* [107, 68] - due to the inferred matter distribution from weak gravitational lensing surveys. The lensing places the mass peak (highest concentration of matter) centered at the galaxies as opposed to the X-ray luminosity peak (gas from the two clusters collide and are shock-heated). As [1] mentions, this is

expected from CDM, where the weakly interacting dark matter particles pass by each other.

This has been used to calculate bounds on the self-interaction cross-section [88], the very one that was used in Chapter 2. It was, however, pointed out in [1] that the superfluid dark matter framework should be considered on its own, since it has two components as opposed to self-interacting dark matter's one.

Instead [1] focuses on whether the relative velocity between the two cluster is sub-sonic or ultra-sonic. Specifically, in the sub-sonic case the superfluid components are expected to flow through each other. Two distinct features from lensing surveys are subsequently expected: mass peaks that coincide with the superfluid cores, and one mass peak coincident with the X-ray peak due to the normal component.

This is not only the case for the "Bullet" cluster, but [1] also claims that this phenomenology can explain the "train wreck" Abell 520 merging system - see *e.g.* [108, 109] - also known as the "Counter-Bullet". The differing property from the "Bullet" cluster is that Abell 520 has a "dark core" centered on the X-ray louminosity peak. This means that, in addition to the peaks at bright galaxies away from the X-ray emitting gas (as it is in the "Bullet" case), there is *also* such a peak located around the gas *without* any corresponding bright galaxies.

In the context of superfluid dark matter, [1] attributes this "dark core" to the peak corresponding to the normal component.

Dynamical friction

A simple understanding of this concept is gained by imagining an incident object (either a globular cluster or a small galaxy) enters larger collection of gas, stars and dark matter at a constant density (*e.g.* a galaxy cluster). Upon entering, the object will lose kinetic energy due to gravitational interactions with the constituents of the collection gaining kinetic energy through conservation of energy[110].

It is pointed out [1] that the reduced dynamical friction due to the superfluid can help alleviate some minor problems with CDM, and lists some examples.

A counter-example in the form of the Fornax dwarf spheroidal is also brought up, leading to the conclusion that more work is necessary.

Vast planar structures and tidal dwarfs

As explained in Chapter 1, the tidal dwarfs of the Milky Way and Andromeda could have been generated following an ancient fly-by event. This works in MOND as there is only stellar dynamical friction, but not in ΛCDM as the dynamical friction within their dark matter halo would would yield a rapid halo merger.

Again, the reduced dynamical friction comes to the rescue, given the infall velocity at fly-by is subsonic. As mentioned in [1], if the fly-by stripped a tiny amount of superfluid dark matter from the host galaxies, the dynamics of the tidal dwarfes will be governed by MOND. This automatically leads to rotation curves that fall on the BTFR [51, 52].

Globular clusters

A globular cluster is a collection of stars in a spherical distribution that exists within the galaxy (paraphrased from [110]).

Stated in [1], these have negligible amounts of dark matter *and* their dynamics are very well described by Newtonian physics using only baryons, which spells trouble for MOND [60]. This is not a problem within the framework of superfluid dark matter, as dark matter is needed to obtain MOND in the first place.

Extragalactic structures

The imposed temperature-dependence of the theory parameters Λ and α could have an impact on the boundary of a collapsed object and the rest of the universe, as opposed to just *within* the collapsed object. This could even be important to consider when studying the cosmic web (walls and filaments between clusters).

Chapter 9

Summary

This thesis has reformulated [1] in SI units with the inclusion of intermediate, and more precise, steps in the calculations.

Initially the introductory chapter is similar, though including more history of dark matter as a concept and the need for it, as was a short description of superfluidity as a property of Bose-Einstein condensates. It was pointed out that phonons within the superfluid are generated by gravitational potentials sourced by baryons.

In Chapter 2, a different model of the mean interparticle separation was used, yielding a higher bound on the dark matter particle mass. This lead to a lower critical temperature on the onset of Bose-Einstein condensation, as well as an ever-so-slightly lower condensed fraction of particles in virialized halos. Consequently, the dark matter particle mass was taken to be in the sub-eV/c^2 range.

The groundwork for the relativistic effective field theory of superfluids at finite temperature was summarized from [89], and subsequently applied to the Newtonian limit. Following this, the zero-temperature, pure condensate was investigated, and the scale Λ_s suppressing higher-order contributions of the theory was identified. The dark matter halo profile was studied, and, due to the more precise calculations, a smaller radial extent of the condensate was found. Subsequently, Λ_s was found to be in the meV range within galaxies.

Starting at zero temperature, the acceleration of baryons due to the superfluid phonons was derived and compared to the critical acceleration of MOND. However, the theory is not stable to perturbations. Including baryons, the scalar acceleration was found to be closer to the MONDian one at all radial distances than in [1]. It was found that the standard gravitational acceleration due to dark matter is not negligible at large radii, in contrast to [1]. Finally, the theory is stable to perturbations, given appropriate conditions.

The speed of sound with the finite-temperature, baryon-including framework was derived, and further applied in the following chapter. This was in opposition of [1], where the sound speed derived in Chapter 3, the condensate-only scenario, was used. Landau's stability criterion for superfluid flow was found to not be satisfied, meaning generation of phonons is guaranteed. Higher-order contributions to the theory are suppressed

down to millimeter scales, ensuring the theory is applicable on galactic scales. The higher bound on the dark matter particle mass found in Chapter 2, lead to an increased critical (thermal) velocity for Bose-Einstein condensation, yielding an even lower bound on coherence breaking with respect to radial distance from the baryonic source. As an example, coherence was found to be broken within the Solar System, meaning dark matter particles are in the normal phase. It is pointed out that coherence breaking occurs when the superfluid reaches lightly relativistic speeds, indicating that this needs to be re-evaluated in a relativistic context.

A relativistic theory was suggested, which was shown to reduce to the proper condensate theory in the non-relativistic, weak-field regime. It implied a significant contribution from three-body interactions. A lower bound on the MONDian regime, with respect to the scalar acceleration, was found, and a starting point for the inclusion of coupling to baryonic matter was suggested.

Dark matter was found to be very well approximated as a zero-temperature superfluid on cosmological scales. By constraining the superfluid to behave like dust, a temperature dependence on the theory scale Λ was suggested. The evolution of cosmological condensate density was calculated, revealing an interesting point in cosmic time. Inclusion of baryons lead to suggesting a temperature dependence of the coupling parameter α. This further implied the critical acceleration within MOND depends on temperature, which for halos correspond to the mass of the halo.

Consequences of such a theory is investigated briefly within the context of standard Bose-Einstein condensate theory and astrophysics. For the former, it was pointed out that the three-body interactions must be properly accounted for, if the theory is to be investigated in the context of Bose-Einstein condensate theory. In case of the latter, the proposed framework provide an origin for the scalar and timelike vector field postulated in TeVeS, the inferred mass peaks in cluster mergers has a natural explanation within the framework of superfluid dark matter, given the relative velocity between clusters is less than that which excites dark matter into the normal phase, as well as how tidal dwarfs fall within the BTFR.

Bibliography

[1] L. Berezhiani and J. Khoury, "Theory of dark matter superfluidity," *Physical Review D*, vol. 92, no. 10, p. 103510, 2015.

[2] G. Bertone and D. Hooper, "A history of dark matter," *arXiv preprint arXiv:1605.04909*, 2016.

[3] F. Zwicky, "Die rotverschiebung von extragalaktischen nebeln," *Helvetica Physica Acta*, vol. 6, pp. 110–127, 1933.

[4] M. Schwarzchild, "Mass distribution and mass-luminosity ratios in galaxies," *Astron. J*, vol. 59, pp. 273–284, 1954.

[5] A. Penzias, "Free hydrogen in the pegasus i cluster of galaxies.," *The Astronomical Journal*, vol. 66, p. 293, 1961.

[6] N. J. Woolf, "On the stabilization of clusters of galaxies by ionized gas," *The Astrophysical Journal*, vol. 148, p. 287, 1967.

[7] B. E. Turnrose and H. J. Rood, "On the hypothesis that the coma cluster is stabilized by a massive, ionized intergalactic gas," *The Astrophysical Journal*, vol. 159, p. 773, 1970.

[8] J. F. Meekins, G. Fritz, T. A. Chubb, H. Friedman, and R. C. HENRY, "Physical sciences: X-rays from the coma cluster of galaxies," *Nature*, vol. 231, no. 5298, p. 107, 1971.

[9] V. C. Rubin and W. K. Ford Jr, "Rotation of the andromeda nebula from a spectroscopic survey of emission regions," *The Astrophysical Journal*, vol. 159, p. 379, 1970.

[10] M. S. Roberts, "A high-resolution 21-cm hydrogen-line survey of the andromeda nebula," *The Astrophysical Journal*, vol. 144, p. 639, 1966.

[11] V. C. Rubin, N. Thonnard, and W. Ford Jr, "Extended rotation curves of high-luminosity spiral galaxies. iv-systematic dynamical properties, sa through sc," *The Astrophysical Journal*, vol. 225, pp. L107–L111, 1978.

[12] T. Lasserre and E. Collaboration, "Not enough stellar mass machos in the galactic halo," *Arxiv preprint astro-ph/0002253*, 2000.

[13] P. Tisserand, L. Le Guillou, C. Afonso, J. Albert, J. Andersen, R. Ansari, É. Aubourg, P. Bareyre, J. Beaulieu, X. Charlot, *et al.*, "Limits on the macho content of the galactic halo from the eros-2 survey of the magellanic clouds," *Astronomy & Astrophysics*, vol. 469, no. 2, pp. 387–404, 2007.

[14] P. A. Ade, N. Aghanim, M. Arnaud, M. Ashdown, J. Aumont, C. Baccigalupi, A. Banday, R. Barreiro, J. Bartlett, N. Bartolo, *et al.*, "Planck 2015 results-xiii. cosmological parameters," *Astronomy & Astrophysics*, vol. 594, p. A13, 2016.

[15] S. Sarkar, "23. big-bang nucleosynthesis,"

[16] R. Miller, K. Prendergast, and W. J. Quirk, "Numerical experiments in spiral structure," in *The Spiral Structure of Our Galaxy*, pp. 365–367, Springer, 1970.

[17] F. Hohl, "Numerical experiments with a disk of stars," *The Astrophysical Journal*, vol. 168, p. 343, 1971.

[18] J. P. Ostriker and P. J. Peebles, "A numerical study of the stability of flattened galaxies: or, can cold galaxies survive?," *The Astrophysical Journal*, vol. 186, pp. 467–480, 1973.

[19] J. R. Bond, G. Efstathiou, and J. Silk, "Massive neutrinos and the large-scale structure of the universe," *Physical Review Letters*, vol. 45, no. 24, 1980.

[20] J. Bond and A. Szalay, "The collisionless damping of density fluctuations in an expanding universe," 1983.

[21] M. Davis, J. Huchra, D. W. Latham, and J. Tonry, "A survey of galaxy redshifts. ii-the large scale space distribution," *The Astrophysical Journal*, vol. 253, pp. 423–445, 1982.

[22] S. D. White, C. Frenk, and M. Davis, "Clustering in a neutrino-dominated universe," *The Astrophysical Journal*, vol. 274, pp. L1–L5, 1983.

[23] P. J. E. Peebles, "Primeval adiabatic perturbations-effect of massive neutrinos," *The Astrophysical Journal*, vol. 258, pp. 415–424, 1982.

[24] D. N. Schramm and G. Steigman, "Relic neutrinos and the density of the universe," *The Big Bang and Other Explosions in Nuclear and Particle Astrophysics. Edited by SCHRAMM DAVID N. Published by World Scientific Publishing Co. Pte. Ltd., 1996. ISBN# 9789812831538, pp. 439-445*, pp. 439–445, 1996.

[25] S. P. Martin, "A supersymmetry primer," in *Perspectives on supersymmetry II*, pp. 1–153, World Scientific, 2010.

[26] G. Bertone, *Particle dark matter: observations, models and searches*. Cambridge University Press, 2010.

[27] T. Mannel, "Theory and phenomenology of cp violation," *Nuclear Physics B-Proceedings Supplements*, vol. 167, pp. 170–174, 2007.

[28] M. E. Peskin, *An introduction to quantum field theory*. CRC Press, 2018.

[29] E. Castellani, "On the meaning of symmetry breaking," *Symmetries in physics: Philosophical reflections*, pp. 321–334, 2003.

[30] R. D. Peccei, "The Strong CP problem and axions," *Lect. Notes Phys.*, vol. 741, pp. 3–17, 2008. [,3(2006)].

[31] L. F. Abbott and P. Sikivie, "A cosmological bound on the invisible axion," *Physics Letters B*, vol. 120, no. 1-3, pp. 133–136, 1983.

[32] M. Dine and W. Fischler, "The not-so-harmless axion," *Physics Letters B*, vol. 120, no. 1-3, pp. 137–141, 1983.

[33] J. Preskill, M. B. Wise, and F. Wilczek, "Cosmology of the invisible axion," *Physics Letters B*, vol. 120, no. 1-3, pp. 127–132, 1983.

[34] G. Steigman and M. S. Turner, "Cosmological constraints on the properties of weakly interacting massive particles," *Nuclear Physics B*, vol. 253, pp. 375–386, 1985.

[35] B. Moore, S. Ghigna, F. Governato, G. Lake, T. Quinn, J. Stadel, and P. Tozzi, "Dark matter substructure within galactic halos," *The Astrophysical Journal Letters*, vol. 524, no. 1, p. L19, 1999.

[36] B. Willman, M. R. Blanton, A. A. West, J. J. Dalcanton, D. W. Hogg, D. P. Schneider, N. Wherry, B. Yanny, and J. Brinkmann, "A New Milky Way companion: Unusual globular cluster or extreme dwarf satellite?," *Astron. J.*, vol. 129, pp. 2692–2700, 2005.

[37] V. Belokurov *et al.*, "Cats and Dogs, Hair and A Hero: A Quintet of New Milky Way Companions," *Astrophys. J.*, vol. 654, pp. 897–906, 2007.

[38] E. J. Tollerud, J. S. Bullock, L. E. Strigari, and B. Willman, "Hundreds of Milky Way Satellites? Luminosity Bias in the Satellite Luminosity Function," *Astrophys. J.*, vol. 688, pp. 277–289, 2008.

[39] S. Walsh, B. Willman, and H. Jerjen, "The Invisibles: A Detection Algorithm to Trace the Faintest Milky Way Satellites," *Astron. J.*, vol. 137, p. 450, 2009.

[40] M. S. Bovill and M. Ricotti, "Where are the fossils of the first galaxies? ii. true fossils, ghost halos, and the missing bright satellites," *The Astrophysical Journal*, vol. 741, no. 1, p. 18, 2011.

[41] M. Boylan-Kolchin, J. S. Bullock, and M. Kaplinghat, "Too big to fail? the puzzling darkness of massive milky way subhaloes," *Monthly Notices of the Royal Astronomical Society: Letters*, vol. 415, no. 1, pp. L40–L44, 2011.

[42] M. Boylan-Kolchin, J. S. Bullock, and M. Kaplinghat, "The milky way's bright satellites as an apparent failure of λcdm," *Monthly Notices of the Royal Astronomical Society*, vol. 422, no. 2, pp. 1203–1218, 2012.

[43] P. Kroupa, C. Theis, and C. M. Boily, "The Great disk of Milky Way satellites and cosmological sub-structures," *Astron. Astrophys.*, vol. 431, pp. 517–521, 2005.

[44] M. Pawlowski, J. Pflamm-Altenburg, and P. Kroupa, "The vpos: a vast polar structure of satellite galaxies, globular clusters and streams around the milky way," *Monthly Notices of the Royal Astronomical Society*, vol. 423, no. 2, pp. 1109–1126, 2012.

[45] M. S. Pawlowski, P. Kroupa, and H. Jerjen, "Dwarf Galaxy Planes: the discovery of symmetric structures in the Local Group," *Mon. Not. Roy. Astron. Soc.*, vol. 435, p. 1928, 2013.

[46] M. S. Pawlowski and P. Kroupa, "The rotationally stabilized VPOS and predicted proper motions of the Milky Way satellite galaxies," *Mon. Not. Roy. Astron. Soc.*, vol. 435, p. 2116, 2013.

[47] R. A. Ibata *et al.*, "A Vast Thin Plane of Co-rotating Dwarf Galaxies Orbiting the Andromeda Galaxy," *Nature*, vol. 493, pp. 62–65, 2013.

[48] A. R. Conn *et al.*, "The Three-Dimensional Structure of the M31 Satellite System: Strong Evidence for an Inhomogeneous Distribution of Satellites," *Astrophys. J.*, vol. 766, p. 120, 2013.

[49] R. A. Ibata, N. G. Ibata, G. F. Lewis, N. F. Martin, A. Conn, P. Elahi, V. Arias, and N. Fernando, "A thousand shadows of Andromeda: rotating planes of satellites in the Millennium-II cosmological simulation," *Astrophys. J.*, vol. 784, p. L6, 2014.

[50] M. S. Pawlowski, P. Kroupa, and K. S. de Boer, "Making counter-orbiting tidal debris-the origin of the milky way disc of satellites?," *Astronomy & Astrophysics*, vol. 532, p. A118, 2011.

[51] F. Bournaud, P. A. Duc, E. Brinks, M. Boquien, P. Amram, U. Lisenfeld, B. S. Koribalski, F. Walter, and V. Charmandaris, "Missing Mass in Collisional Debris from Galaxies," *Science*, vol. 316, p. 1166, 2007.

[52] G. Gentile, B. Famaey, F. Combes, P. Kroupa, H. S. Zhao, and O. Tiret, "Tidal dwarf galaxies as a test of fundamental physics," *Astron. Astrophys.*, vol. 472, p. L25, 2007.

[53] B. Famaey and S. McGaugh, "Modified Newtonian Dynamics (MOND): Observational Phenomenology and Relativistic Extensions," *Living Rev. Rel.*, vol. 15, p. 10, 2012.

[54] M. Milgrom, "M. milgrom, astrophys. j. 270, 365 (1983).," *Astrophys. J.*, vol. 270, p. 365, 1983.

[55] M. Milgrom, "A modification of the newtonian dynamics as a possible alternative to the hidden mass hypothesis," *The Astrophysical Journal*, vol. 270, pp. 365–370, 1983.

[56] M. Milgrom, "A modification of the newtonian dynamics-implications for galaxies," *The Astrophysical Journal*, vol. 270, pp. 371–389, 1983.

[57] O. E. Gerhard and D. N. Spergel, "Dwarf spheroidal galaxies and non-newtonian gravity," *The Astrophysical Journal*, vol. 397, pp. 38–43, 1992.

[58] M. Milgrom, "MOND and the seven dwarfs," *Astrophys. J.*, vol. 455, p. 439, 1995.

[59] S. S. McGaugh and J. Wolf, "Local group dwarf spheroidals: correlated deviations from the baryonic tully-fisher relation," *The Astrophysical Journal*, vol. 722, no. 1, p. 248, 2010.

[60] R. Ibata, A. Sollima, C. Nipoti, M. Bellazzini, S. C. Chapman, and E. Dalessandro, "The globular cluster NGC 2419: a crucible for theories of gravity," *Astrophys. J.*, vol. 738, p. 186, 2011.

[61] S. McGaugh and M. Milgrom, "Andromeda Dwarfs in Light of MOND," *Astrophys. J.*, vol. 766, p. 22, 2013.

[62] S. McGaugh and M. Milgrom, "Andromeda Dwarfs in Light of MOND. II. Testing Prior Predictions," *Astrophys. J.*, vol. 775, p. 139, 2013.

[63] A. L. Serra, G. W. Angus, and A. Diaferio, "Implications for dwarf spheroidal mass content from interloper removal," *Astronomy & Astrophysics*, vol. 524, p. A16, 2010.

[64] H. Zhao, B. Famaey, F. Lüghausen, and P. Kroupa, "Local Group timing in Milgromian dynamics. A past Milky Way-Andromeda encounter at z>0.8," *Astron. Astrophys.*, vol. 557, p. L3, 2013.

[65] C. Nipoti, P. Londrillo, and L. Ciotti, "Galaxy merging in MOND," *Mon. Not. Roy. Astron. Soc.*, vol. 381, p. 104, 2007.

[66] O. Tiret and F. Combes, "Interacting Galaxies with MOND," *ASP Conf. Ser.*, vol. 396, p. 259, 2008.

[67] F. Combes and O. Tiret, "Mond and the galaxies," in *AIP Conference Proceedings*, vol. 1241, pp. 154–161, AIP, 2010.

[68] D. Clowe, M. Bradac, A. H. Gonzalez, M. Markevitch, S. W. Randall, C. Jones, and D. Zaritsky, "A direct empirical proof of the existence of dark matter," *Astrophys. J.*, vol. 648, pp. L109–L113, 2006.

[69] J. D. Bekenstein, "Relativistic gravitation theory for the MOND paradigm," *Phys. Rev.*, vol. D70, p. 083509, 2004. [Erratum: Phys. Rev.D71,069901(2005)].

[70] M. Feix, C. Fedeli, and M. Bartelmann, "Asymmetric Gravitational Lenses in TeVeS and Application to the Bullet Cluster," *Astron. Astrophys.*, 2007. [Astron. Astrophys.480,313(2008)].

[71] S. Dodelson and M. Liguori, "Can Cosmic Structure form without Dark Matter?," *Phys. Rev. Lett.*, vol. 97, p. 231301, 2006.

[72] C. Skordis, D. F. Mota, P. G. Ferreira, and C. Boehm, "Large Scale Structure in Bekenstein's theory of relativistic Modified Newtonian Dynamics," *Phys. Rev. Lett.*, vol. 96, p. 011301, 2006.

[73] G. W. Angus, A. Diaferio, B. Famaey, and K. J. van der Heyden, "Cosmological simulations in MOND: the cluster scale halo mass function with light sterile neutrinos," *Mon. Not. Roy. Astron. Soc.*, vol. 436, p. 202, 2013.

[74] G. W. Angus, A. Diaferio, B. Famaey, G. Gentile, and K. J. van der Heyden, "Modified Baryonic Dynamics: two-component cosmological simulations with light sterile neutrinos," *JCAP*, vol. 1410, no. 10, p. 079, 2014.

[75] L. Blanchet, "Gravitational polarization and the phenomenology of MOND," *Class. Quant. Grav.*, vol. 24, pp. 3529–3540, 2007.

[76] L. Blanchet and A. Le Tiec, "Model of Dark Matter and Dark Energy Based on Gravitational Polarization," *Phys. Rev.*, vol. D78, p. 024031, 2008.

[77] H. Zhao, "Reinterpreting MOND: Coupling of Einsteinian gravity and spin of cosmic neutrinos?," 2008.

[78] J.-P. Bruneton, S. Liberati, L. Sindoni, and B. Famaey, "Reconciling MOND and dark matter?," *JCAP*, vol. 0903, p. 021, 2009.

[79] B. Li and H. Zhao, "A Realistic Cosmology Without Cold Dark Matter," *Phys. Rev.*, vol. D80, p. 064007, 2009.

[80] C. M. Ho, D. Minic, and Y. J. Ng, "Cold Dark Matter with MOND Scaling," *Phys. Lett.*, vol. B693, pp. 567–570, 2010.

[81] C. M. Ho, D. Minic, and Y. J. Ng, "Quantum Gravity and Dark Matter," *Gen. Rel. Grav.*, vol. 43, pp. 2567–2573, 2011. [Int. J. Mod. Phys.D20,2887(2011)].

[82] C. M. Ho, D. Minic, and Y. J. Ng, "Dark Matter, Infinite Statistics and Quantum Gravity," *Phys. Rev.*, vol. D85, p. 104033, 2012.

[83] C. Pethick and H. Smith, "Bose-einstein condensation in dilute gases," *Bose-Einstein Condensation in Dilute Gases, by CJ Pethick, H. Smith, Cambridge, UK: Cambridge University Press, 2008*, 2008.

[84] `https://www.dropbox.com/s/f5k77llfodg7cep/lecture4notes_2017.pdf?dl=0`.

[85] `https://www.dropbox.com/s/rjifo72avpkxoxl/lecture5notes_2017.pdf?dl=0`.

[86] P. Sikivie and Q. Yang, "Bose-einstein condensation of dark matter axions," *Physical Review Letters*, vol. 103, no. 11, p. 111301, 2009.

[87] R. Kippenhahn, A. Weigert, and A. Weiss, *Stellar structure and evolution*, vol. 282. Springer, 1990.

[88] S. W. Randall, M. Markevitch, D. Clowe, A. H. Gonzalez, and M. Bradač, "Constraints on the self-interaction cross section of dark matter from numerical simulations of the merging galaxy cluster 1e 0657–56," *The Astrophysical Journal*, vol. 679, no. 2, p. 1173, 2008.

[89] A. Nicolis, "Low-energy effective field theory for finite-temperature relativistic superfluids," 2011.

[90] D. Son and M. Wingate, "General coordinate invariance and conformal invariance in nonrelativistic physics: Unitary fermi gas," *Annals of Physics*, vol. 321, no. 1, pp. 197–224, 2006.

[91] S. M. Carroll, *Spacetime and geometry: An introduction to general relativity*. 2004.

[92] S. Dubovsky, T. Grégoire, A. Nicolis, and R. Rattazzi, "Null energy condition and superluminal propagation," *Journal of High Energy Physics*, vol. 2006, no. 03, p. 025, 2006.

[93] S. Endlich, A. Nicolis, R. Rattazzi, and J. Wang, "The quantum mechanics of perfect fluids," *Journal of High Energy Physics*, vol. 2011, no. 4, p. 102, 2011.

[94] `https://www.astro.princeton.edu/~gk/A403/polytrop.pdf`.

[95] P. J. McMillan, "Mass models of the milky way," *Monthly Notices of the Royal Astronomical Society*, vol. 414, no. 3, pp. 2446–2457, 2011.

[96] O. Y. Gnedin, W. R. Brown, M. J. Geller, and S. J. Kenyon, "The mass profile of the galaxy to 80 kpc," *The Astrophysical Journal Letters*, vol. 720, no. 1, p. L108, 2010.

[97] `https://www.space.com/29270-milky-way-size-larger-than-thought.html`.

[98] B. Gripaios, "Lectures on effective field theory," *arXiv preprint arXiv:1506.05039*, 2015.

[99] `https://ssd.jpl.nasa.gov/horizons.cgi#top`.

[100] H. Fahr, T. Kausch, and H. Scherer, "A 5-fluid hydrodynamic approach to model the solar system-interstellar medium interaction," *Astronomy and Astrophysics*, vol. 357, pp. 268–282, 2000.

[101] R. Essig, J. A. Jaros, W. Wester, P. H. Adrian, S. Andreas, T. Averett, O. Baker, B. Batell, M. Battaglieri, J. Beacham, *et al.*, "Dark sectors and new, light, weakly-coupled particles," *arXiv preprint arXiv:1311.0029*, 2013.

[102] R. Swaters, R. Sanders, and S. McGaugh, "Testing modified newtonian dynamics with rotation curves of dwarf and low surface brightness galaxies," *The Astrophysical Journal*, vol. 718, no. 1, p. 380, 2010.

[103] J. González and F. Guzmán, "Interference pattern in the collision of structures in the bose-einstein condensate dark matter model: Comparison with fluids," *Physical Review D*, vol. 83, no. 10, p. 103513, 2011.

[104] A. P. Cooper, D. Martínez-Delgado, J. Helly, C. Frenk, S. Cole, K. Crawford, S. Zibetti, J. A. Carballo-Bello, and R. J. Gabany, "The formation of shell galaxies similar to ngc 7600 in the cold dark matter cosmogony," *The Astrophysical Journal Letters*, vol. 743, no. 1, p. L21, 2011.

[105] `https://link.springer.com/content/pdf/10.1023%2FA%3A1015934027224.pdf`.

[106] J. Dubinski and R. Carlberg, "The structure of cold dark matter halos," *The Astrophysical Journal*, vol. 378, pp. 496–503, 1991.

[107] D. Clowe, A. Gonzalez, and M. Markevitch, "Weak lensing mass reconstruction of the interacting cluster 1E0657-558: Direct evidence for the existence of dark matter," *Astrophys. J.*, vol. 604, pp. 596–603, 2004.

[108] A. Mahdavi, H. y. Hoekstra, A. y. Babul, D. y. Balam, and P. Capak, "A Dark Core in Abell 520," *Astrophys. J.*, vol. 668, pp. 806–814, 2007.

[109] D. Clowe, M. Markevitch, M. Bradač, A. H. Gonzalez, S. M. Chung, R. Massey, and D. Zaritsky, "On dark peaks and missing mass: a weak-lensing mass reconstruction of the merging cluster system a520," *The Astrophysical Journal*, vol. 758, no. 2, p. 128, 2012.

[110] B. W. Carroll and D. A. Ostlie, "An introduction to modern astrophysics," 2007.